People's and Democratic Republic of Algeria
Ministry of Higher Education and Scientific Research

Med Khider University of Biskra

Faculty of Exact Sciences and Nature and Life

Department of Matter Sciences

Thesis

Presented to obtain the degree of

Doctorate

Speciality:

Physics of Materials

Study of Thin layers of Tin Sulfide (SnS) Elaborated by Chemical Means for technological applications

Presented by:

Imane bouhaf kherkhachi

To the Jury composed by:

A. Zerarka	Professor	University Med Khider of Biskra	President
A. Attaf	Professor	University Med Khider of Biskra	Reporter
S. Rahmane	Professor	University Med Khider of Biskra	Examiner
N. Attaf	Professor	University of Constantine 1	Examiner
M. L. Benkidir	Professor	University of Tebessa	Examiner
M.S. Aida	Professor	University of Constantine 1	Guest

Academic Year: 2016-2017

Acknowledgements

Firstly, I thank **GOD** the whole powerful for having agreed his infinite kindness, courage, the force and patience to complete this modest work.

After that, I make a point of profoundly thanking to my supervisor Mister **Attaf Abdallah**, Professor at the department of sciences of matter at Faculty of Exact Sciences and Sciences of Nature and Life in Mohamed Khider University of Biskra, for his help, support, guidance and encouragement.

Mr: A.Zerarka, A Professor at the University of Biskra, S. Rahman, Professor at the University of Biskra, N. Attaf, Professor at the University of Constantine 1 and M.L. Benkidir, Professor in Universty of Tebessa, find here the expression of my sincere thanks for the honor they do for me in accepting and spending a valuable part of their time to review the manuscript and participate in Jury defense. I also wish to thank MS Aida, Professor Universty of Constantine 1.

I wish to thank my parents for their unconditional love and support, I am very grateful for what they have done for me. Also I thank my husband and all my family.

I thank all the members of thin films and Applications Laboratory (LPCMA) and Laboratory of Semiconductors Materials of our university.

Table of contents

ACKNOWLEDGEMENTS

General introduction……………………………………………………………...……...1

References…………………….………………………………………….…….…....4

Chapter I: Physical properties of tin sulfide and deposition techniques

I.1.Introduction……………………………………………………….………………….…....6

I.2.Semiconductor type IV-VI……………………….……………….……………………….6

I.2.1. Trends in Group IV……………………………………………….……………….……6

I.2.2. Trends in Group VI……………………………………………….……………….……6

I.2.2.1. Chalcogen and metal chalcogenides……………………………….….…………….…6

I.2.2.1. a. Chalcogen…………………………………………………………….…….….….6

I.2.2.1. b. Metal chalcogenides……………………………………………………….….….....8

I.2.2.1. c. Metal sulfides………………………………….…………………….…………….9

I.2.3. Some properties of the elementary constituents of IV-VI compounds….……….….…..9

I.2.4. Crystal structure of IV-VI elements……………………….…………………….…….10

I.3. Tin sulfide……………………………….………………………..……………......11

I.3.2. Physical properties of tin sulfide…………………...……………….……………….....11

I.3.2.1. The macroscopic appearance of tin sulfide………..………...….……….….…….....11

I.3.2.2. Growth Kinetics……………..………..…………………………………………......11

I.3.2.3. Structural properties……………..…………….……………………..…………......12

I.3.2.3.a.Crystal Structure……………………..……………………………………..…......12

I.3.2.4. Optical properties……………………..……………………………………......19

I.3.2.4.a.Transmittance………………………….…………………………………………......19

I.3.2.5.Electrical properties………………………………………………………….….…....21

I.4.System Sn-S………………………………………...………………………….........22

I.5. Enthalpies of formation ……..…………………………...……………………...…….24

I.6. Applications of tin sulfide thin films………………………………………………..…...24

I.6.1. Photovoltaic Applications………………………………………………………..….24

I.6. 2.Other Applications……………………………………………………………......….26

I.7. Thin film deposition techniques………………………………………………….…...26

I.7.1. Physical vapor deposition………………………………………………….………..27

I.7.1.1. Sputtering……………………………………………………………………28
I.7.1.2.Molecular Beam Epitaxy (MBE)…………………………………….………29
I.7.1.3. Thermal Evaporation……………………………………………………...30
I.7.1.3. a. Thermal evaporation by resistive heating…………………………….....30
I.7.1.3. b. Electron-Beam (e-Beam) Evaporation……………………………….…31
I.7.2. Chemical Vapor Deposition (CVD)……………………………….…...31
I.7.2.1. Plasma enhanced CVD (PECV)…………………………………….…..32
I.7.2.2. Atmospheric Pressure CVD (APCVD)……………………………….....32
I.7.2.3. Chemical Bath Deposition……………………………………………...33
I.7.2.4. Electrochemical Deposition (ECD)……………………………………….33
I.7.2.5.Spray pyrolysis………......………………………………………………34
References……………………...…………………………………………..….…37

Chapter II: Technical preparation and characterization of tin sulfide thin films

II.1.Introduction……………………………………………………………....43
II.2.Tin sulfide thin films prepared by ultrasonic spray……………………….…..43
II.2.1. Experimental setup used in our study………………………………….…..43
II.2.2. Experimental procedure………………………………………….........44
II.2.2.1.Preparation of substrates…………………………………………………..44
II.2.2.2. Cleaning of the substrates……………………………………………….…..44
II.2.2.3.Chemical composition envisaged for the development of thin layers of tin sulfide……………………………………………………………….…......45
II.2.2.4.The deposition processes…………………….……………………….......45
II.3. Characterization of thin films……………………….……………………..47
II.3.1.Adhesion Test………………………………………………………….…47
II.3.2.Thickness calculation……………………...……………………………..47
II.3.3. Structural characterization…….……………………..……………………..48
II.3.3.1. X-ray diffraction………………………………………………………......48
II.3.3.1.a. Determination of the grains size……………………………………..50
II.3.3.1.b. Determination of lattice parameter………………………….……….50
II.3.3.1.c. Stress determination……………………………………………….…...50
II.3.3.1.d.The texture coefficient (TC)…………………………………….……51

II.3.3.1.e.The dislocation density (δ)……………………………………………………….51
II.3.3.1.f.The number of crystallites n_c……………………………………….…………...51
II.3.4.Optical characterization………...………………………………………………....52
II.3.4.1.UV-visible spectroscopy……………………………...……………….......52
II.3.4.1.a. Film thickness……………………………………...…………………...53
II.3.4.1.b.The absorption coefficient……………………………………..……....….54
II.3.4.1. c. Optical gap…………………………………………………………..………54
II.3.4.1.d. Disorder calculating……………………………...…………………..55
II.3.4.1.e. Refractive index and dielectric constant…………………………...………...56
II.3.4.2.Photoluminescence spectroscopy………………………………………………56
II.3.4.2.a. Physical principle………………………………......................................57
II.3.4.2.b. Photoluminescence peak positions: Energy levels…………………………..58
II.3.5.Infrared Spectroscopy…………………………...…………………………..58
II.3.6.Electrical characterization with four point probe method………………….….…60
References…………………………………………………………………….….….62

Chapter III: Deposition times influence on tin sulfide thin films using $SnCl_2$ and $SnCl_4$ sources precursors

III.1.Introduction……………………………………………………………………..65
III.2. The film thickness and growth rate……………………………………….……65
III.3. Structural studies……………………………………...……………….……….66
III.3.1.Texture coefficient, Crystallites size, Strain, dislocation density and lattice parameters……………………………………………………………………….....70
III.4. Optical studies………………………………………………………...…..76
III.4.1.Transmittance ……..…………………………...……………………….….76
III.4.2.Optical band gap…………………………………………………….…...77
III.4.3.Photoluminescence studies…………………….……………………….…..79
III.5.Electrical studies …………………………………………………….……..…..80
III.6.Conclusion……………………………………………………………......…81
References…………………...……………………………………………..…….82

Chapter IV: Effect of solution flow rate on properties of tin sulfide thin films

IV.1. Party A: Solution flow rate affects on tin sulfide thin films prepared at 4 min…......85
IV.1.1.The film thickness and deposition rate …………….……………………..…..85
IV.1.2. Structural studies……………………………...…………………………...…86
IV.1.2.1. Lattice parameters, Crystallites size, Strain and Dislocation density …………..86
IV.1.3. Optical studies……………………………….……..…………………….……..…89
IV.1.3. 1.The transmittance…………………………………………………………….……89
IV.1.3.2.The absorbance………………………………………………………......…..89
IV.1.3.3.The optical band gap and disorder……………………………………….....…90
IV.1.4. Electrical studies………………………………………………………………...91
IV.2.Party B: Solution flow rate affects on tin sulfide thin films prepared at 6 min….….92
IV.2.1.The film thickness and deposition rate……………………………………….…....92
IV.2.2. Structural properties………………………………………………………….…92
IV.2.2.1.Lattice parameters, crystallites size, strain and dislocation density…………..….94
IV.2.3.Optical properties…………………………………………………………….…..…96
IV.2.3.1.The transmittance……………………………………………….................96
IV.2.3.2.The optical band gap and disorder……………………………..……………......97
IV.2.3.3.Photoluminescence properties……………………………………………….…...98
IV.2.3.4.The reflectance………………………………...…………………….……......99
IV.2.3.4.a.The refractive index…………………………….………………………….…....100
IV.2.3.4.b.The extinction coefficient……………………….…………………………....101
IV.2.3.4.c.The dielectric constant………………………………………………..…….102
IV.2.4.FTIR studies……………………………………………………..………….……102
IV.3. Conclusion………………………………………………………………..……...104
References……………………………...…………………………………..…....105

Chapter V: Substrate temperature effect on properties of tin sulfide thin films

V.1.Party A: Influence of substrate temperature for films deposited at 4 min and 50ml/h……………………………………………………………………………......108

V.1.1.The film thickness……………………..…………………………………...……......108
V.1.2. Structural studies……………………………………………………..……..……109
V.1.2.1.Crystallites size, Strain, Dislocation density, Texture coefficient and lattice parameters……………………..…………………………………………………………111
V.1.3. Optical studies…………………………………………………………………….113
V.1.3.1.Transmittance …………………………..113
V.1.3.2.Optical band gap……………………………………………………………....114
V.1.3.3. Photoluminescence studies……………………...…………………………...…115
V.1.4. Electrical studies…………………………………………………………......….116
V.2. Party B: Influence of substrate temperature for films deposited at 6 min and 40 ml/h……………………………………………………………………………………….117
V.2.1.The film thickness and the deposition rate……………………………………...…117
V.2.2.Structural studies………....……………………………………………………...118
V.2.2.1.Lattice parameters, Crystallites size, Strain and Dislocation density…………...120
V.2.3. Optical studies……………………………………………………………….…121
V.2.3.1.Transmittance ………………....……………………………………………121
V.2.3.2.The absorption coefficient……………………………………………………….122
V.2.3.3.The optical band gap and disorder………...……………………………………..123
V.2.3.4.Photoluminescence studies……………………………………..…………......124
V.2.3.5.The reflectance……………………….……………………..…………......124
V.2.3.5.a.The refractive index and extinction coefficient……………………………......125
V.2.3.5.b.The dielectric constant……………………………………..……………..126
V.2.4. FTIR studies…………………………………………………………...…127
V.3. Conclusion…………………………………………………………………..…....128
References…………………………………………………..………………..…129

General conclusion and perspectives………………………………..……..………131

List of Figures

Chapter I

Fig.I.1: Macroscopic appearance of tin sulfide ………………..………………………....11
Fig.I.2: Variation of film thickness with substrate temperature…………………………..12
Fig.I.3: The unit cell of the a) orthorhombic structure and b) zinc blende of SnS ……..…12

Fig.I.4: CdI_2-type crystal structure of SnS_2, (a) trigonal unit cell, (b) and layered structure (dark spheres represent S and light spheres represent Sn) 13
Fig.I.5: Orthorhombic crystal structure of Sn_2S_3, (a) unit cell, and (b) chain structure. (Black spheres represent S, dark grey spheres represent Sn(IV) and light spheres represent Sn(II))..14
Fig.I.6: X-ray diffraction patterns of Sn_xS_y thin films prepared by a)various solution rates,b) various substrate temperatures T_S=320°C,370 °C, 420 °C and 470°C, c) substrate temperatures T_S=300°C,350 °C, 400 °C, 450 °C and 500 °C 15
Fig.I.7: Optical absorption spectra of SnS thin films deposited by CBD with different deposition time 19
Fig.I.8: Transmittance spectra for SnS_2 thin film prepared at a 373 K b 398 K and c 423 K 20
Fig.I.9: The phase diagram of the system Sn-S 23
Fig.I.10: Schematic diagram of SnS based solar cell 25
Fig.I.11: Solar cell structure 25
Fig.I.12: Schematic diagram of the structure for the fabricated diodes 26
Fig.I.13: Presentation of the main deposition methods of thin films........................27
Fig.I.14: Schematics of the sputtering process 28
Fig.I.15: Schematic diagram of the molecular beam epitaxy apparatus 29
Fig.I.16: Schematic of Thermal evaporation by resistive heating............................30
Fig.I.17: Schematic diagram of e-Beam evaporation 31
Fig.I.18: A schematic of the modified PECVD system..32
Fig.I.19: Schematic diagram of APCVD system 33
Fig.I.20: Experimental device used for the preparation of thin layers by CBD..............33
Fig.I.21: General schematic diagram for electrodeposition process.........................34
Fig.I.22: Sketch diagram of spray pyrolysis system 35
Fig.I.23: Presentation of the different processes that may occur in Spray CVD as the deposition temperature..36

Chapter II

Fig.II.1: Installation used in the deposition technique ultrasonic Spray.....................43
Fig.II.2: Different steps for obtaining a thin layer..47
Fig.II.3: Crystal planes family in Bragg condition..48
Fig.II.4: Schematic diagram of the diffractometer..49

Fig.II.5: Type diffractometer (D8 ADVANCE)…………………… ………….........49

Fig.II.6: Illustrate the peak widths FWHM (ΔΘ=β)………………………..……….......50

Fig.II.7: The principle of operation of UV-visible……………………..……..…….52

Fig.II.8: Thin absorbing film on thick transparent substrate system……………...……53

Fig.II.9: Method of interference fringes to determinate the thickness……………..……..54

Fig.II.10: Determination of Eg…..55

Fig.II.11: Determination of the disorder by extrapolation starting from the variation of ln(α) has in function of hv……………………………………………………………………56

Fig.II.12: Typical experimental set-up for PL measurements……………………………57

Fig.II.13: Radiative recombination paths: (a) band-toband; (b) donor to valence band; (c) conduction band to acceptor. (d) Nonradiative recombination via an intermediate state....58

Fig.II.14: Stretching vibrations……………………………………………………………59

Fig.II.15: Bending vibrations…………………………………………………………...59

Fig.II.16: Linear four-point probe configuration. The sample thickness is t and a is the distance from the edge or boundary of the sample……………………………….………..61

Chapter III

Fig.III.1: Variation of film thickness as a function of deposition time…………………..65

Fig.III.2: Variation of deposition rate as a function of deposition time…………………66

Fig.III.3: XRD pattern of SnS thin film sample with different deposition time……....…66

Fig.III.4: ASTM files of SnS_2 and SnS……………………………………………........67

Fig.III.5: XRD pattern of Sn_xS_y thin film sample with different deposition time……..….68

Fig.III.6: Variation of preferential orientation as a function of deposition time for (001) plane…………………………………………….………………………………….…..71

Fig.III.7: Variation of the crystallite size as a function of the deposition time…………..73

Fig.III.8: Variation of strain ε in the films network as a function of the deposition time...74

Fig.III.9: Variation of dislocation density with deposition time…………………………75

Fig.III.10: Variation of number of crystallites with deposition time of SnS thin films…………………………………………………………………………………..75

Fig.III.11: Transmission curves for films 1 at different deposition time…………...……76

Fig.III.12: Transmission curves for films 2 at different deposition time………………...77

Fig.III.13: The variation of band gap energy at different deposition time……….….......78

Fig.III.14: Variation of disorder of Sn_xS_y at different deposition time………...……...78

Fig.III.15: PL Spectra Vs Wavelength plot of Sn_xS_y thin films prepared at different deposition time………………………………….…………………………….……...79
Fig.III.16: Electrical resistivity of SnS thin films……………………….….….………81

Chapter IV

Fig.IV.1: Variation of the films thickness and deposition rate as function of deposition time…………………………..………………………………………..………….......85
Fig.IV.2: X-ray spectra of the samples of SnS_2………………...………………………86
Fig.IV.3: Crystallite size and strain as a function of flow rate……………….…………..87
Fig.IV.4: Variation of the dislocation density with flow rate of SnS_2 thin films……..…...88
Fig.IV.5: UV–visible transmittance spectrum of SnS_2 deposited at different flow rates....89
Fig.IV.6: Spectral dependence of absorbance for SnS_2 films synthesized at different flow rate……………………………………………………………………………………....90
Fig.IV.7: Variation of optical band gap energy and disorder of SnS_2 at different flow rates…………………………………………………………………………………..90
Fig.IV.8: Variation of electrical resistivity with different flow rate…………….……...91
Fig.IV.9: Deposition rate dependence on solution flow rate, inset shows variation of film thickness as a function of solution flow rate………………………………………………92
Fig.IV.10: XRD diffraction pattern of tin sulfide thin films prepared with different flow rate………………………………………………………………….……….…..…93
Fig.IV.11: ASTM files of Sn_2S_3………………………………………………………..94
Fig.IV.12: Dependence of crystallite size and strain on flow rate…………………….…....96
Fig.IV.13: Optical transmittance spectra of tin sulfide thin films as a function of solution flow rate……………………………………………………………………….........97
Fig.IV.14: Variation of optical band gap and urbach energy of SnS at different flow rate……………………………………………………………………..…………97
Fig.IV.15: Variation of crystallite size and optical band gap of SnS with various flow rates………………………………………………………………….……………98
Fig.IV.16: Photoluminescence spectra of SnS sprayed thin films……….…………......99
Fig.IV.17: Variation of reflectance for the SnS thin films deposited at various solution flow rate…………………………………………………………………….……100
Fig.IV.18: Variation of refractive index (n) for tin sulfide thin films grown at different flow rate……………………………………………………………….………101

Fig.IV.19: Plot of extinction coefficient 'k' of SnS grown for different flow rate……………………………………………………………………………...………..101
Fig.IV.20: Variation of the real (ε_1) and imaginary (ε_2) parts of dielectric constant of SnS thin films as-grown at different flow rate……………………………………………….……..102
Fig.IV.21: FTIR spectra of SnS films at different flow rate……………………….……103

Chapter V

Fig.V.1: Vaiation of film thickness as a function of substrate temperature…..……….…...108
Fig.V.2: XRD pattern of SnS thin film sample with different substrate temperatures……………………...……………………………………………….....109
Fig.V.3: Color of films Sn_xS_y with different substrate temperatures…………………....110
Fig.V.4: Substrate temperature effect on the texture coefficient……………………..…....112
Fig.V.5: Transmittance spectrum of tin sulfide thin films prepared at different substrate temperature…………………..…………………………………………….…………….…113
Fig.V.6: Variation of optical band gap of films with T_S…………………….…..……....114
Fig.V.7: PL spectra of tin sulfide at different substrate temperature………………..……...115
Fig.V.8: Variation of electrical resistivity with substrate temperature for as-deposited films………………………………………………………………………………........116
Fig.V.9: Variation of film thickness and deposition rate as a function of substrate temperature……………………………………………………………………………......117
Fig.V.10: XRD pattern of Sn_xS_y films prepared at substrate temperature…………….....118
Fig.V.11: Substrate temperature effect on the film texture……………………….......119
Fig.V.12: Transmittance spectra of tin sulfide thin film prepared at different temperature……………………………………………………………………………......122
Fig.V.13: Spectral shape of α versus wavelength of SnS thin layers system grown at different substrate temperature……………………………………………………...122
Fig.V.14: Variation of optical band gap and disorder of the tin sulfide thin films grown at different substrate temperature……………………………………………………...123
Fig.V.15: PL spectra of different substrate temperature……………………………....124
Fig.V.16: Spectral shape of reflectance R of SnS thin layers for different substrate temperature………………………………………………………………………………125
Fig.V.17: Variation of refractive index (n) and extinction coefficient (k) for tin sulfide thin films grown at different substrate temperature……………………….………………..126

Fig.V.18: Variation of real and imaginary part of the dielectric constant of the tin sulfide thin films……………………………………………………………………………....126
Fig.V.19: FTIR spectra of SnS thin films deposited at various substrate temperature.....127

List of Tables

Chapter I

Tab.I.1: Elements of the column 16 (VIA)……………..………..…………………...……7
Tab.I.2: Electronic Structures chalcogen elements…..………..……………………….….…8
Tab.I.3: Main properties of group IV elements…...…………..…………………………....9
Tab.I.4: Main properties of the elements of Group VI…………………………………....10
Tab.I.5: Basic Parameters at 300 K……………………………..……………………..….13
Tab.I.6: Structure, preferred grain size and orientation of thin films of SnS prepared by different techniques……………………………………………………………….……….17
Tab.I.7: Influence of source nature and substrate temperature on the crystal structure of tin sulfide………………………………………………………….……………..……………18
Tab.I.8: The optical band gap of SnS material by different techniques…………………..20
Tab.I.9: The optical band gap of SnS_2 and Sn_2S_3 material by different techniques….......21
Tab.I.10: Electrical properties of SnS material………...……………………………...…21
Tab.I.11: Electrical resistivity of the material SnS_2……...……………………...…..….22
Tab.I.12: Electrical Properties for the Sn_2S_3…..………...…………………..……………22
Tab.I.13: Enthalpies of formation for tin sulfide…...………...………………….………24

Chapter II

Tab.II.1: Deposition parameters of three series of thin layers of tin sulfide…..……….....45

Chapter III

Tab.III.1: Structural properties of the tin sulfide films**1** on different deposition time…...70
Tab.III.2: Structural properties of films **2** on different deposition time…………………71

Chapter IV

Tab.IV.1: Lattice parameters of SnS_2 thin film..…..87
Tab.IV.2: Structural parameters of SnS_2 thin film………………………….…………....95
Tab.IV.3: Crystallite size Dependence on flow rate with (211), (001), (112) and (151) plans…………………………………………………………………….……..……...95

Chapter V

Tab.V.1: Structural parameters of spray ultrasonic Sn_xS_y films…………………………...111

Tab.V.2: Lattice parameters of SnS_2 films deposited on the different substrates…..…...112

Tab.V.3: Lattice parameters of SnS_2 films deposited on the different substrates temperatures……………………………………………………………………….…..120

Tab.V.4: Structural parameters of spray ultrasonic Sn_xS_y film………………………..…121

General introduction

Solar PV technology is one of the renewable technologies which have a potential to shape a clean, reliable, scalable and affordable electricity system for the future [1].

To achieve cost-effective thin film solar cells for large-scale production of solar energy, the absorbing semiconductor material used in the device needs to satisfy many requirements. First, the constituent elements should be inexpensive, non-toxic, and abundant. Second, to obtain high energy conversion efficiency, the material should have appropriate optical and electrical properties such as a suitable optical band gap, a high optical absorption coefficient, a high quantum yield for the excited carriers, a long carrier diffusion length, and a low recombination velocity [2]. Thin-film solar cells are commercially used in several technologies, including cadmium telluride (CdTe), copper indium gallium diselenide (CIGS), and amorphous thin-film silicon (a-Si). Amorphous Si (a-Si) PV modules are the primitive solar cells that are first to be manufactured industrially. Amorphous (a-Si) solar cells can be manufactured at a low processing temperature, thereby permitting the use of various low cost, polymer and other flexible substrates. These substrates require a smaller amount of energy for processing [3]. Therefore, a-Si amorphous solar cell is comparatively cheaper and widely available. The mainissue of a-Si solar cell is the poor and almost unstable efficiency. The cell efficiency automatically falls at PV module level. Currently, the efficiencies of commercial PV modules vary in the range of 4% - 8%. They can be easily operated at elevated temperatures, and are suitable for the changing climatic conditions where sun shines for few hours [4]. Thin-film CdTe solar cells are one of the most promising thin-film PV devices with a band gap of 1.45 eV it has an excellent match with the solar spectrum. Since these are direct band gap semiconductors with high absorption coefficient, very thin absorber layer are needed to absorb the photons. Theoretical efficiencies for these devices are about 26%. Laboratory efficiencies of 16.5% for thin-film CdTe solar cell has been demonstrated by NREL scientists [5]. Chalcopyrite based solar modules combine advantages of thin film technology with the efficiency and stability of conventional crystalline silicon cells. It is therefore believed that chalcopyrite based modules can take up a large part of the photovoltaic market growth once true mass production is started [6]. Chalcopyrites are compounds based on the use of elements from groups I, III and VI of the

periodic table and include copper indium diselenide ($CuInSe_2$), copper gallium indium diselenide ($CuGa_{1-x}In_xSe_2$) and copper indium disulphide ($CuInS_2$). One refers to these cells as CI(G)S solar cells. As with amorphous silicon and cadmium telluride these materials have direct energy band gaps and high optical absorption coefficients for photons with energies greater than the energy band gap making it possible for a few microns of absorber layer material to absorb most of the incident light [7]. But there were material disadvantages in the toxicity of Cd and the rarity of indium and tellurium. Although tellurium is currently in low demand, up-scaled production of CdTe could potentially produce a price spike that would exclude CdTe from being an economic solar energy conversion material.

Searching for thin film materials for solar energy conversion and other related applications has been recently identified. Compared to other studies, using metal chalcogenides, as a class of materials, had shown somewhat superior performance [8]. Among the new materials that have attracted considerable attention in the binary is composed of tin sulfide due to its interesting physico-chemical properties, and which could also replace other material such as quaternary $CuInGaSe_2$ in photovoltaics [9]. Tin sulfides are materials of technological importance, which are being explored as semiconductors, anode materials for Li ion batteries, photoconductors, photocatalysts and absorber layer materials in photovoltaic solar cell devices [10]. In the phase diagram of the Sn–S binary system, there are three stoichiometric compounds known, with different tin to sulfur ratios: SnS, Sn_2S_3 and SnS_2 that are the most interesting [11] materials according to technological standpoint. In addition, the tin sulfide SnS has many advantages for photovoltaic applications such as the gap that can approach the optimum for the conversion of solar energy (1.50 eV) [12], low cost, non-natural toxic and easily developed because these components are very abundant on earth. Moreover, SnS_2 as an n-type semiconductor, has a layered hexagonal structure with a larger band gap varying (0.8–2.88 eV), it is a good light absorber (absorption coefficient of 10^4 cm^{-1}) [13], it is known for its intriguing optical, electrical properties and potential applications. Several deposition techniques have been used to prepare tin sulfide thin films, including: chemical bath deposition method (CBD), thermal evaporation, RF sputtering, electrochemical deposition, hot wall method, novel hydrothermal method, successive ionic layer adsorption and reaction method (SILAR), pulseelectro-deposition method, spray pyrolysis, electron beam evaporation, plasma-enhanced chemical vapor deposition (PECVD), and dip coating method.

The purpose of the following work is to study of thin layers of tin sulfide (SnS) prepared by spray ultrasonic technique for technological applications .The ultrasonic spray method adopted in this work is an inexpensive technique, easy to implement and offers the possibility to deposit films on large areas and develop the various component layers of the solar cell.

The work described in this thesis is presented in 5 chapters, as follows:

The first chapter will include general properties of semiconductors IV-VI especially on tin sulfide (crystallographic structure, optical and electrical properties ......) and their applications. Finally we give the different techniques for depositing tin sulfide.

In the second chapter, firstly we describe the ultrasonic spray pyrolysis technique to deposit tin sulfide thin film (SnS). After that, we will depict the various experimental techniques for characterization of our samples.

In the third chapter, we studied the influence of deposition time on the structural, optical and electrical properties of SnS thin film produced by ultrasonic spray.

The fourth chapter is dedicated to the effect of the solution flow rate on the sprayed SnS thin films properties.

In the last chapter, the effect of the substrate temperature on tin sulfide thin films deposited by ultrasonic spray method is offered.

Finally, we report general conclusion about the results obtained in this work.

References of General Introduction

[1] V.V. Tyagi, Nurul A.A.Rahim, N.A.Rahim, JeyrajA./L.Selvaraj, J.Progress in solar PV technology: Research and achievement. Renewable and Sustainable Energy Reviews 20 (2013) 443–461.

[2] R. H. Bube, Photovoltaic Materials, Series on Properties of Semiconductor Materials Vol. 1 Imperial College Press London (1998).

[3] M.Imamzai, M.Aghaei, Y. Hanum Md Thayoob, M. Forouzanfar, A Review on Comparison between Traditional Silicon Solar Cells and Thin-Film CdTe Solar Cells, Proceedings of National Graduate Conference, Tenaga Nasional University, Putrajaya Campus 8-10 (2012) 1-5.

[4] M.A. Maehlum, Best Thin Film Solar Panels-Amorphous, Cadmium Telluride or CIGS, J. Energy Informative The Homeowner's Guide To Solar Panels (2015).

[5] X. Wu. High Efficiency Polycrystalline CdTe Thin-Film Solar Cells, J.Solar Energy 77 (2004) 803–814.

[6] J. Poortmans, V. Arkhipov. Thin Film Solar Cells: Fabrication, Characterization and Applications, "Chapter 6: Chalcopyrite Based Solar Cells", R. Klenk, M.C. Lux-Steiner, (John Wiley, Chichester, England) (2006) 237-275.

[7] R.W. Miles, K.M. Hynes, I. Forbes. "Photovoltaic Solar Cells: An Overview of State-of-the-art Cell Development and Environmental Issues", J.Progress in Crystal Growth and Characterization of Materials 51(2005) 1-42.

[8] Abriksov NKH, Bankia VF, Poretskaya LV, Shelimova LE, Skudnova EV. Plenum 1969.

[9] B.G. Jeyaprakash, R. Ashok kumar, K.Kesavan, A. Amalarani, J.American Science 6(2010) 3.

[10] Shuang Liu, X. Y., Libao Chen, Qiuhong Li, Taihong Wang, J.Solid State Sci 12(2010)712-718.

[11] T. Chattopadhyay, A. Werner, HG von Schnering, J. Review Phys. Appl 19 (1984) 807-813.

[12] J. Yang, Q. Tian, Z. Chen, X. Xu, L. Zha, J.Materials Letters 67 (2012) 32-34.

[13] B. Thangaraju and P Kaliannan, J. Phys. D. Appl. Phys 33(2000) 1054-1059.

Chapter I

Physical properties of tin sulfide and deposition techniques

I.1.Introduction

We present in this chapter the general properties of semiconductors IV-VI and tin sulfide (crystallographic structure, optical and electrical properties ......). In addition, we give those technological applications of tin sulfide and various deposition techniques.

I.2 .Semiconductor type IV-VI

Metal chalcogenide semiconductors are used as sensors, and polarizers as thermoelectric cooling materials [1].

I.2.1.Trends in Group IV

The chemistry of silicon, germanium, tin and lead is very different from that carbon. While the latter properties are strictly those of a non-metal, the metallic character of its congeners increases when descending from the group: tin, especially lead, are clearly metal. All group elements, with the exception of lead, have at least one solid phase having the diamond structure. In the case of tin, diamond variety (gray tin) is metastable with respect to another form (white tin) in which each tin atom has six neighbors (octahedral environment strongly deformed). Lead has a compact cubic structure.

• The electronegativity decreases lead to silicon;

• The tendency to catenation decreases in the order C >> Si > >> Ge ≈ Sn >>Pb parallel to the binding energy E-E;

• The coordination number is limited to 4 for carbon, but can exceed 4 other dogs because of the availability of d orbitals from silicon;

• In the oxidation state IV, all tetrahedral elements form compounds which can be resolved into enantiomers with all four substituents are different;

• The oxidation state II is more stable when down in the group. It is the most stable state for the lead;

• In the oxidation state II, the compounds possess a lone pair of electrons that can be stereochemically active ($SnCl^{-3}$ is pyramidal) [1].

I.2.2. Trends in Group VI

I.2.2.1. Chalcogen and metal chalcogenides

I.2.2.1. a. Chalcogen

- **History**

In 1869, when Mendeleev proposed his table of chemical elements, the four first elements of the oxygen family were already known. The group of these elements represents the latest so-called "Chalcogen".

The term "Chalcogen" was proposed around 1930 by Warner Fisher, when he worked in the group of "Wilhelm Blitz" at the University of Hanover, to designate elements of the group16. This term derived from the ancient Greek χαλκός (khalkos) meaning "copper - brass (bronze)" followed by the Greek γεννάω suffix (gene) or Latin generare (birth) was quickly accepted by the German chemists, including Heinrich Remy recommended its official use in 1938, with the agreement of members of the International Union Committee on Inorganic Chemistry (IUPAC later). Then it was internationally recognized that the elements: oxygen, sulfur, selenium and tellurium; which were called "Chalcogen" and their compounds "chalcogenides".

Chalcogen family currently has six elements: oxygen (O), sulfur (S), the Selenium (Se), tellurium (Te), polonium (Po) and element 116 - ununhexium (Uuh) [2].

• Place the family of elements "chalcogens" in the periodic table

Column 16 or VIA (chalcogen) of the periodic table, to the right of this group of four columns (Table.I.1), consists of three non-metal elements (O, S, Se), two-metals (Te, Po) and a metal (Uuh).

Tab.I.1*: Elements of the column 16 (VIA).*

	Column N°			
Period N°	13	14	15	16
2	B	C	N	O
3	Al	Si	P	S
4	Ga	Ge	As	Se
5	In	Sn	Sb	Te
6	Tl	Pb	Bi	Po
7	Uut	Uu q	Uu p	Uuh

All elements of this family have six electrons in the valence shell (ns^2 np^4) or ns^2 (n-1) d^{10} np^4 as shown in table.I.2 that is why they have a strong tendency to capture two

electrons or form two covalent bonds to acquire a saturated layer, in order to respect the octet rule [2] .

Tab.I.2*: Electronic Structures chalcogen elements.*

Element	Symbol	Electronic structure
Oxygen	O	[He] $2s^2$ $2p^4$
Sulfur	S	[Ne] $3s^2$ $3p^4$
Selenium	Se	[Ar] $3d^{10}$ $4s^2$ $4p^4$
Tellurium	Te	[Kr] $4d^{10}$ $5s^2$ $5p^4$
Polonium	Po	[Xe] $4f^{14}$ $5d^{10}$ $6s^2$ $6p^4$
ununhexium	Uuh	[Rn] $5f^{14}$ $6d^{10}$ $7s^2$ $7p^4$

The sulfide component represents 0.60% of the land mass but only 0.34% of the mass of the earth's crust. These are sulfides and sulfates (sixteenth place for classification abundance).The sulfur promotes the oxidation state + VI, selenium and tellurium the oxidation state + IV.

I.2.2.1. b. Metal chalcogenides

The elements of column 6 formed with metals and nonmetals of binary and ternary compounds. While with the transition metals, S, Se and Te form non-stoichiometric compounds, glasses and sometimes alloys. Some of them are investigated for their optical, electrical and magnetic properties [2]. Today research into chalcogenide prepared by various techniques has resulted in many applications: infrared optics, optical fibers, thermal imaging, photovoltaic cells of the third generation, and materials for magnetic information storage. Chalcogenides are known for their following properties:

- They are non-balanced and highly metastable substances. Exposure to light can cause their transformation to a state close to equilibrium.
- They have orbits unbound (free pairs), which form the top of the valence band states. These orbits can be transferred to related orbits and vice versa.
- "Free volume" of the chalcogen is relatively large, making the flexible structure.

The largest photo-induced change of the optical properties was found for systems with the largest free volume.

Based on the foregoing, significant changes due to the exposure to light, in the structure and these properties are changes: structure, refractive index, photodecomposition, thickness, absorption coefficient and reactivity (solubility in chemical solvents). Some of these changes can be caused by densification, polymerization, the homogenization of films,

and the formation of defects (charged or neutral) and localized electronic states in the tails of bands conduction and valence, etc [2].

I.2.2.1. c. Metal sulfides

Metal sulfides are advanced materials with intriguing physical and chemical properties. They have received great attention and have been studied for decades. Naturally occurring metal sulfides also constitute an important source of metals. Some elements of the periodic table that do not exist in elemental form on earth are abundant in sulfide ores. Lead is one of these metals that can be rarely found in free elemental form but exists as a sulfide ore, galena (PbS), which is the major source of lead. Other metal sulfide mineral sources like pyrite (FeS_2), sphalerite (ZnS), cinnabar (HgS), stibnite (Sb_2S_3) and chalcocite (Cu_2S) are also present in nature. Apart from being major metal sources, metal sulfides alleviate many recent challenges especially in the field of energy as the requirement of cost effective, efficient and environmentally benign advanced energy storage and conversion devices, including solar cells, fuel cells, and lithium ion batteries is gaining importance. They are considered materials of great significance due to their exceptional optical, electronic and mechanical properties, and are widely used as solid lubricants, catalysts, sensors, in thermoelectric devices, solar cells, light emitting diodes, as lithium battery electrodes, photoconductors and shockwave resistant materials [3].

I.2.3. Some properties of the elementary constituents of IV-VI compounds

The main properties of elements of group IV of the Periodic Table: Carbon (C), silicon (Si), germanium (Ge), Tin (Sn) and lead (Pb) are shown in the following table:

Tab.I.3: *Main properties of group IV elements.*

Physical properties	C	Si	Ge	Sn	Pb
Atomic number	6	14	32	50	82
Atomic weight (g / mol)	12.011	28.0855	72.59	118.710	207.2
Density (g/cm^3)	2.62	2.33	5.32	7.30	11.4
Crystal structure	Diamond	Diamond	Diamond	Diamond	-
network constant (Å)	3.56683	5.43095	5.64613	6.48920	-
Melting temperature (°K)	4100	1685	1210.4	505.06	600.6
Boiling temperature (°K)	4470	3540	3107	2876	2023

The properties of the elements of group VI: Oxygen (O), Sulphur (S), selenium (Se), tellurium (Te) is shown in table.I.4.

Tab.I.4: *Main properties of the elements of Group VI.*

Physical properties	O	S	Se	Te
Atomic number	8	16	34	52
Atomic weight (g/ mol)	15.9994	32.06	78.96	127.60
Density (g/cm^3)	1.429	2.62	2.33	5.32
Crystal structure		rhomboedric	hexagonal	hexagonal
network constant (Å)	-	-	a = 4.355 -4.750 c = 4.72 – 4.949	a = 4.4570 c = 5.9290
Melting temperature (°K)	50.35	388.36	494	722.65
Boiling temperature (°K)	90.18	717.75	958	1261

All these elements of IV and VI groups can together form compounds: oxides (SiO_2, SnO_2), sulfides (SnS, GeS), selenide (SnSe, PbSe), telluride (PbTe, GeTe) and other compounds [4].

Therefore, the IV-VI semiconductors are formed by the association of atoms from column IV with those in column VI of the periodic table of the chemical elements (The elements shown in both tables I.3 and I.4).

I.2.4. Crystal structure of IV-VI elements

Crystallography MN compounds (poor Metals and Non-metals) some problems due to the polymorphism of these compounds.

The new IV-VI semiconductor MX (M = Ge, Sn, Pb, X = S, Se, Te) are isoelectronic with the group V element and crystallizes under ambient conditions with three different structures, which are similar to those elements of the group V. the lighter compounds GhG GeSe, SnS and SnSe crystallize with the GHG standard structure (B16) which is bit like the black phosphorus structure [5]. The heavier compounds SnTe, PbS, PbSe and PbTe crystallize with the NaCl structure (B1) [6], a bit like the simple cubic phase high pressure black phosphorus [7]. GeTe crystallizes with the rhombohedral structure and is analogous to the binary gray arsenic, structure (A7) [4].

I.3. Tin sulfide

Works on SnS dates back to the beginning of the twentieth century SnS was first reported by a German mineralogist Herzenberg in 1932 [8]. Since then, reports are available on the various structural, optical and electronic properties of the material.

Binary compounds based on Sn-S system have a high potential use in optoelectronic devices. Tin sulfide form a variety of phases, such as SnS, SnS_2, Sn_2S_3, Sn_3S_4, etc. due to polyvalent coordination features tin and sulfur. From a technological standpoint, tin mono-sulfide (SnS) disulfide tin (SnS_2) and the compound of Sn_2S_3 are among the most interesting materials [9]. And especially the two forms: SnS_2 and SnS are the most important technological point of view [10].

I.3.2. Physical properties of tin sulfide

I.3.2.1.The macroscopic appearance of tin sulfide

Most researchers have found that the color of tin sulfide thin films attributed to their appeared phases and the temperature [10-13]. Lee A. Burton et al found three phases of SnS, with dark gray SnS, black needles of Sn_2S_3, and yellow flakes of SnS_2 (See figure.I.1) [14].

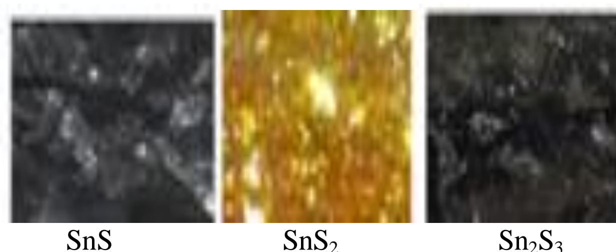

Fig.I.1: *Macroscopic appearance of tin sulfide [14].*

I.3.2.2. Growth Kinetics

The thickness of the tin sulfide film varies depending on several deposition parameters, such as the temperature, the deposition time, molarity of solution and flow rate. Figure.I.2 shows the variation of the thickness of SnS films deposited by a chemical technique (CBD) depending on the deposition temperature. The kinetics of growth film on function deposition temperature is generally in three stages: incubation or nucleation, growth nucleons or films, stunting movies and a fourth stage corresponding to the reducing the thickness [11].

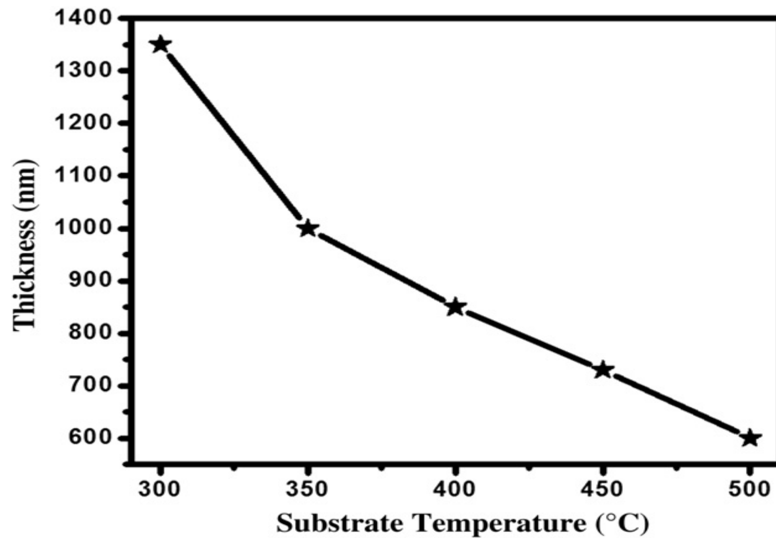

Fig.I.2: Variation of film thickness with substrate temperature [11].

I.3.2.3. Structural properties

I.3.2.3. a. Crystal Structure

There are mainly three types of crystal structure for SnS [15]:

- The orthorhombic structure.
- Zinc blende structure.
- The NaCl structure.

Most films of SnS generally has orthorhombic structure (which theoretically has the following lattice parameters: a = 0.398 nm, b = 0.433 nm, c = 1.118 nm reference database code. 01-075-0925).Only literatures reported preparing the zinc blende structure or NaCl films SnS [15].

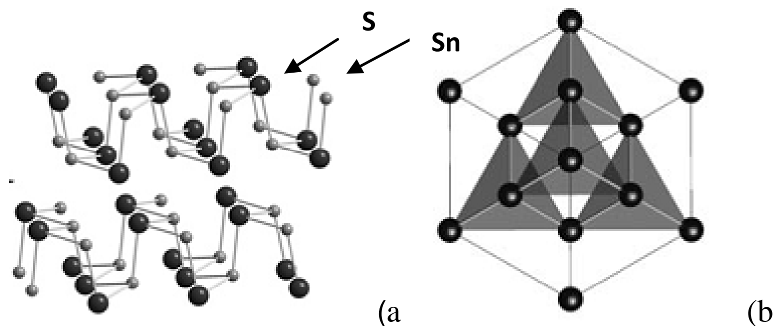

Fig.I.3: The unit cell of the a) orthorhombic structure [15] and b) zinc blende of SnS [16].

From this figure we see that the ZB structure is more compact and hard than that of the orthorhombic, indeed the GOLD structure is formed by sheets which are connected by Vander Waals forces (weak forces) [17].

Table.I.5 shows the basic parameters at 300 K of tin sulfide.

Tab.I.5: *Basic Parameters at 300 K [18].*

Crystal structure	Orthorhombic
Debye temperature	270 K
Density	5.08 g/cm^3
Linear thermal expansion coefficient	$\alpha = 2.8*10^{-7}$ K^{-1}
Heat capacity	$C_P = 45$ J mol^{-1} K^{-1}
Lattice constants	a= 4.33 Å, b = 11.18 Å et c = 3.98 Å

Tin disulfide (SnS_2) is a semiconductor layer to CdI_2 type structure [19], or PbI_2 with a primitive cell Hexagonal (a = 0.3648 nm, c = 0.5899 nm) [20, 13]. It is composed of tin atoms sheets sandwiched between two sheets clamped sulfur atoms [19].

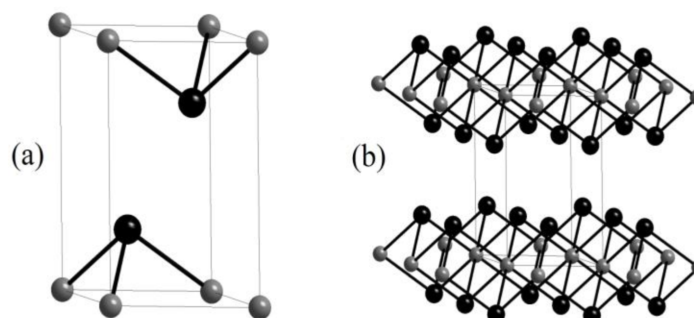

Fig.I.4: *CdI_2-type crystal structure of SnS_2, (a) trigonal unit cell, (b) and layered structure (dark spheres represent S and light spheres represent Sn) [3].*

It can also be in the trigonal structure [7], but in very rare cases.

Sn_2S_3 naturally occurs as a mineral named ottemanite. It exists in four polymorphs, α, β, γ, and δ- Sn_2S_3, as shown in the phase diagram in figure.I.5 [21].Sn-NMR studies reveal that it is the only mixed valence compound in the Sn-S system, consisting of a mixture of Sn(II) and Sn(IV) ions[22]. It usually forms needle shaped crystals and exhibits an orthorhombic structure in space group *Pnma* with a = 8.878 Å, b = 3.751 Å and c = 14.020 Å [23, 24]. The structure consists of Sn (IV) ions that occupy chain-center positions with octahedral symmetry, thus forming infinite double strings of SnS_6 octahedra parallel to the c-axis. Sn (II) atoms are attached laterally, occupying chain-end positions possessing trigonal pyramidal symmetry [25].

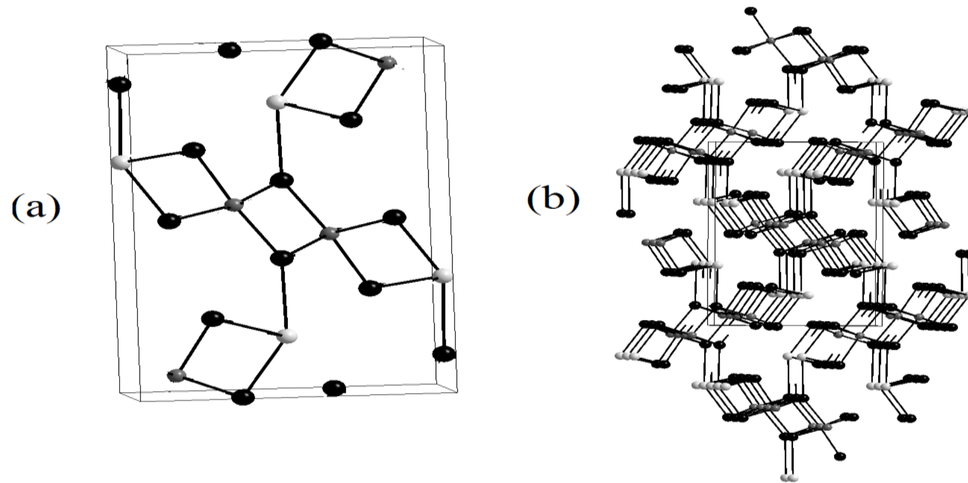

***Fig.I.5**: Orthorhombic crystal structure of Sn_2S_3, (a) unit cell, and (b) chain structure. (Black spheres represent S, dark grey spheres represent Sn (IV) and light spheres represent Sn (II)) [3].*

The crystal structure and physical properties of tin sulfide thin films are sensitive to the method and the deposition conditions.

The XRD diffraction spectra recorded in films prepared by spray pyrolysis with various substrate temperature and solution flow rate shown in following figure.

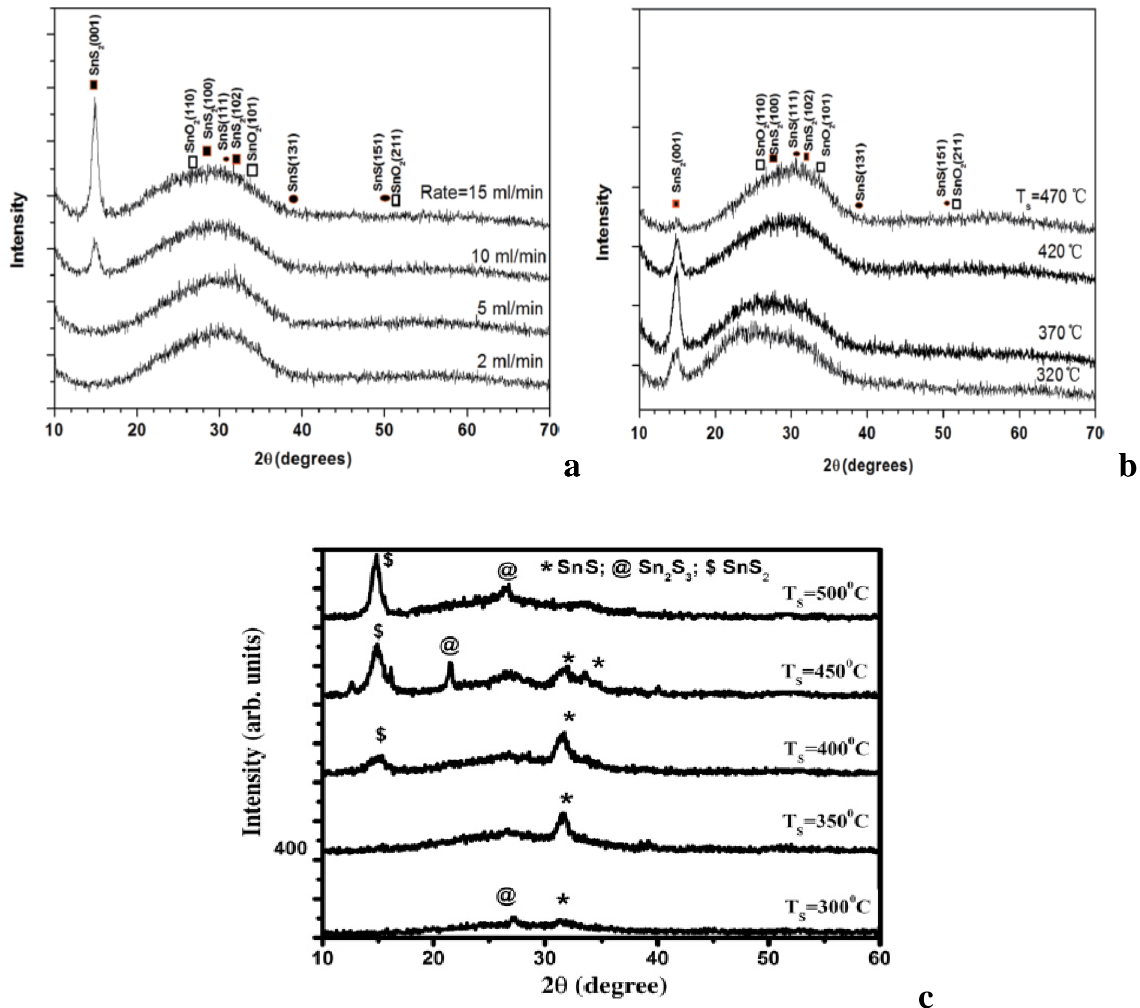

***Fig.I.6**:X-ray diffraction patterns of Sn_xS_y thin films prepared by :a) various solution rates, b)various substrate temperatures T_S=320°C,370 °C, 420 °C and 470 °C [26],c) substrate temperatures T_S=300°C,350 °C, 400 °C, 450 °C and 500 °C [11].*

Figure.I.6 shows the XRD patterns of the deposited Sn_xS_y films with different spray rates and various substrate temperatures. The XRD patterns of thin films prepared with spray rates of 2 and 5 mL/min display an amorphous structure and thin films prepared by solution rates of 10 and 15 mL/min display a polycrystalline structure corresponding to SnS_2 and SnO_2 phases [26]. The XRD patterns of films prepared with various substrate temperatures indicates that T_s = 370°C is the best substrate temperature for the highest structural order. Increasing the substrate temperature higher than 370 °C would lead to the scope of sulfur from the lattice and, finally, the formation of an amorphous structure. As can be seen, the temperature range of 320–370 °C corresponds to the highest domination of the SnS_2 phase. When T_s increases to 420 °C, the peak corresponding to SnS_2 disappears [26]. But in the last spectra when T_S was in the range 300 °C to 400 °C, all the films were

uniform, free of pinholes and crack. Their films had predominant SnS phase, crystallized in herzenbergate orthorhombic structure [11].

In the table.I.6 we have summarized the structure, grain size and preferred orientation reported in the literature for tin sulfide deposited by different deposition techniques. From this table note that the hexagonal structure of tin sulfide is the most stable and the most observed when compared by orthorhombic structure but the zinc blende rarely observed. Many studies have confirmed the influence of factors on the crystal structure of tin sulfide films deposited by spray pyrolysis technique. Among which we mention: the substrate temperature, deposition time, the nature and concentrations of source solutions, pH, and the type of substrate and flow rate.

Tab.I.6: *Structure, preferred grain size and orientation of thin films of SnS prepared by different techniques*

Technique	Parameters studied	Structure	D(nm)	(hkl)	Phase	Ref
Chemical bath deposition CBD	Deposition time	Orthorombic	23 nm	(1 1 0)	SnS	[27]
	The ammonia content in the reaction bath	Hexagonal	25-40 nm	(001)	SnS_2	[28]
	Copper doped concentrations y= [Cu]/[Sn]	zinc blend (ZB)	43- 53 nm	(111)	SnS	[29]
co-evaporation	Substrate temperature: 80–325°C	hexagonal+ orthorhombic	/	(001)+(130)+ (111)	SnS_2+ Sn_2S_3+ SnS	[30]
plasma-enhanced chemical vapor deposition (PECVD)	Different substrates: - Soda-lime glass - Silicon slices - FTO coated glass	Hexagonal	-25.8 nm. -21.6 nm. -16.2 nm.	(001)	SnS_2	[31]
spray pyrolysis	Substrate temperature: 348 K- 423 K	- hexagonal +orthorhombic	-35nm -53 nm -71 nm	(002) (104) (100)	SnS_2+ Sn_2S_3	[32]
	Substrate temperature: 300–350°C	Orthorhombic	-200–250 nm	(111)	SnS	[33]
	Substrate temperature: 320–488 °C	Orthorhombic + hexagonal	-14.6 nm	(111),(001), (002),(211), (110)	SnS+ SnS_2+ Sn_2S_3+ SnO_2	[34]
	Substrate temperature: 300°C-500°C	Orthorhombic+ hexagonal	-10nm	(111)	SnS+ Sn_2S_3 SnS_2	[11]
Dip coating	150–300 °C	Hexagonal	14 nm	(001)	SnS_2	[10]
Dip technique	Temperature 200°C-360°C	hexagonal+ orthorhombic	1 µm.	(001)+(040)	SnS_2+ SnS	[13]

M.Calixto-Rodriguez [34], et al prepared films SnS by the spray pyrolysis technique on glass substrates at temperature between 320–488 °C. The films deposited at T_s between 320 and 455 °C show one peak located at 2θ=31.54° which corresponds to the preferential orientation (111) of the SnS phase with orthorhombic structure. While thin films deposited at T_s between 376 and 396 °C show better recrystallization for the SnS phase and two small peaks corresponds SnS_2 and Sn_2S_3.However, when T_s is increased up to 488°C the peak corresponding to the SnS_2 disappears, and the material is almost completely converted to SnO_2. It is to explain the emergence of SnO_2 by considering the carrier gas employed, as the oxygen from air oxidize the tin of the solution prior to react with sulfur, due to the higher energies involved in the process [34]. On the other hand, the presence of the phase SnO_2 at high temperature is due to the vaporization of sulfur since it is known as a very volatile element that is why the oxygen replaces. This has been confirmed by several authors [35-37].

According to our literature review, the hexagonal structure of SnS_2 phase can be stable only to smaller crystallite sizes [1, 10], however the structure of orthorhombic which corresponding SnS and Sn_2S_3phase is observed for larger sizes [33]. (See table .I.7)

Furthermore the nature of the precursor source of tin (Sn) can be decisive for the film structure. Table.I.7 relates to the nature of the source of Sn solution and the types of crystal structures obtained for tin sulfide films deposited by spray pyrolysis.

***Tab. I.7**: Influence of source nature and substrate temperature on the crystal structure of tin sulfide.*

Source of Sn	T (°C)	Structure	Ref
$SnCl_2.2H_2O$	300-500°C	Orthorhombic + hexagonal	[11]
	200°C -300 °C	Orthorhombic	[38]
	300–375 °C	Orthorhombic	[39]
	300–350 °C	Orthorhombic	[33]
	350°C	Hexagonal + Orthorhombic	[1]
	27 °C	Hexagonal	[40]
$SnCl_4.5H_2O$	280 °C	Hexagonal	[41]
	70 °C	Hexagonal	[42]
	250-500 °C	Hexagonal	[31]
	150–300 °C	Hexagonal	[10]
	180 °C	Hexagonal	[43]
	60 °C -180°C	Hexagonal	[44]
	350°C	Hexagonal	[1]

Thorough the table can be note that the hexagonal structure is observed when using $SnCl_4.5H_2O$ but when using $SnCl_2.2H_2O$ the hexagonal and orthorhombic structure are appeared.

I.3.2.4. Optical properties

The study of the optical properties of tin sulfide layer is very important for the reason that of its use as an absorber layer in solar cells.Transmittance, the absorbance, reflectance and studies of photoluminescence.

I.3.2.4. a. Transmittance

The tin sulfide films have low optical transparency which allows using them as layers absorbent in photovoltaic cells. In general, the transmittance is a function of the deposition parameters such as thickness, the gap, and the crystal structure of the film. In figure.I.7 we reported typical spectra transmittance of SnS film deposited by CBD technique. The films have a little transmittance in the visible region of the solar spectrum 400 to 800 nm and they characterized by absence of the interference fringes in their transmittance spectra. This indicates that the tin sulfide films have rough surfaces [27].

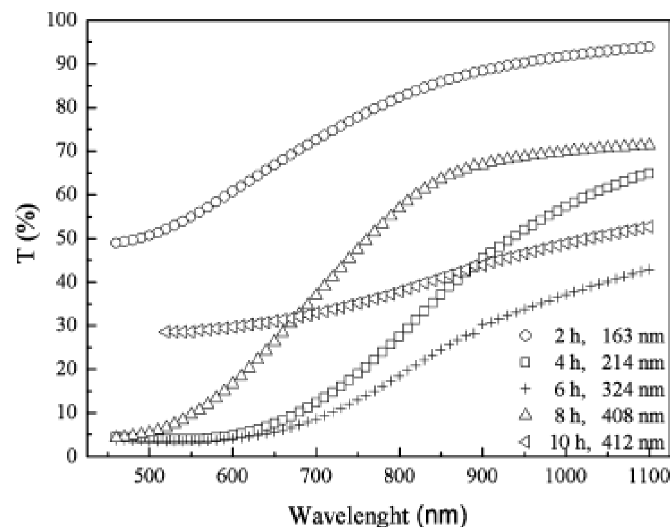

Fig.I.7: *Optical absorption spectra of SnS thin films deposited by CBD with different deposition time [27].*

Tin sulfide SnS is a potential candidate for the thin film solar cells, because the theoretical photovoltaic conversion efficiency of tin sulfide SnS solar cells can reach 25%. [45] Which allows the use as absorbent in photovoltaic cells [17]. In addition, there are

many advantages of tin sulfide SnS for photovoltaic applications such as the gap (1.30 eV), which can approach the optimum for the conversion of solar energy (1.50 eV) [15]. Transitions are direct with high absorption coefficients, which allow the use in thin layers and as an absorber in solar devices [17]. The large absorption coefficient (> 10^4 cm^{-1}). Refractive index 3.5.

The gap Eg values of SnS determined by research results of various researchers by variety of methods are given in the table.I.8.

Tab.I.8: *The optical band gap of SnS material by different techniques*

Technique	Cathodic electrodeposition	Spray	CBD	Thermal evaporation	Pulsed electrodeposition	co-evaporation
Eg (eV)	1.15 [46]	1.30-140 [38]	1.75 - 1.15 [15]	2.15 – 2.30 [45]	1.46 – 2 [47]	1.75 [30]

Tin disulfide SnS_2 is very interesting properties related to optical absorption in the visible region [48]. It has a large absorption coefficient in the visible region (> 10^4 cm^{-1}) [49], and a band gap that varies in the range 0.8-2.88 eV [41], and a strong performance for the photoconductivity. These properties indicate that this is a good material for solar cells as an absorber or a window material and also for applications optoelectronic devices.

Figure.I.8 shows the transmittance spectra of SnS_2 thin films prepared by spray pyrolysis technique at different substrate temperatures.

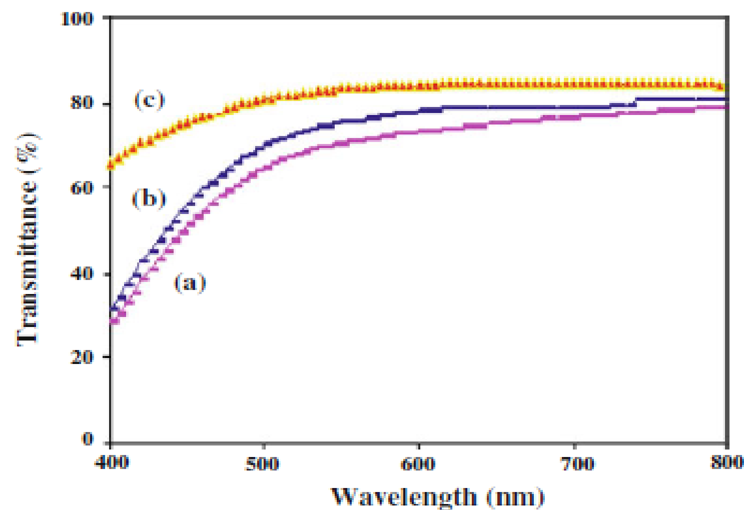

Fig.I.8: *Transmittance spectra for SnS_2 thin film prepared at a 373 K b 398 K and c 423 K [32] .*

The optical band gap Eg values of SnS_2 and Sn_2S_3 deposited by various methods is tabulated in the table.I.9.

Tab. I.9: *The optical band gap of SnS_2 and Sn_2S_3 material by different techniques.*

Technique	SILAR	Dip coating	Spray pyrolysis	PECVD	CBD	Co-evaporation
Eg (eV)	2.6 eV [12]	3.25 eV [10]	2.80 - 2.65 eV [32] 2.87 eV [13] 1.99-2.38 eV [34] 2 eV [50]	2.68-2.95 eV [31]	3.3 -3.7 eV [28] 2.12-2.03 eV[51]	2.1-2.3 eV [30]

I.3.2.5. Electrical properties

Tin sulfide (SnS) attracted much attention in recent years also for these electrical properties. Full study was interested in the study of electrical properties of this material in order to optimize.

The electrical resistivity of SnS films (for orthorhombic structure and without annealing) in the dark is normally in the range of 10^5 to 10^6 Ωcm. And the electrical resistivity of SnS films zinc blend (without annealing) in the dark is measured what is around 1.7×10^7 Ωcm [1]. It is normally accepted that too high electrical resistivity is not beneficial for the application in solar cells. But there are methods developed thin films that have proven they can prepare films of SnS with a resistivity in the dark as low as studying the theory, as the deposition technique to study chemical bath by Gao Chao, Honglie Shen and Sun Lei who proved that the resistivity of SnS in the dark can be as low as 10^2-10^3 Ωcm. And this can be particularly useful for the preparation of the solar cells at low cost using SnS as light absorption layer. In addition, the SnS has both p and n type conduction [24].The following table.I.10 includes electrical properties of tin sulfide and that following method of preparation:

Tab.I.10*: Electrical properties of SnS material.*

Growth technique	Type	Carrier density (cm^{-3})	Mobility ($cm^2V^{-1}S^{-1}$)	Resistivity (Ωcm)	Activation energy (eV)	Ref.
CBD	P	-	8.99×10^5	2.53×10^5	0.527	[52]
Electron-beam evaporation	-	10^{17}	1.2	51	-	[53]
Spray	P	1.6×10^{15}	130	37 – 25	0.46	[35]

Compared with the SnS, the SnS_2 has the opportunity to represent both p-type and n-type conduction [41]. But under certain conditions it represents an electrical conductivity

of n-type, with magnitude, and on preparation technique. These two characteristics make this compound suitable for the role of a window material in the structure of heterojunction. From different searches the value of the electrical resistivity was evaluated as shown in table.I.11:

Tab.I.11: *Electrical resistivity of the material SnS_2.*

Method	Substrate temperature	Resistivity (Ωcm)	Ref
Spray pyrolysis	348-423 k	1.48-0.55	[32]
	340 -380°C	10^5–10^7	[54]
SILAR	350–470 K	10^3	[12]
Close-spaced vacuum sublimation (CSS)	473-723 K.	10^4 - 10^7	[55]

For the activation energy E_a of this material studies we prove that varies from 0.25 to 1.52 eV [49]. Sn_2S_3 has also been reported as an intrinsic n-type material [50] with activation energy of about 0.15 eV [56]. The value of the electrical conductivity was evaluated as shown in table.I.12:

Tab. I.12: *Electrical Properties for the Sn_2S_3.*

Method	Conductivity (Ω cm^{-1})	Carrier concentration (cm^{-3})
spray pyrolysis	4.35 -10^{-3} ~67	9.4 -10^{14} [50] ~10^{15} [35]
plasma-enhanced chemical vapour deposition (PECVD)	2.5x10^{-5} [56]	-

I.4.System Sn-S

The appearance of the gaseous phase for high sulfide concentration makes difficult the explanation of the phase equilibrium in the system Sn-S. The T-x projection of the p-T-x phase diagram of Sn-S is shown in figure. I.9. In the system Sn-S was revealed two compounds: SnS and SnS_2, which melt congruently. During the study of elasticity of SnS vapor, it was established that the melting point of SnS in a neutral atmosphere is 1153 ÷ 5 K, and the boiling point at normal air pressure is 1503 K. The maximum melting point (1154 ± 2 K) for SnS was found for sulphur pressure 3.34 × 10^3 Pa, and for SnS_2 (1143 K) for sulphur pressure of 4 × 10^6 Pa.

In the temperature interval 858 ÷ 875 K for SnS one observes an effect that corresponds to

the polymorphous transformation. The studies of the phase transformations of the SnS crystals in the temperature range 295 ÷ 1000 K by XRD and neutron diffraction , have shown that these crystals exhibit a structural transitions from low temperature α-phase (*B16* spatial group *Pbnm*) to high temperature β-phase with type II lattice (*B33*, spatial group *Cmcm*). The transition α→β is a second order transition of the displacement type. The transition is produced by the continuous shift of the Sn and S atoms along the axis [100]. The transition is related to the soft modes on the boundary of the brillouin zone of the β-phase. SnS_2, known as “plated gold”, are golden-yellow platelets or scaly crystals shiny and very soft. As reported in, the dependence of the dissociation pressure of SnS_2 on the temperature is expressed by the equation [57]:

$$\text{Lg } p \text{ (Torr)} = [(4736+200)/T] + 6.88 \pm 0.15 \quad (I.1)$$

SnS_2 is stable at room temperature in air, does not dissolve in water, decomposes in the royal water with the formation of tin chloride and release of sulphur, and, also, dissolves in sulphur solutions of the alkali metals and ammonium sulphate. By heating in air, SnS_2 completely transforms into SnO_2. Several researchers supposed the formation of Sn_2S_3 and Sn_3S_4 by peritectical reaction [57].

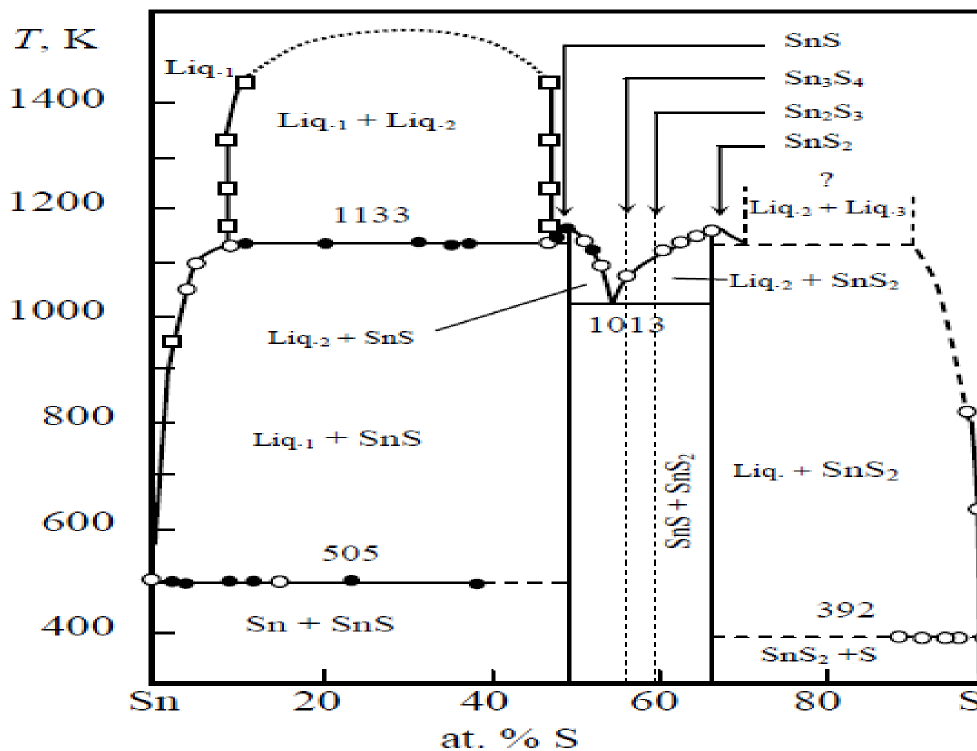

Fig.I.9: *The phase diagram of the system Sn-S [57].*

I.5. Enthalpies of formation

Enthalpies of formation are key to understanding the relative stabilities of a multiphasic system as they indicate which conformation the system would preferentially adopt. Indeed, simple thermodynamic arguments have been shown to play a fundamental role in the design, optimization, and performance of solar cell devices due to, issues associated with phase mixing and separation across interfaces [58].

We define the enthalpies according to the reaction:

$$x\ Sn(s) + yS(s) \rightarrow Sn_xS_y \qquad (I.2)$$

The enthalpies of formation for tin sulfide shown in table .I.13.

Tab.I.13: *Enthalpies of formation for tin sulfide [58]*

phase	space group	ΔH_f^{DFT} (in eV and kJ mol^{-1})		ΔH_f^{exp} (kJ mol^{-1})
SnS	*Pnma*	−1.03	−99.35	−100 to −108
SnS	*Fm$\bar{3}$m*	−0.95	−91.66	
SnS	*F$\bar{4}$3m*	−0.29	−27.80	
SnS_2	*P$\bar{3}$m1*	−1.36	−130.99	−148 to −182
Sn_2S_3	*Pnma*	−2.39	−230.35	−249 to −297

I.6. Applications of tin sulfide thin films

In recent years, much attention has been focused on tin sulfide (SnS) because of its potential use in the fabrication of various applications such as holographic recording systems, solar collectors and solar photovoltaic cells since its constituent elements are inexpensive, environmentally-friendly and easily available in nature whereas SnS_2 having a wide energy band gap is more suitable for photoconductive and photoelectrochemical cells and can be used as window layers, n-p heterojunction of n-SnS_2/p-SnS quantum well structures and the substrate for deposition of organic layers.

I.6.1. Photovoltaic applications

SnS came into limelight as a candidate mainly for the development of solar cell devices due to its narrow band gap and high absorption. In this direction, variety photovoltaic devices have been realized by using p-SnS films as absorber layer and other n-type materials as window layers.

Noguchi et al. prepared SnS films-based photovoltaic (PV) devices with the configuration of n-CdS/p-SnS on indium doped tin oxide (ITO) substrate with Ag as Ohmic contacts. All the layers were developed using thermal evaporation method, and the schematic diagram of the device is shown in figure.I.10 [59]. Under dark, the as-deposited devices exhibit a high diode quality factor of 3.5 and saturation current density of 2.83×10^{-4}A cm^{-2}.

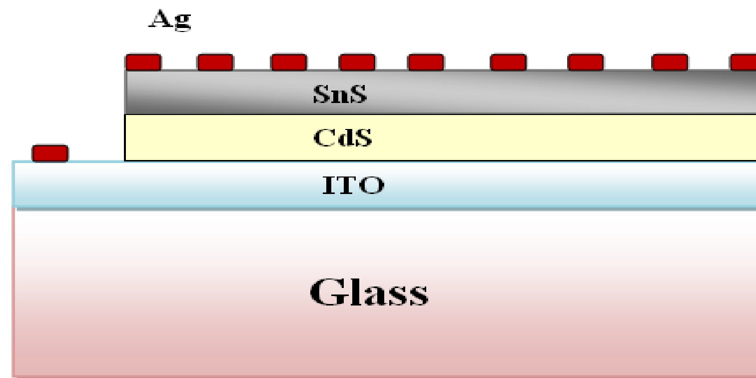

Fig.I.10: *Schematic diagram of SnS based solar cell.*

Miyawaki et al. developed ZnS/SnS solar cell devices by depositing ZnS films on 0.6 mm thick p-type SnS thin films using photochemical and electrochemical deposition methods, respectively [60]. The as-deposited device showed good rectifying behavior and under 100 mW cm^{-2} light these structures exhibited I_{sc} and Voc as 0.95 mA cm^{-2} and 135 mV, respectively.

Masaya Ichimura et al have fabricated ZnO/SnS heterostructures. Figure.I.11 shows the structure of the cell fabricated. SnS was deposited first on the ITO substrate, and then ZnO was deposited. Indium electrode was fabricated by vacuum evaporation [61].

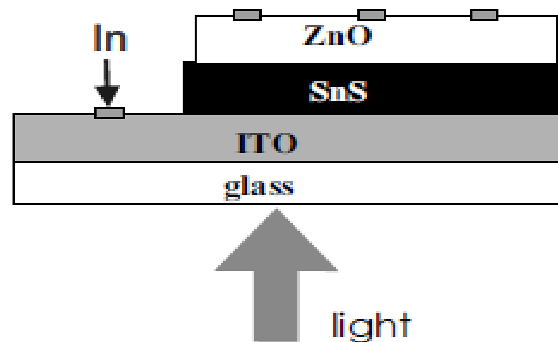

Fig.I.11: *Solar cell structure [61].*

Sanchez-Juarez et al. have fabricated SnS_2/SnS heterojunction thin film diodes by plasma-enhanced chemical vapor deposition (PECVD) .Using SnS_2 as a window material and SnS as absorber material [62] (Figure.I.12).

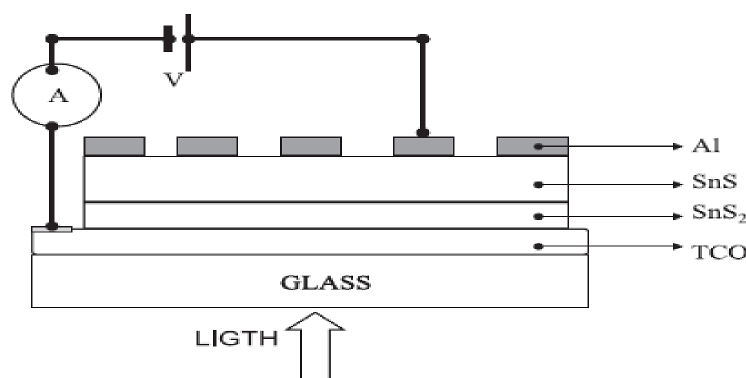

***Fig.I.12**: Schematic diagram of the structure for the fabricated diodes [62].*

I.6.2.Other Applications

Tin sulfide has also received good attention in different fields including photoelectrochemical cells, lithium-ion batteries, infra-red detectors, etc.

SnS_2 is an attractive material as an alternative of carbon anode for Li ion batteries. As anode materials of rechargeable Li-ion batteries, SnS_2 exhibited good electrochemical properties, which revealed a higher reversible capacity about 502 m Ahg^{-1} and stable cyclic retention at 50th cycle [63].

I.7. Thin film deposition techniques

Generally any thin film deposition follows the sequential steps: a source material is converted into the vapor form (atomic/molecular/ionic species) from the condensed phase (solid or liquid), which is transported to the substrate and then it is allowed to condense on the substrate surface to form the solid film [64]. Depending on how the atoms/molecules/ions/clusters of species are created for the condensation process, the deposition techniques are broadly classified into two categories: physical methods and chemical methods. The methods summarized in figure.I.13.

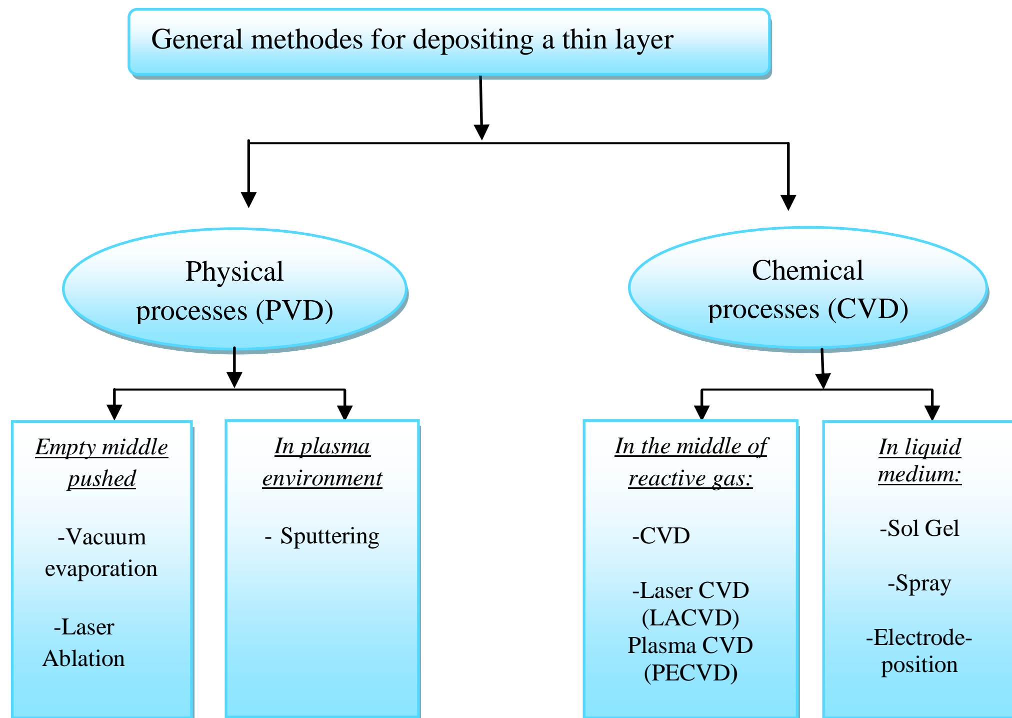

Fig.I.13: *Presentation of the main deposition methods of thin films.*

SnS thin films have been prepared by using various chemical and physical methods such as pulse electrodeposition , spray pyrolysis, rf sputtering, vacuum evaporation, chemical vapour deposition,chemical bath deposition (CBD), cathodic electrodeposition electrochemical deposition, thermal evaporation, hydrothermal method, solvothermal method, SILAR method, electrodeposition method dip techniques, and physical vapour deposition (PVD).

I.7.1. Physical vapor deposition

The PVD processes include mainly resistive heating, flash evaporation, electron beam heating, laser heating, arc evaporation, sputtering, etc. In the realization of a layer can be distinguished the following three steps:

- The creation of or the species to be deposited, in the form of atoms, molecules or clusters (groups of atoms or molecules).
- Transport of these species vapor from the source to the substrate.
- Deposit on the substrate and growth layer.

The methods, which were used for the deposition of SnS films, are briefly described below.

I.7.1.1.Sputtering

Sputtering is one of the most versatile techniques used for the deposition of thin film when device quality films are required. Sputtering process produces films with better controlled composition, provides films with greater adhesion and homogeneity and permits better control of film thickness. The sputtering process involves the creation of gas plasma usually an inert gas such as argon by applying voltage between a cathode and anode. The target holder is used as cathode and the anode is the substrate holder. Source material is subjected to intense bombardment by ions. By momentum transfer, particles are ejected from the surface of the cathode and they diffuse away from it, depositing a thin film onto a substrate. Sputtering is normally performed at a pressure of 10^{-2} –10^{-3} Torr.

Usually there are two modes of powering the sputtering system; DC and RF biasing. In DC sputtering system a direct voltage is applied between the cathode and the anode. This method is restricted for conducting materials only. RF sputtering is suitable for both conducting and non-conducting materials; a high frequency generator (13.56 MHz) is connected between the electrodes of the system. Magnetron sputtering is a process in which the sputtering source uses magnetic field at the sputtering target surface.

Magnetron sputtering is particularly useful when high deposition rates and low substrate temperatures are required [64].

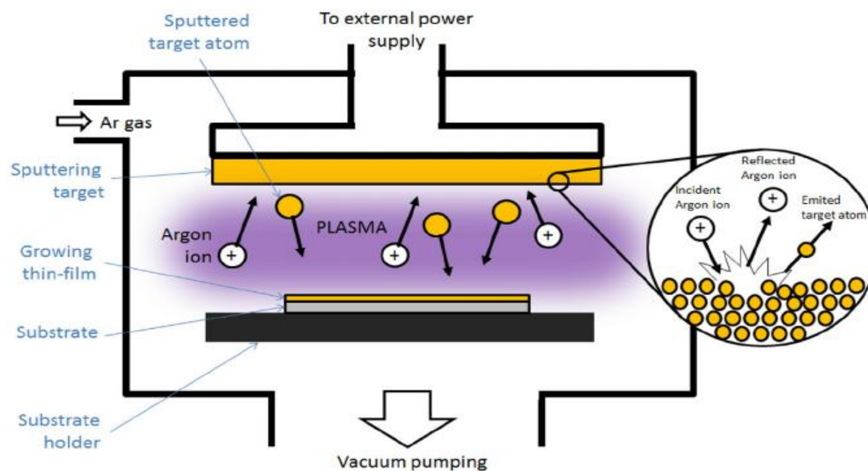

***Fig.I.14**: Schematics of the sputtering process [65].*

SnS films have been obtained on glass substrates using RF-sputtering by others studies [66, 67].

I.7.1.2.Molecular Beam Epitaxy (MBE)

The BME is a technique which makes it possible to create single-crystal deposits. This technique was developed for the semiconductors growth (Si, GaAs, CdTe, ZnSe...) because it makes it possible to carry out homo-epitaxies (material A on support A) with low temperature (400-600°C for Si). Thus one eliminates diffusion problems of the doping agents for example. Moreover, low temperatures of epitaxy imply to work with slow speeds (qq. A°/s) in order to leave time to the atoms sometimes happen at surface to migrate by diffusion of surface towards crystallographic sites. In order to obtain pure films, taking account into these slow speeds, thus it is necessary to work with very thorough vacuums, called UHV (Ultra High-Vacuum). The principle of the deposits is very simple: it is enough to evaporate the material which one wants to deposit by heating it by effect joule or by electronic bombardment (gun with electrons). Moreover, under UHV, the mean free path traversed by an atom is very large what implies that flows of evaporated atoms are directional, atoms moving in straight line without any shock before settling on the substrate. For this reason one speak about molecular or atomic jets. This technique also makes it possible to make hereto- epitaxies (deposit of B on a different support A), taking account into the low temperatures of epitaxy which eliminates the mechanism from inter-diffusion of A and B [68]. Epitaxial grown SnS films have been obtained by MBE technique by several studies [69].

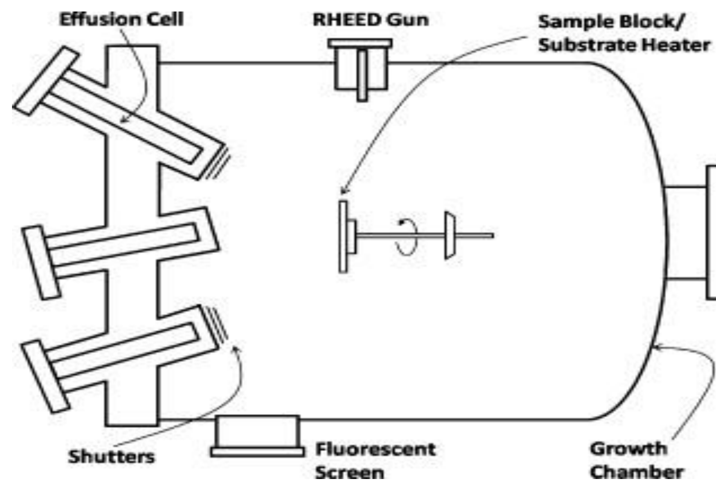

Fig.I.15: *Schematic diagram of the molecular beam epitaxy apparatus [70].*

I.7.1.3. Thermal evaporation

Thermal evaporation techniques (resistive-, electron beam-, and flash- evaporation are the simplest techniques as compared to all other physical vapor deposition (PVD) techniques. This technique basically involves on the transformation of source material into vapor, transport of this vapor onto the substrate surface and finally condensation of the vapor on the substrate to form the thin film.

I.7.1.3. a. Thermal evaporation by resistive heating

Thermal evaporation is the most widely used technique for the preparation of thin films of metals, alloys, and also many compounds, as it is very simple and convenient. Here the only requirement is to have a vacuum environment in which sufficient amount of heat is given to the evaporants to attain the vapor pressure necessary for the evaporation. The evaporated material is allowed to condense on a substrate kept at a suitable temperature. When evaporation is made in vacuum, the evaporation temperature will be considerably lowered and the formation of the oxides and incorporation of impurities in the growing layer will be reduced. Evaporation is normally done at a pressure of 10^{-5} Torr. At this pressure a straight line path for most of the emitted vapor atoms is ensured for a substrate to source distance of nearly 10 to 50 cm. The characteristics and quality of the deposited film will depend on the substrate temperature, rate of deposition, ambient pressure, etc. and the uniformity of the film depends on the geometry of the evaporation source and its distance from the source. The deposition by thermal evaporation is simple, convenient and is widely use [64]. High quality SnS films have been obtained by resistive evaporation [59, 71, 72].

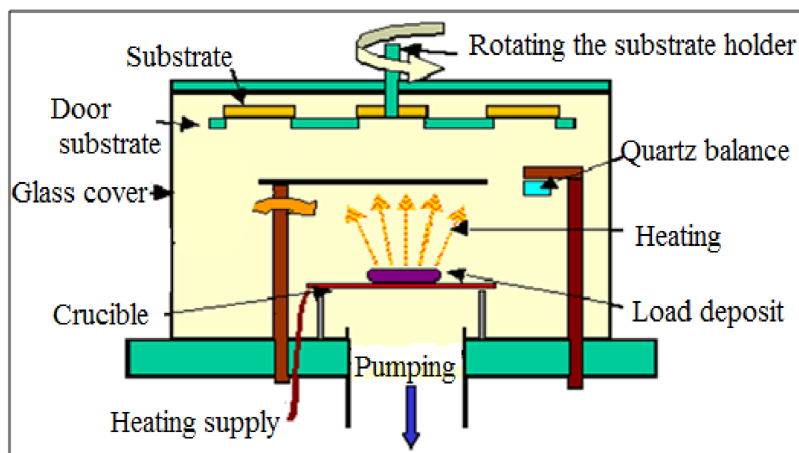

Fig I.16: Schematic of Thermal evaporation by resistive heating.

I.7.1.3. b. Electron-Beam (e-Beam) Evaporation

In electron beam evaporation (EBE) a stream of electrons is accelerated through fields of typically 5–10kV and focused onto the surface of the material for evaporation. The electrons lose their energy very rapidly upon striking the surface and the material melts at the surface and evaporates. That is, the surface is directly heated by impinging electrons, in contrast to conventional heating modes. Direct heating allows the evaporation of materials from water-cooled crucibles. Such water-cooled crucibles are necessary for evaporating reactive and in particular reactive refractory materials to avoid almost completely the reactions with crucible walls. This allows the preparation of high purity films because crucible materials or their reaction products are practically excluded from evaporation. Electron beam guns can be classified into thermionic and plasma electron categories. In the former type the electrons are generated thermionically from heated refractory metal filaments, rods or disks. In the latter type, the electron beams are extracted from plasma confined in a small space [64].

Fig I.17: *Schematic diagram of e-Beam evaporation [73]*

I.7.2.Chemical Vapor Deposition (CVD)

A deposition technique, in which chemical components react on the surface of the substrate to form a solid film, is called chemical deposition technique [74].

I.7.2.1.Plasma enhanced CVD (PECV)

Plasma-enhanced chemical vapor deposition (PECVD) is a process used to deposit thin films from a gas state (vapor) to a solid state on a substrate. Chemical reactions are involved in the process, which occur after creation of plasma of the reacting gases. The plasma is generally created by RF (AC) frequency or DC discharge between two electrodes, the space between which is filled with the reacting gases. Good quality SnS and SnS_2 films have been achieved by PECVD [75, 76].

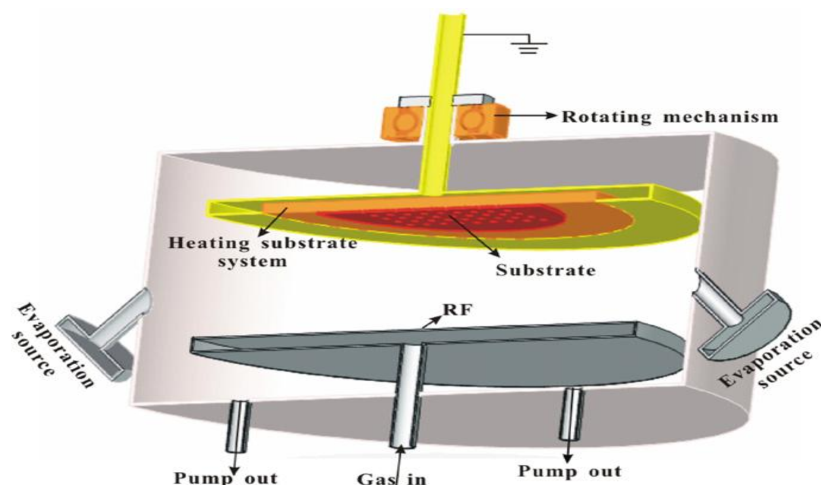

Fig.I.18: *A schematic of the modified PECVD system [76].*

I.7.2.2.Atmospheric Pressure CVD (APCVD)

Is one of the modifications of the conventional CVD process. In the PACVD system, electric power is supplied to the reactor to generate the plasma. The power is supplied by an induction coil from outside of the chamber, or directly by diode glow-discharge electrodes. Usually the working pressure is in the range of 10 to 100 Pa. In the plasma, the degree of ionization is typically only 10^{-4}, so the gas in the reactor consists mostly of neutrals. Ions and electrons travel through the neutrals and get energy from the electric field in the plasma. The average electron energy is 2 to 8 eV, which corresponds to electron temperatures of 23,000 to 92,800 K. In contrast, the heavy, much more immobile, ions cannot effectively get enough coupling energy from the electric field. The ions in the plasma show slightly higher energy than the neutral gas molecules at room temperature. Typically the temperature of the ions in plasma is around 500 K. A APCVD system is schematically presented in figure.I.19. Good quality SnS films were obtained using APCVD technique [77- 81].

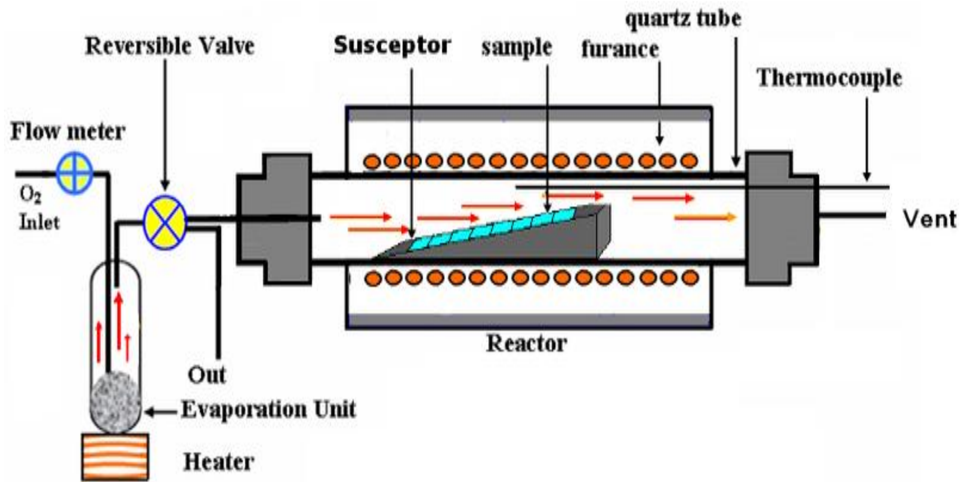

Fig.I.19: *Schematic diagram of APCVD system [82].*

I.7.2.3.Chemical Bath Deposition (CBD)

The chemical bath deposition (CBD) refers to deposit films on a solid substrate by a reaction produced in an aqueous solution. The chemical bath deposition can occur in two ways according to the deposition mechanism: by homogeneous nucleation in solution or on a substrate hétéronucléation. In heterogeneous nucleation, the particles, or even individual ions can adsorb on the substrate. The energy required forming an interface between the particles and the solid substrate is often less than that required for homogeneous nucleation. Heterogeneous nucleation is therefore preferred to homogeneous nucleation energy [83]. SnS films have been prepared by chemical bath deposition [17, 84, 85].

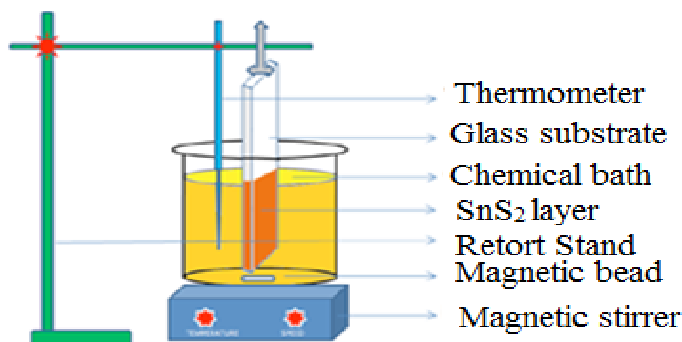

Fig.I.20: *Experimental device used for the preparation of thin layers by CBD [28].*

I.7.2.4. Electrochemical deposition (ECD)

Electrodeposition, also known as electrochemical deposition or electro crystallization, it is one of the most useful techniques for preparing thin films on the surface of conducting substrate.

Besides advantages such as low temperature, the electrodeposition is the simplest of the chemical methods, and it has many advantages like [86]:

- Toxic gaseous precursors need not to be used (unlike gas phase methods).
- Deposition on complex shapes is possible.
- Structurally and compositionally modulated alloys and compounds can be deposited which are not possible with other deposition techniques.
- In most of the cases the deposition can be carried out at room temperature enabling to form the semiconductor junctions without interdiffusion.
- The deposition process can be controlled more accurately and easily.

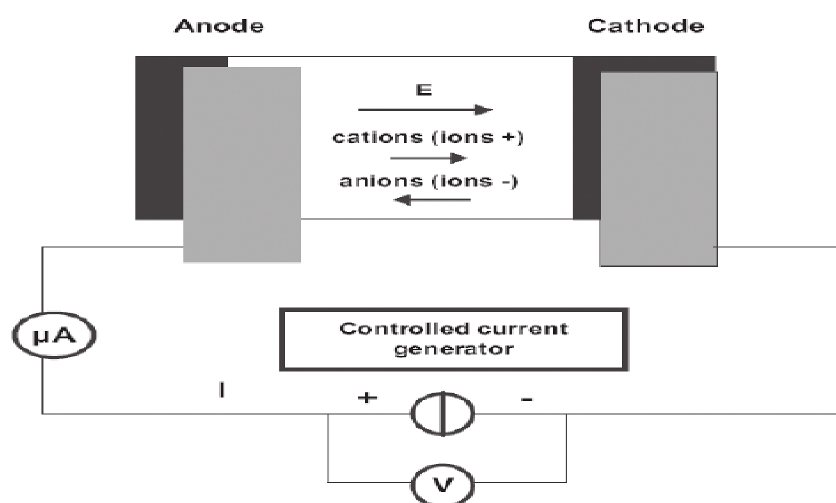

Fig.I.21: *General schematic diagram for electrodeposition process [87].*

I.7.2.5.Spray pyrolysis

The spray pyrolysis technique involves the spraying the solution, which contains the solvable salts of the constituent elements of the desired compound, onto a heated substrate. The sprayed droplet upon reaching the surface of hot-substrate undergoes pyrolytic decomposition and forms a single crystallite or a cluster of crystallites of the product. The volatile by products and the excess solvents escape in the vapor phase. Here, the heated substrate provides the thermal energy necessary for the decomposition and subsequent recombination of the constituent species. This is followed by sintering and recrystallization of the clusters of crystallites giving rise to continuous film. A spray system (Figure.I.22) consists of a spray head connected to two channels and substrate heater cum controller. The purified compressed air/nitrogen and solution are fed to the spray nozzle from opposite sides and are then sprayed onto hot-substrates kept at below the spray nozzle. The substrate temperature is controlled using a temperature controller.

SnS films have been obtained using spray pyrolysis technique by many researchers [11, 88, 89].

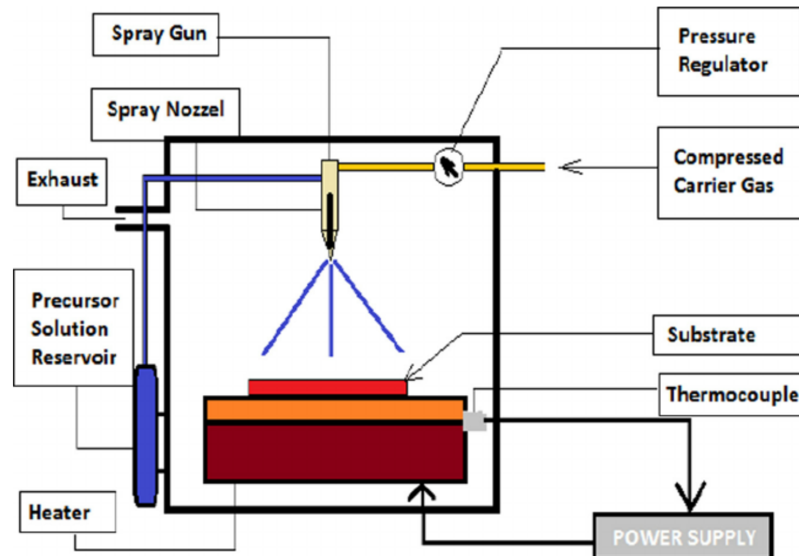

Fig.I.22: *Sketch diagram of spray pyrolysis system [90].*

The choice of this technique was motivated under many advantages:

- Large choice of precursors is possible, the compound must be soluble in a solvent, and the solution may be atomized.
- Ability to deposit a wide range of materials.
- Simple method of providing the precursor by means of a spray.
- High growth rate for mass transport of the precursor can be very high.
- Environment controllable reaction just under atmospheric pressure gas.
- Easy realization of such reactors.

One of major problems of this technique is the control of the evaporation of the generated spray. In fact, too fast or too slow evaporation causes a reaction of unwanted precursors affecting the properties of the deposit. In other words, if the drops reach the hot substrate before a complete evaporation, spray pyrolysis reaction takes place of the expected Spray CVD mechanism. According to the area where evaporation occurs, four different processes can take place, figure.I.23 illustrates the different possible configurations. These processes depend on the deposition temperature and diffusion of the precursors in this gradient.

Process I: The droplets of the aerosol directly projected onto the hot substrate. The solvent evaporates and the decomposition of the precursor takes place to give the product layer. For thick films, the process requires sequential deposition to obtain dense films (<1 micron). Obviously, this process takes time. In addition, when the film thickness increases, the layer tends to become porous and cracks can appear. This process corresponds to the principle of pyrolysis spray.

Process II: solvent is evaporated before reaching the hot substrate surface. The precursor reacts with the surface and decomposes or undergoes chemical reactions to form the layer of the desired material. It does not pass through the gas phase.

Process III: The solvent is evaporated during the approach of the substrate surface. Pass the precursor in the gas phase in the vicinity of the hot surface. The precursor vapor is adsorbed to the surface; diffuse then reacts to form the product by decomposition and / or following the chemical reactions. This mechanism is similar to the heterogeneous deposition of CVD processes. This method tends to produce dense film with excellent adhesion.

Process IV: If the deposition temperature is very high, the decomposition and / or chemical reactions take place in the vapor phase, leading to homogeneous nucleation (similar to a homogeneous reaction CVD). The formation of fine particles of product is carried out in gas phase. They are then deposited on the substrate. The film thus formed has a porous nature and very low adhesion to the substrate. The powder can be directly collected in the gas phase for the production of ultrafine particles [91].

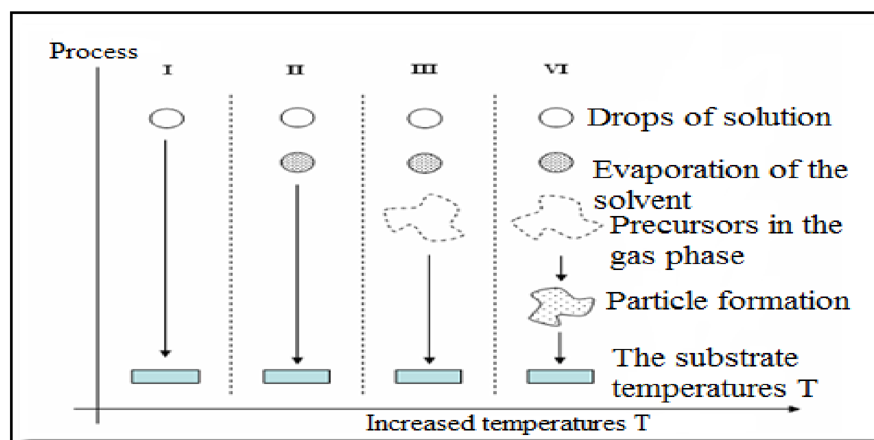

Fig .I.23*: Presentation of the different processes that may occur in Spray CVD as the deposition temperature [91].*

References of first chapter

[1] K. kamli, « Elaboration et caractérisations physico-chimique des couches minces de sulfure d'étain par spray ultrasonique: Effet des sources d'étain», Memory of magister, University of Med Khider-Biskra, (2013).

[2] S. Hariech, «Élaboration et caractérisation des films minceschalcogénures à base de cadmium et de cuivre pour desapplications photovoltaïques», doctorate thesis, University of Constantine 1, (2013)

[3] R. Kaur, «Non-hydrolytic Sol-gel Synthesis of Tin Sulfides», The Master of Science Degree in Chemistry, University of Toledo, (2014).

[4] T. Chattopadhyay, A. Werner, H. G. von Schnering, Revue Phys. Appl 19 (1984) 807-813.

[5] H. Wiedemeier, H. G. Von Schnering, Z. Krist 148 (1978) 295.

[6] R. W. G. Wyckoff, Crystal Structure (John Wiley) 1 (1963) 89.

[7] T. Kikegawa, H. Iwasaki, Acta Crystallogr B 39 (1983) 158.

[8] R. Herzenberg, Rev. Miner 4 (1932) 33.

[9] M. Calixto-Rodriguez, H. Martinez, A. Sanchez-Juarez, J. Campos-Alvarez, A. Tiburcio-Silver, M.E. Calixto, J.Thin Solid Films 517 (2009) 2497–2499.

[10] S.K. Panda, A. Antonakos, E. Liarokapis, S. Bhattacharya, S. Chaudhuri. J. Materials Research Bulletin 42 (2007) 576–583.

[11] T. H. Sajeesh, A.R. Warrier, C. Sudha Kartha, K.P. Vijayakumar, J.Thin Solid Films 518 (2010) 4370–4374.

[12] B.R .Sankapal, R.S. Mane, C.D. Lokhande, J. Res. Bull 35 (2000) 2027-2035.

[13] Sekhar C. Ray, Malay K. Karanjai, Dhruba DasGupta, J. Thin Solid Films 350 (1999) 72-78.

[14] L.A. Burton, D.Colombara, R.D. Abellon, F. C. Grozema, L.M. Peter, T.J. Savenije, G. Dennler, A. Walsh, J.Chem. Mater 25 (2013) 4908−4916.

[15] C.Gao, H. Shen, L. Sun, J.Applied Surface Science 257 (2011) 6750-6755.

[16] E.C. Greyson, J.E. Barton, T.W. Odom, J.Small 2 (2006) 368 – 371.

[17] A. Akkari, « Synthése et caractérisation physico-chimiques de couches minces de sulfure d'étain en vue de leur utilisation dans des dispositifs photovoltaïques », doctorate Thesis, University of Montpellier II, (2011).

[18] O. Madelung, *Semiconductors: Data handbook* (2004) 1981-1989 Springer.

[19] J. Yang, Q. Tian, Z. Chen, X. Xu, L. Zha, J. Materials Letters 67 (2012) 32–34.

[20] F. Tan, S. Qu, X. Zeng, C. Zhang, M. Shi, Z. Wang, L. Jin, Y. Bi, J. Cao, Z. Wang, Y. Hou, F. Teng, Z. Feng, J.Solid State Communications 150 (2010) 58–61.

[21] R. C .Sharma, Y. A .Chang, J. Bull. Alloy Phase Diagrams 7 (1986) 269-273,307-268.

[22] M. Cruz, J.Morales, J. P. Espinos, J. Sanz, J. Solid State Chem (2)175 (2003) 359-365.

[23] R. Kniep, D. Mootz, U .Severin, H .Wunderlich, J.Acta Crystallogr, Sect. B 38 (1982) 2022-2023.

[24] M. Cruz, J.Morales, J. P. Espinos, J.Sanz, J. Solid State Chem 175 (2003) 359-365.

[25] M. R. Fadavieslam, N. Shahtahmasebi, M. Rezaee-Roknabadi, M. M. Bagheri-Mohagheghi, J.Semiconductors 32(2011) 113002.

[26] D.Mootz, H.Puhl, J.Acta Crystallogr 23 (3) (1967) 471-476.

[27] E .Guneri, C.Ulutas, F.Kirmizigul, G. Altindemir, F. Gode, C. Gumus, J.Appl Surf Sci 257 (2010)1189–1195.

[28] K.T. Ramakrishna Reddy, G. Sreedevi, K. Ramya and R.W. Miles, J. Energy Procedia 15(2012) 340-346.

[29] A. Akkari, M. Reghima, C. Guasch, N. Kamoun-Turki, J. Mater Sci 47 (2012) 1365–1371.

[30] V. Robles, J. F. Trigo, C. Guillén, J. Herrero, J. Mater Sci 48 (2013) 3943–3949.

[31] S.Wang, S.Wang, J. Chen, P.Liu, M.Chen, H. Xiong, F.Guo, M. Liu, J.Nanopart Res 16 (2014) 2610.

[32] K. Vijayakumar, C. Sanjeeviraja, M. Jayachandran, L. Amalraj, J.Mater Sci: Mater Electron 22 (2011) 929–935.

[33] N. Koteswara Reddy, K.T. Ramakrishna Reddy, J.Thin Solid Films 325 (1998) 4–6.

[34] M.Calixto-Rodriguez, H.Martinez, A.Sanchez-Juarez, J.Campos-Alvarez, A. Tiburcio-Silver, M.E. Calixto, J.Thin Solid Films 517 (2009) 2497–2499.

[35] N. Koteeswara Reddy, K.T. Ramakrishna Reddy, J. Solid-State Electronics 49 (2005) 902–906.

[36] G.H. Yue, D.L. Peng, P.X. Yan, L.S. Wang, W. Wang, X.H. Luo, J.Alloys and Compounds 468 (2009) 254–257.

[37] N. Koteswara Reddy, K. T. Ramakrishna Reddy, G.Fisher, R.Best, P.K.Dutta, J. Phys. D: Appl. Phys 32(1999) 988–990.

[38] B.G. Jeyaprakash, R. Ashok kumar, K.Kesavan, A. Amalarani, J.American Science 6(3) (2010) 22-26.

[39] N. Koteeswara Reddy, K.T. Ramakrishna Reddy, J. Thin Solid Films 325 (1998) 4–6.

[40] N.G. Deshpande, A.A. Sagade, Y.G. Gudage, C.D. Lokhande, Ramphal Sharma, J. Alloys and Compounds 436 (2007) 421–426.

[41] C. Khélia, K. Boubaker, T. Ben Nasrallah, M. Amlouk, S. Belgacem, J.Alloys and Compounds 477 (2009) 461–467.

[42] M. Liu, J. Yang, Q.Qu, P. Zhu, W. Li, J.Power Sources 273 (2015) 848-856.

[43] J.Gajendiran, V **.**Rajendran**,** J.Adv. Nat. Sci:Nanosci. Nanotechnol 2 (2011) 015001.

[44] R. Wei, T. Zhou, J. Hu, J. Li, J.Materials Research Express 1 (2014) 025018.

[45] S. Cheng, G. Conibeer, J.Thin Solid Films 28887 (2011) 5.

[46] B. Subramanian, C. Sanjeeviraja, M. Jayachandran, J.Materials Chemistry and Physics 71 (2001) 40–46.

[47] P. LU, H. Jia, Y. Yang, S. Cheng, J.Semiconductor Photonics and Technology, 1007-0206 (2010) 04-0132-05.

[48] S.S. Hegde, A.G. Kunjomana, K. Ramesh, K.A. Chandrasekharan, M. Prashantha, International Journal of Soft Computing and Engineering (IJSCE) 1(2011) 2231-2307.

[49] L. Amalraj, C. Sanjeeviraja, M. Jayachandran, J. Crystal Growth 234 (2002) 683–689.

[50] M. Khadraoui, N. Benramdane, C. Mathieu, A. Bouzidi, R. Miloua, Z. Kebbab, K. Sahraoui, R. Desfeux , J.Solid State Communications 150 (2010) 297-300.

[51] E. Güneri, F. Göde, B. Boyarbay, C.Gümüş, J.Materials Research Bulletin 47(2012) 3738–3742.

[52] E.Guneri, F.Gode, C.Ulutas, F.Kirmizigul, G.Altindemir, C.Gumus, J.Chalcogenide Letters 7 (2010) 685-694.

[53] H.K. Park, J. Jo, H. K.Hong, G.Y. Song, J.Heo, J. Current Applied Physics 15 (2015) 964-969.

[54] M. Calixto-Rodríguez, A. Sánchez-Juárez, J. Superficies y Vacío 20 (2007) 34-38.

[55] A. Voznyi , V. Kosyak , A. Opanasyuk , N. Tirkusova , L. Grase , A. Medvids ,G. Mezinskis, J. Materials Chemistry and Physics 173 (2016) 1-10.

[56] Sanchez-Juarez. A, Ortiz. A, J.Semicond. Sci. Technol 17 (2002) 931.

[57] D. I. Bletskan, J. Ovonic Research 1 (2005) 61 – 69.

[58] Lee A. Burton and Aron Walsh, J. Phys. Chem 116 (2012)24262−24267.

[59] H. Noguchi, A. Setiyadi, H. Tanamura, T. Nagatomo, O. Omoto, J.Solar Ener. Mater. Solar Cells 35 (1994) 325–331.

[60] T. Miyawaki, M. Ichimura, J.Mater. Lett 61 (2007) 4683–4686.

[61] M. Ichimura, H. Takagi, Proceedings of ISES Solar World Congress Solar Energy and Human Settlement, (2007).

[62] A. Sanchez-Juarez, A. Tiburcio-Silver, A. Ortiz, J.Thin Solid Films 480 (2005) 452–456.

[63] S.Liu, X.Yin, L.Chen, Q. Li, T .Wang, J. Solid State Sci 12 (2010) 712–718.

[64] A.Aldrin, «Preparation and characterization of certain II-VI, I-III-VI_2 semiconductor thin films and transparent conducting oxides», PhD thesis, Cochin University of Science and Technology, Kerala, India, (2004).

[65] R. S. Pessoa, M. A. Fraga, L. V. Santos, N. K. A. M. Galvão, H. S. Maciel, M. Massi, In Anti-Abrasive Nanocoatings (2015) 455-479.

[66] W.Guang-Pu, Z.Zhi-Lin, Z. Wei-Ming, G. Xiang-Hong, C. Wei-Qun, H. Tanamura, M. Yamaguchi, H. Noguchi, T. Nagatomo,O. Omoto, IEEE First World Conference on Photovoltaic Energy Conversion, Hawaii (1994) 365.

[67] K. Hartman, J. L. Johnson, M. I. Bertoni, D. Recht, M. J. Aziz, M. A. Scarpulla, T. Buonassisi, J.Thin Solid Films 519 (2011) 7421–7424.

[68] Introduction to thin films and networks (Stéphane Andrieu). Franco-Romanian school: Magnetism of nanoscopic systems and hybrid structures - Brasov (2003).

[69] H. Nozaki, M. Onoda, M. Sekita, K. Kosuda, and T. Wada, J.Solid State Chem. 178, (2005) 245–252.

[70] G.M.Uddin, Z.Cai, K.S.Ziemer, A.Zeid, S.Kamarthi, J.Manuf.Sci.Eng 132 (2010) 9.

[71] N. K. Reddy, K. Ramesh, R. Ganesan, K. T. R. Reddy, K. R. Gunasekhar, E. S. R. Gopal, J.Appl. Phys. A Mater, Sci. Process 83 (2006)133–138.

[72] M. Devika, K. T. R. Reddy, N. K. Reddy, K. Ramesh, R. Ganesan, E. S. R. Gopal, K. R. Gunasekhar, J. Appl. Phys (2) 100 (2006) 023518.

[73] D. A. Jameel, International Journal of Modern Physics and Applications 1(2015)193-199.

[74] J. H. Park, Chemical Vapor Deposition. ASM International, (2001).

[75] A. Ortiz, J. C. Alonso, M. Garcia, J. Toriz, J.Semicond. Sci. Technol 11(1996) 243–247.

[76] L. L.Cheng, M. H. Liu, S. C. Wang, M.X.Wang, G.D.Wang, Q.Y. Zhou, Z.Q Chen, J. Semicond. Sci.Technol 28 (2013) 8.

[77] L. S. Price, I. P. Parkin, T. G. Hibbert, and K. C. Molloy, J.Chem. Vapor Deposit 4 (1998) 222–225.

[78] L. S. Price, I. P. Parkin, M. N. Field, A. M. E. Hardy, R. J. H. Clark, T. G. Hibbert, K. C. Molloy, J. Mater. Chem 10 (2000) 527–530.

[79] T. G. Hibbert, M. F. Mahon, K. C. Molloy, L. S. Price, I. P. Parkin, J. Mater. Chem 11 (2001) 469–473.

[80] A. T. Kana, T. G. Hibbert, M. F. Mahon, K. C. Molloy, I. P. Parkin, L. S. Price, J.Polyhedron 20 (2001)2989–2995.

[81] Z. T. Khodair, A. R. Alsrraf, M .I. Manssor, N. A. Bakr, J. Electron Devices 15 (2012) 1200-1208.

[82] I. P. Parkin, L. S. Price, T. G. Hibbert, K. C. Molloy, J. Mater. Chem 11 (2001)1486–1490.

[83] H. Moualkia, « Elaboration et Caractérisation de Couches Minces de Sulfure de Cadmium (CdS) », Doctorate thesis, University of Mentouri-Constantine, (2010).

[84] R. D. Engelken, H. E. Mccloud, C. Lee, M. Slayton, H.Ghoreishi, J. Electrochem. Soc 134 (1987) 2696–2707.

[85] A. Bouhdjer, «Study of thin layers of Indium oxide (In_2O_3) elaborated by chemical means», Doctorate thesis, University of Med Khider-Biskra, (2016).

[86] I. Gurrappa, L Binder, J. Science and Technology of Advanced Materials 9 (2008) 043001.

[87] P. Pramanik, P. K. Basu, S. Biswas, J. Thin Solid Films 150 (1987) 269–276.

[88] M. Kumar, A. Kumar, A.C. Abhyankar, J.Ceramics International 40 (2014) 8411–8418.

[89] S. Lopez, A. Ortiz, J .Semicond. Sci. Technol 9 (1994) 2130–2133.

[90] N. K. Reddy, K. T. R. Reddy, J. Mater. Chem. Phys 102 (2007)13–18.

[91] G. Jérôme, «Elaboration de couches minces d'oxydes transparents et conducteurs par spray CVD assiste par radiation infrarouge pour applications photovoltaïque», Doctorat thesis, National School of Arts Superior and Crafts of Paris, (2009).

Chapter II

Technical preparation and characterization of tin sulfide thin films

II.1.Introduction

In this chapter, we present the depositing system used to develop tin sulfide. Then, we will describe the different experimental techniques for characterization our samples.

II.2. Tin sulfide thin films prepared by ultrasonic spray

SnS thin films can be prepared by several techniques such as chemical bath deposition method (CBD) [1], thermal evaporation [2], RF sputtering [3], electrochemical deposition [4], hot wall method [5], novel hydrothermal method [6], successive ionic layer adsorption and reaction method (SILAR) [7], pulse electro-deposition method [8], dip coating method [9], electron beam evaporation [10], close-spaced vacuum sublimation (CSS) [11],and spray pyrolysis [12]. Among them, spray pyrolysis method is a cost effective technique to prepare tin sulfide thin film, since it is a low cost and can be used to deposit uniform coatings on large surface area. Also this technique is excellent for depositing films homogeneous and acceding. From the advantages mentioned above we have selected this development process and we adopted it for use in our work.

II.2.1. Experimental setup used in our study

In laboratory of Physics of Thin Films and Applications (LPCMA) of the University of Biskra. We used ultrasonic spray pyrolysis technique to deposit tin sulfide films, this technique is illustrated in the following figure:

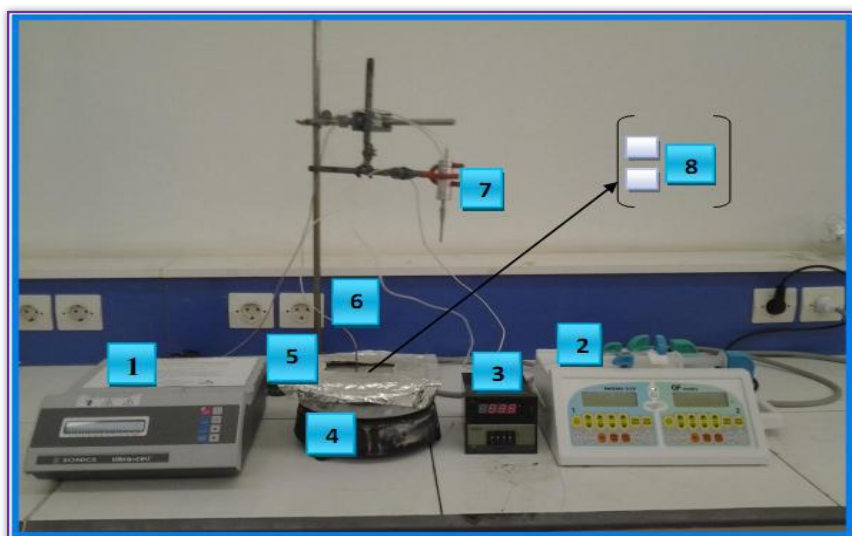

Fig.II.1: *Installation used in the deposition technique ultrasonic spray.*

1- Ultrasonic generator with 40 KHz frequency permits to generate the ultrasonic waves and submit them to the atomizer. **2-** Syringe pump to control the flow rate.

3- Temperature regulator related to a thermocouple to control the temperature.

4- Resistance to heat the substrate.

5- Substrate holder.

6- Thermocouple.

7- Atomizer to decompose the solution to fine droplets.

8- Substrate.

II.2.2. Experimental procedure

In this section, we present the procedure for preparation of substrates that we used for the elaboration of thin layers of tin sulfide, as well as the proposed chemical composition for the deposited of SnS thin films.

II.2.2.1. Preparation of substrates

To prepare thin films of tin sulfide (SnS) by ultrasonic spray we used glass substrates for studying the structural, optical and electrical properties of these films.

II.2.2.2. Cleaning of the substrates

We clean the substrate in order eliminates the traces from greases and impurities onto the surface of glass then ameliorate my film adhesion.

The process of cleaning of the surface of the substrates is as follows:

-Firstly using a pen with diamond point to cut the substrates.

-Rinsing with the water distilled and then with acetone during 10 min.

-Rinsing with distilled water.

-Washing in methanol at ambient temperature.

- Cleaning in a water bath distilled.

-Drying with using a drier.

All this treatment is to prevent pollution from dust release and other impurities.

II.2.2.3. Chemical composition envisaged for the development of thin layers of tin sulfide

The choice of chemical precursor and their concentrations in the solvent have a strong influence on the quality of films.

In this study thin layers of tin sulfide were deposited on glass substrates using ultrasonic spray technique. The spraying solution consisted of a tin Chloride II ($SnCl_2.2H_2O$), tin chloride IV ($SnCl_4.5H_2O$) and thiourea ($CS(NH_2)_2$). The molarity of sulfide (M_{Sn}) was 0.05mol/l and the molarity of thiourea (M_S) was 0.1mol/l both of them were dissolved in methanol 30 ml. The distance between nozzle and substrate was 5 cm all of them were kept constant; however all other experimental conditions demonstrated in table.II.1

Tab. II.1*: Deposition parameters of three series of thin layers of tin sulfide.*

Sample	**Tin chloride II $SnCl_2(2H_2O)$ and tin chloride IV $SnCl_4(5H_2O)$**						**Tin chloride II ($SnCl_2(2H_2O)$)**										
	Serie 1						**Serie 2**					**Serie 3**					
Deposition time (min)	2	4	6	8	10	13	4			6		4			6		
Flow rate (ml)	50						25	30	40	50	60	50			40		
Substrate temperature (C°)	300						300					100	150	200	300	350	400

II.2.2.4.The deposition process

We divide our study into three series:

Serie 1 : After cleaning of substrates, place it onto the ohmique resistance which the power supply is connected to the temperature controller, then heat the substrate from room temperature to the temperature chosen to deposits (300°C); When the recommended

temperature is reached we fix flow rate 50 ml, and ultrasonic amplitude wave 40%. However, the spraying deposition time varied from 2 to 13 min, using two precursors: tin (II) chloride and tin (IV) chloride.

Serie 2: We follow the same procedure to prepare a second series of SnS thin films by using tin (II) chloride $SnCl_2$ as a source of Sn, but the deposition time is fixed at 4 then 6 min and the flow rate varies from 25 to 60 ml /h.

Serie 3: We follow the same procedure to prepare a third series of SnS thin films by using tin (II) chloride $SnCl_2$ as a source of Sn, we divide the experimental conditions into two parts:

- The solution flow rate was 50 ml/h, deposition time was 4 min however the substrate temperature varied from 100°C to 400°C.
- The solution flow rate was 40 ml/h, deposition time was 6 min however the substrate temperature varied from 100°C to 400°C.

We have a very fine droplets are sprayed onto the heated substrate; that causes the activation of the chemical reaction between the compounds. At the end of the process, stop heating and leave a substrates to cool slowly to room temperature, to prevent thermal shock that may crack the glass, finally after cooling we can get our samples of tin sulfide thin film.The formation of SnS and SnS_2 phase from a solution can be schematized by the global reaction [13]:

$$SnCl_2 + (NH_2)_2CS + 2H_2O \longrightarrow SnS + 2NH_4Cl + CO_2 \quad (II.1)$$

$$SnCl_2 + 2(NH_2)_2CS + 2O_2 \longrightarrow SnS_2 + 2NH_4Cl + N_2 + 2CO_2 \quad (II.2)$$

$$SnCl_4 + 2(NH_2)_2CS + 2O_2 \longrightarrow SnS_2 + 2NH_4Cl_2 + N_2 + 2CO_2 \quad (II.3)$$

We can summarize the steps to obtain tin sulfide thin films in the following chart:

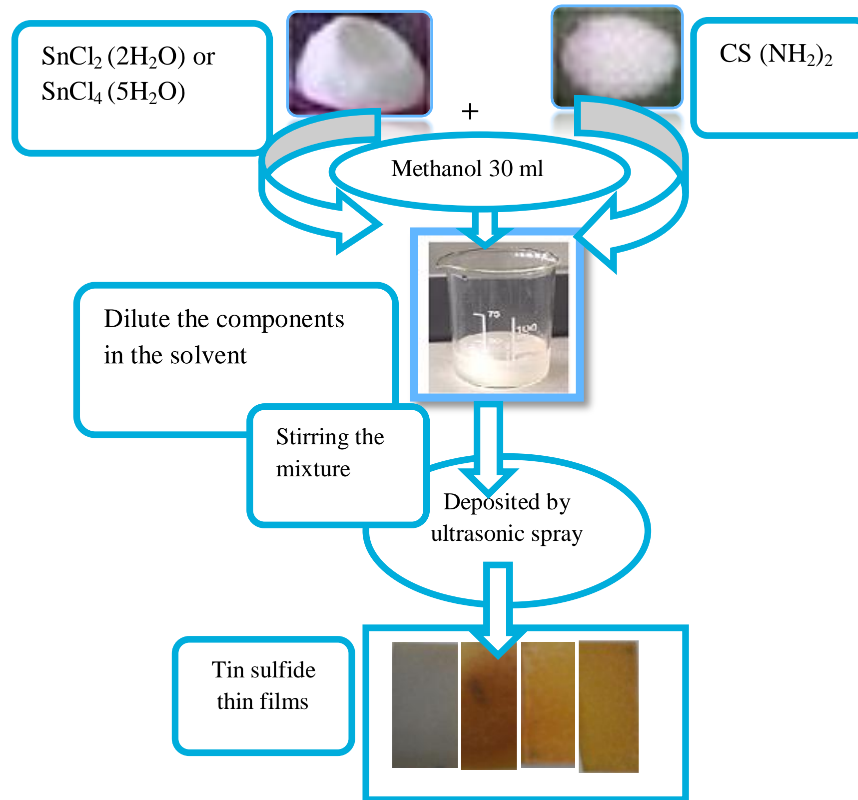

Fig.II.2: Different steps for obtaining a thin layer

II.3. Characterization of thin films

II.3.1.Adhesion Test

Before doing any characterization on the as prepared and heat treated films, adhesion strength between the films and the substrates were evaluated by applying the Scotch tape test on the deposited films. Generally, adhesion strength is considered to be "good" if the film adheres to the substrate and it doesn't peel off the substrate [14].

II.3.2.Thickness calculation

After deposition, the thin film thickness (e) was evaluated using the weight difference method with the following relation [15]:

$$e = \frac{m}{\rho .A} \qquad (II.4)$$

Where m is the mass of the film deposited on the substrate, ρ is the density of the deposited material in the bulk form and A (in cm^2) is the effective area on which the film was deposited.

II.3.3. Structural characterization

II.3.3.1. X-ray diffraction

The structural characterization of thin films was done by analysis (XRD) which allows having information on the crystallographic growth directions [16].

- ***Principle:***

When a monochromatic X-ray beam strikes a crystal under an angle θ, and a constructive interference peak in the reflection intensity is observed if the Bragg law is verified (Figure.II.3).

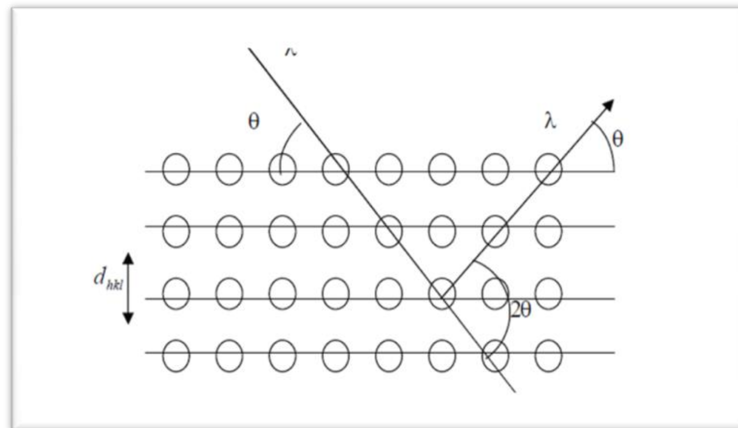

Fig. II.3*: Crystal planes family in Bragg condition [16].*

This law relates the distance d between the parallel crystal planes, the wavelength λ of X-rays and the angle of incidence θ by:

$$2d_{hkl} \sin\theta = n.\lambda \tag{II.5}$$

n = 1, 2 ... order of diffraction.

The diffraction pattern is a recording of the diffracted intensity versus the 2θ angle with the direct beam figure.II.4 .The study of the diffraction pattern can be traced back to a lot of information on:

- The crystalline phases (peak position);
- Crystallite size and / or the internal stress (width half-height peaks);
- The stacking faults (peak shape) orientation of crystallites (absence or presence of reflections) [17].

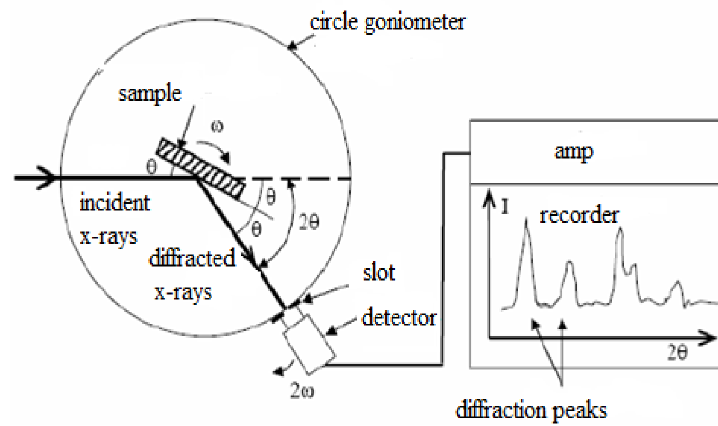

Fig.II.4: *Schematic diagram of the diffractometer [17].*

Our study were used: D8 ADVANCE diffractometer (University of Biskra) and X'Pert (Research Center and Energy Technologies at Tunisia) (Figure.II.5); rays were produced from a radiation source CuKα copper anode having a wavelength $\lambda = 1.54183$ Å.

Fig. II.5*: Type diffractometer (D8 ADVANCE) and* (X'Pert)

II.3.3.1.a. Determination of the grains size

The average grain size of the film can be calculated using the Scherrer's formula [18]:

$$D = \frac{(0.94.\lambda)}{\Delta\theta_{hkl}.\cos\theta_{hkl}} \quad \text{(II.6)}$$

Where β is the full width at half maximum intensity in radians, λ is the wavelength of CuK_{α} radiation source, and θ is the Bragg angle.

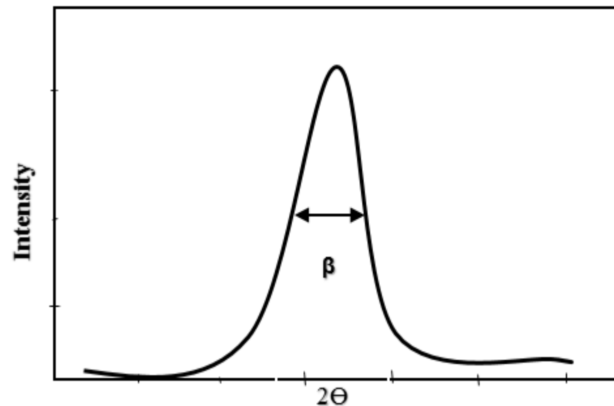

Fig.II.6: *Illustrate the peak widths FWHM (ΔΘ=β).*

II.3.3.1.b. Determination of lattice parameter

The lattice parameter values for different crystallographic systems can be calculated from the following equations using the (hkl) parameters and the interplanar spacing d [19, 20].

Hexagonal system: $$\frac{1}{d^2} = \frac{4}{3}\left(\frac{h^2+hk+k^2}{a^2}\right) + \frac{l^2}{c^2} \quad \text{(II.7)}$$

Orthorhombic system: $$\frac{1}{d^2} = \frac{h^2}{a^2} + \frac{k^2}{b^2} + \frac{l^2}{c^2} \quad \text{(II.8)}$$

II.3.3.1.c. Stress determination

The relation that links the stress($\boldsymbol{\sigma_{ij}}$[**Pa**]), the strain tensor ($\boldsymbol{\varepsilon_{kl}}$), and the elastic constants *(C_{ijkl})* are given by Hooke's law:

$$\sigma_{ij} = C_{ijkl} \, . \, \varepsilon_{kl} \quad \text{(II.9)}$$

The elastic constants are not always available in the literature (as in the case of our material), and as the strain varies in a manner proportional with the stress, one can use this relation between the two variables have a idea about the variation stress layers studied and that using the following formula of strain (ε) [21]:

$$\varepsilon = \frac{\beta.cos\theta}{4} \quad (II.10)$$

II.3.3.1.d.The texture coefficient (TC)

The preferential orientation of the dominant phase of the sample has been determined by means of the texture coefficient (TC) using the expression [22, 23]:

$$TC(hkl) = \frac{I(hkl)/I_0(hkl)}{\frac{1}{N}\sum_n I(hkl)/I_0(hkl)} \quad (II.11)$$

Where I_0 (h k l) is the standard intensity of the (h k l) plane, I (hkl) is the observed intensity of the (h k l) plane and N is the reflection number and n is the number of diffraction peaks.

II.3.3.1.e.The dislocation density (δ)

Knowing the crystallite size values one can estimate the dislocation density (δ), defined as the length of dislocation lines per unit volume of the crystal has been calculated by using the Williamson and Smallman's formula [24]:

$$\delta = \frac{1}{D^2} \quad (II.12)$$

II.3.3.1.f.The number of crystallites n_c

The number of crystallites per unit surface area n_c has been calculated using the following formula [25].

$$nc = \frac{e}{D^3} \quad (II.13)$$

II.3.4.Optical characterization

Optical methods used to characterize a large number of parameters. They have the advantage on electrical methods to be non-destructive and do not require achieving, always delicate, ohmic contacts. They only require a transparent substrate in the wavelength range. two types of optical methods can be distinguished:

- Methods that analyze the optical properties of the material such as; measurements of transmittance and reflectance, and the ellipsometric measurements. These spectroscopic measurements to determine the thickness of the material, the optical gap and refractive index.
- The methods studying the optical response of the material to a stimulus such as the photo-luminescence and cathode

II.3.4.1.UV-visible spectroscopy

This technique rests on the knowledge of the distances between interference rings in the spectra of transmission in the visible and the near infra-red. One uses a recording spectrophotometer with double beams, of which it principle of operation is represented in figure.II.7.

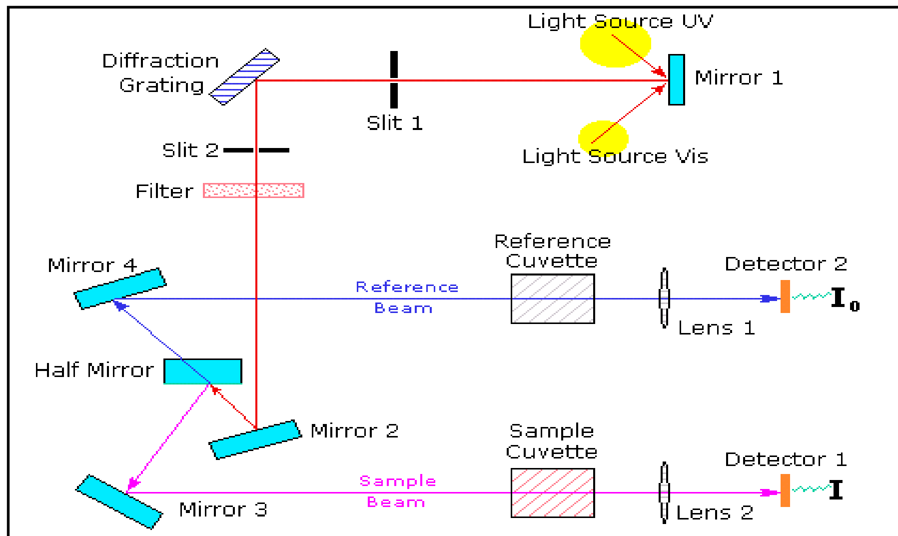

Fig.II.7: *The principle of operation of UV-visible*

Using a spectrometer we can measure the optical properties (transmittance, the energy gap, the energy of activation...) the transmission spectrometer used is

Perkin Elmer LAMBDA 25 UV/ VIS Spectrometer with double beam one for their reference (glass) the other with the sample (glass – film), there spectral range extends from wavelength λ=200 nm to 2000 nm.Spectra obtained give the variation of transmittance expressed as a percentage according to their wavelength.

In addition, thanks to the interferences, one can determine the following parameters: The film thickness, the optical gap, the disorder, the absorption coefficient and the refraction index can be calculated using the following relations [26].

II.3.4.1.a. Film thickness

The physical constants used in calculations are defined in figure.II.8:

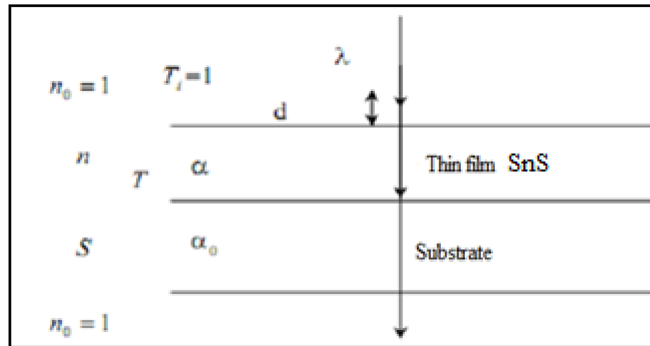

Fig.II.8: *Thin absorbing film on thick transparent substrate system.*

T is the transmittance, α is the absorption coefficient of film, λ is the incidental light wavelength, n and s are respectively the refraction indexes of the film and the substrate and d represents the film thickness. Using the physical parameters defined in figure (II.9) and the spectrum of transmission obtained, one can determine the film thickness as follow [27]:

$$d=\lambda_1\lambda_2/2(\lambda_2 n_1 - \lambda_1 n_2) \qquad (II.14)$$

Where: n_1 and n_2 are the refraction index of the film for the wavelength λ_1 and λ_2 we can calculate n_1 and n_2 from the following relation [28]:

$$n_{1(2)} = \left[N_{1(2)} + (N_{1(2)}^2 - s^2)^{1/2}\right]^{1/2} \qquad (II.15)$$

And $N_{1\,(2)}$ can be obtained using this relation [28]:

$$N_{1(2)} = 2s(T_M - T_{m1(2)})/T_M T_{m1(2)} + (s^2 + 1)/2 \qquad (II.16)$$

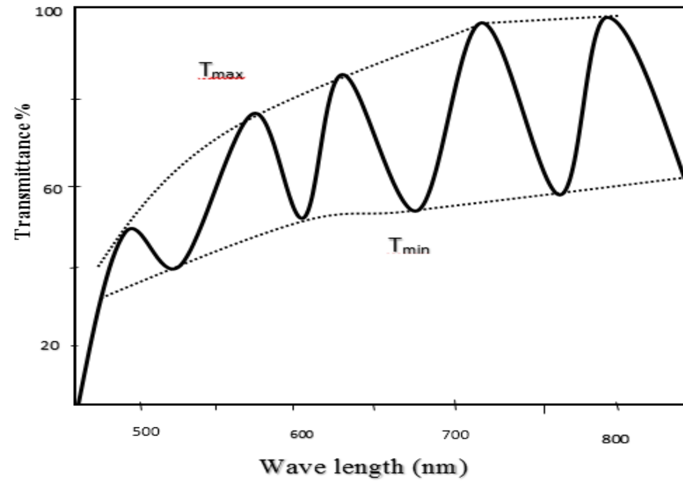

Fig.II.9: Method of interference fringes to determinate the thickness

II.3.4.1.b.The absorption coefficient

In the spectral field where the light is absorbed, and by knowing the film's thickness, we can determine the absorption coefficient for each value of transmittance T in (%) which corresponds to energy by the law of Beer-Lambert:

$$T=\frac{I}{I_0}\times 100 \tag{II.17}$$

Where:

$$\frac{I}{I_0}=\exp(-\alpha d)=\frac{T}{100} \tag{II.18}$$

Where: I_0 is the incidental light intensity, I the transmitted light intensity, α coefficient of absorption and d the thickness of the film. This relation can be written:

$$\alpha=\frac{1}{d}\ln\left(\frac{I_0}{I}\right) \tag{II.19}$$

If we express T (λ) in (%), this expression becomes:

$$\alpha=\frac{1}{d}\ln\left(\frac{100}{T}\right) \tag{II.20}$$

This approximate relation is established, by neglecting the reflexions with all interfaces; air/film, air/substrate.

II.3.4.1. c. Optical gap

In high energy, absorption results from electronic transitions between wide states of band to band. It is usually described by Tauc law [29]:

$$\alpha\,(h\nu)=A(h\nu-E_g)^m \tag{II.21}$$

Where: hν is the photon energy, Eg is optical gap m and A are constants, m characterizes the optical type of transition and takes the values 1/2, 2 (1/2 for allowed direct transitions or 2 for allowed indirect transitions). In order to determine the nature of the transition from films produced in this study, we will plot the curves $(\alpha h\nu)^2 = f(h\nu)$.
We can obtain Eg Value as it showing in figure.II.10.

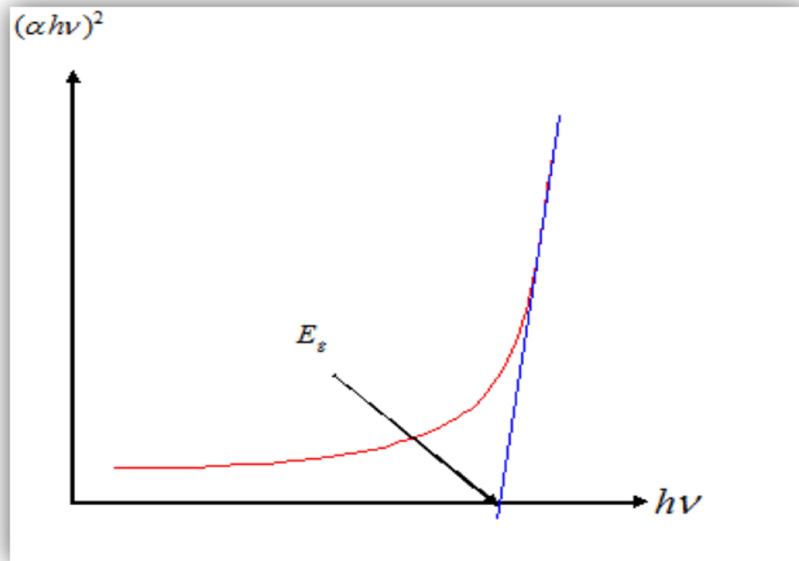

Fig.II.10: *Determination of Eg.*

II.3.4.1.d. Disorder calculating

Another important parameter which characterizes the material disorder is Urbach energy, according to the Urbach law of the expression of the absorption coefficient is as follow:

$$\alpha = \alpha_0 \exp \frac{h\nu}{E_{00}} \quad \text{(II.22)}$$

By drawing the ln (α) as a function of hν, one can determinate E_{00} value [30]:

$$\ln(\alpha) = \ln \alpha_0 + \frac{h\nu}{E_{00}} \quad \text{(II.23)}$$

The following figure presents how we can estimate E_{00}

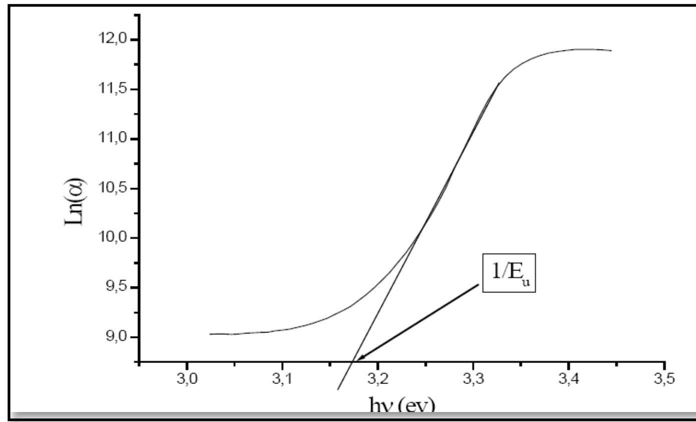

Fig.II.11: *Determination of the disorder by extrapolation starting from the variation of ln (α) has in function of hν.*

II.3.4.1.e. Refractive index and dielectric constant

The refractive indices (n) were determined from the reflectance (R) data using [31]:

$$n = \frac{1+R}{1-R} + \sqrt{\frac{4R}{(1-R)^2} - k^2} \qquad \text{(II.24)}$$

Where the extinction coefficient calculated by the formula:

$$K = \frac{\alpha\lambda}{4\pi} \qquad \text{(II.25)}$$

The dielectric constant of films was designed using the relation [32]:

$$\varepsilon = \varepsilon_1 + \varepsilon_2 \qquad \text{(II.26)}$$

Where the respective real and imaginary parts have been calculate using the relations:

$$\varepsilon_1 = n^2 - k^2$$

$$\varepsilon_2 = 2nk \qquad \text{(II.27)}$$

II.3.4.2.Photoluminescence spectroscopy

Photoluminescence spectroscopy (PL) is an optical technique for characterizing semiconductors and insulating materials. Its principle is based on the excitation of electrons by monochromatic radiative source of low wavelength laser type or other lamps.

The spectrum emitted in return by this excitement is called radiative phenomenon photoluminescence.

The energy emitted by the material studied is always lower than the excitation source. In generally, the emission to a solid is very low, hence the use of laser and a system of performance detection. Photoluminescence can be used to study the band structure or the levels of impurities in a semiconductor.

Other luminescence phenomena using other sources excitatory exist, for following. Electroluminescence is the light emitted by a body traversed through an electric current, catholuminescence the result of bombardment by an electron beam, is triboluminescence due to mechanical excitation while the chemiluminescence follows a chemical reaction

II.3.4.2.a. Physical principle

In photoluminescence spectroscopy, the photons are directed onto the semiconductor surface with a higher energy than the energy gap of the material studied. Photons incidents monochromatic laser source, is either reflected or absorbed or transmitted by the material and the absorbed photons create electron-hole pairs in the semiconductor.Indeed, the electron absorbing the incident photon passes from the valence band to conduction band. When the electron loses energy by radiative recombination and recombines with the hole, the emitted photons comprising the photoluminescence spectrum. The different wavelength component that spectrum reflect the different energy level transitions allowed in the material. Therefore, the PL spectrum provides information about the nature of defects as vacancies, interstitial atoms or impurities in the network.

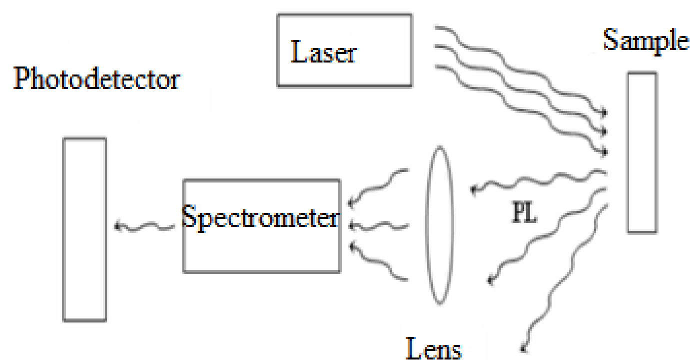

Fig.II.12: *Typical experimental set-up for PL measurements [33].*

II.3.4.2.b. Photoluminescence peak positions: Energy levels

In the bulk of a crystalline material, translational symmetry leads to the formation of electronic energy bands. Defects and impurities break the periodicity of the lattice and perturb the band structure locally. The perturbation usually can be characterized by a discrete energy level that lies within the band gap. Depending on the defect or impurity, the state acts as a donor or acceptor of excess electrons in the crystal. Electrons or holes are attracted to the excess or deficiency of local charge due to the impurity nucleus or defect, and coulomb binding occurs. The situation can be modeled as a hydrogenic system where the binding energy is reduced by the dielectric constant of the material. Because electrons and holes have different effective masses, donors and acceptors have different binding energies. When the temperature is sufficiently low, carriers will be trapped at these states. If these carriers recombine radiatively, the energy of the emitted light can be analyzed to determine the energy of the defect or impurity level. Shallow levels, which lie near the conduction or valence band edge, are more likely to participate in radiative recombination, but the sample temperature must be small enough to discourage thermal activation of carriers out of the traps. Deep levels tend to facilitate nonradiative recombination by providing a stop-over for electrons making their way between the conduction and valence bands by emitting phonons. Several intrinsic and impurity transitions are illustrated in figure.II.13 [34].

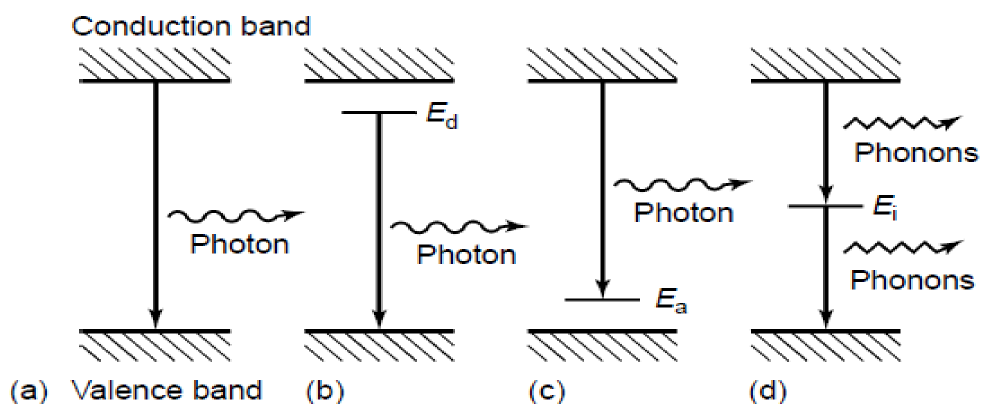

Fig.II.13: *Radiative recombination paths: (a) band-toband; (b) donor to valence band; (c) conduction band to acceptor. (d) Nonradiative recombination via an intermediate state [34].*

II.3.5. Infrared Spectroscopy

Infrared spectroscopy is an absorption method in the wavelength region of 1 to 100 µm in that extends the region of the visible light to longer wavelengths and smaller

frequencies/energies. The energy of infrared light is no longer sufficient to induce transitions of valence electrons. Instead, infrared radiation excites vibrational and rotational motions in molecules. Except for the differences in the energy transfer from the radiation to the molecule, the principles of IR spectroscopy are the same as those of VIS/UV spectroscopy or other spectroscopic techniques.

- **Molecular rotations**

Rotational transitions are of little use to the spectroscopist. Rotational levels are quantized, and absorption of IR by gases yields line spectra. However, in liquids or solids, these lines broaden into a continuum due to molecular collisions and other interactions.

- **Molecular vibrations**

The positions of atoms in molecules are not fixed; they are subject to a number of different vibrations. Vibrations fall into the two main catagories of stretching and bending.

Stretching: Change in inter-atomic distance along bond axis

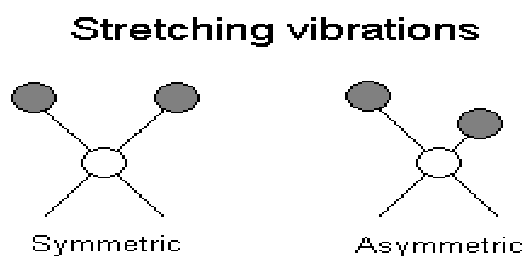

Fig.II.14: *Stretching vibrations*

Bending: Change in angle between two bonds. There are four types of bend: rocking, scissoring, wagging and twisting

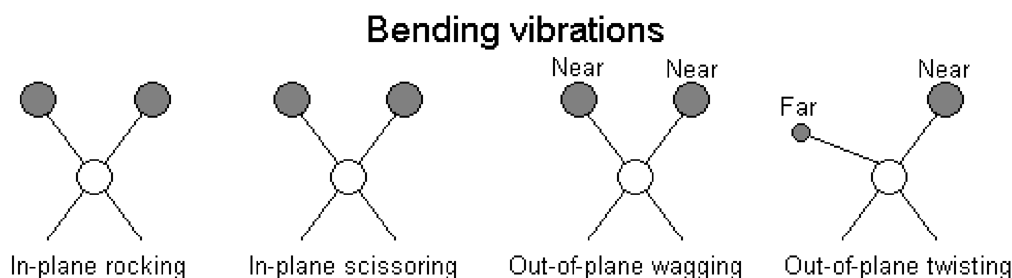

Fig.II.15: *Bending vibrations*

II.3.6. Electrical characterization with four point probe method

In order to eliminate or at least minimize the contact contribution to the measured resistance value, techniques based on separate current injection and voltage drop measurements have been developed. Firstly, the two-probe technique can be used. This measurement is very simple, but it is affected by several parameters: lateral contact geometry, probe spacing, and minority carrier injection near the lateral contacts. The main disadvantage of this technique is the need for lateral contacts. This requirement is overcome with the four-point probe technique, where two probes are used for current injection and the other two probes are used to measure the voltage drop. The more usual probe geometry configuration is when the four probes are placed in a line, as shown in figure.II.16. The voltage at probe 2, V_2, induced by the current flowing from probe 1 to probe 4 is given by:

$$V_2 = \frac{\rho I}{2\pi} \cdot \left(\frac{1}{s_1} - \frac{1}{s_2 + s_3}\right) \qquad \text{(II.28)}$$

The voltage at probe 3 is:

$$V_3 = \frac{\rho I}{2\pi} \cdot \left(\frac{1}{s_1 + s_2} - \frac{1}{s_3}\right) \qquad \text{(II.29)}$$

Then, by measuring $V = V_2 - V_3$, the voltage drop between probes 2 and 3, and the current I through probes 1 and 4, the resistivity can be determined using (II.28) and (II.29) as:

$$\rho = \frac{2\pi V / I}{\left(\frac{1}{s_1} + \frac{1}{s_2} - \frac{1}{s_2 + s_3} - \frac{1}{s_1 + s_2}\right)} \qquad \text{(II. 30)}$$

Thus, a direct measurement of the resistivity can be made using a high-impedance voltmeter and a current source. When the probe spacings are equal ($s_1 = s_2 = s_3 = s$), which is the most practical case, then (II.30) becomes:

$$\rho = 2\pi s \cdot \frac{V}{I} \qquad \text{(II.31)}$$

Equations (II.30) and (II.31) are valid only for semi-infinite samples; that is, when both the thickness t and the sample surface are very large ($\rightarrow\infty$), and the probes' locations must be far from any boundary. Because these relations can be applied only to large ingots, then in many cases a correction factor f must be introduced in order to take into account

the finite thickness and surface of the sample and its boundary effects. Further, for epitaxial layers, f must also consider the nature of the substrate – whether it is a conductor or an insulator. Thus, (II.31) becomes:

$$\rho = 2\pi\, s \cdot \frac{V}{I} \cdot f \tag{II.32}$$

For a thin semiconductor wafer or thin semiconducting layer deposited on an insulating substrate, and for the condition $t < s/2$, which represents most practical cases because the probe spacing s is usually on the order of a millimeter, then the correction factor due to the thickness is:

$$f = \frac{(t/s)}{2\ln 2} \qquad \text{so that:} \qquad \rho = 4.532\, t\, \frac{V}{I} \tag{II.33}$$

We used a four-point device (EPS alessi-08) at the university Mohamed Kheider Biskra.

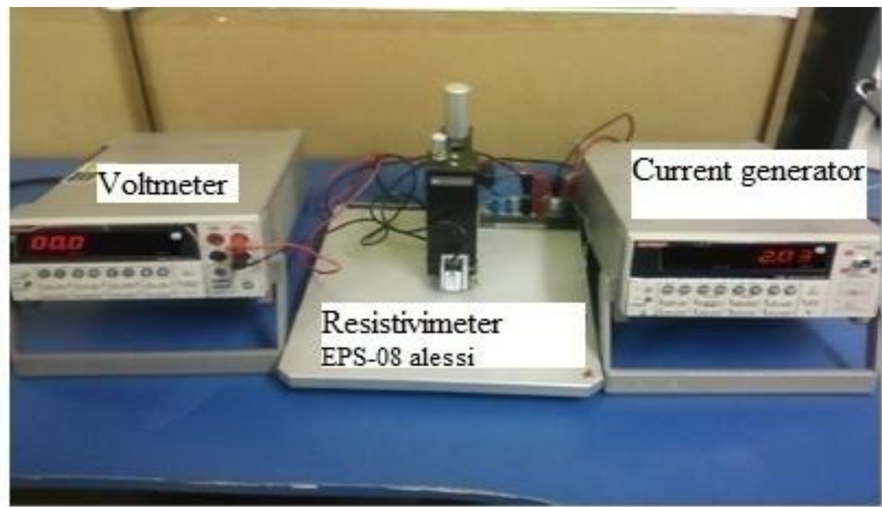

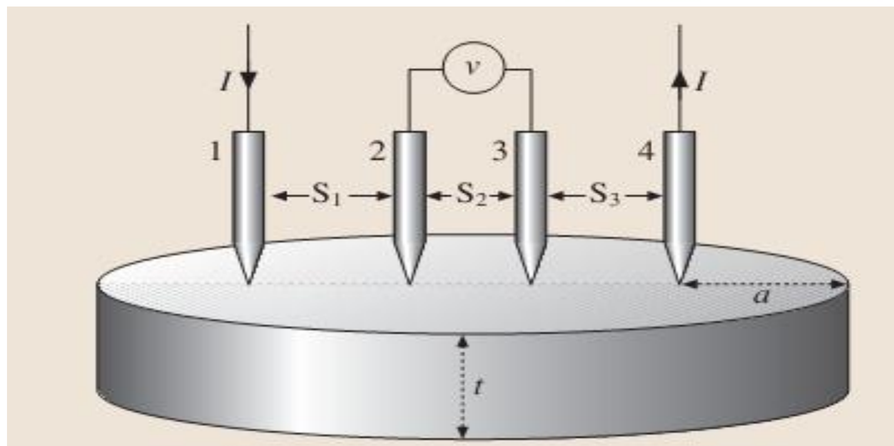

Fig.II.16: *Linear four-point probe configuration. The sample thickness is t and a is the distance from the edge or boundary of the sample [35].*

References of second chapter

[1] A.J. Ragina, K.C. Preetha, K.V. Murali, K. Deepa, T.L, J.Remadevi, J.Adv Appl Sci Res 2 (2011) 438-444.

[2] J. Priyal, P .Arun, J.Semiconductors 34 (2013) 9.

[3] K. Hartman, J. Johnson, M. Bertoni, D. Recht, M. J. Aziz, J.Thin Solid Films 519 (2011) 7421–7424.

[4] R .Mariappan, T. Mahalingam, V. Ponnuswamy, J.Optik 122 (2011) 2216–2219.

[5] A. Bashkirov.S, FGremenok .V, A Ivanov .V, J.Fizika i Tekhnika Poluprovodnikov 45 (6) (2011)765–769.

[6] H. Zhu, D. Yang, Y. Ji, H. Zhang, X. Shen, J.materials science 40 (2005)591–595.

[7] B. Ghosh, M. Das, P. Banerjee, S. Das, J. Applied Surface Science 254 (2008) 6436–6440.

[8] Cheng, Y. Chen, Y. He, G. Chen, J.Materials Letters 61 (2007) 1408–1412.

[9] SK .Panda, A.Antonakos, E. Liarokapis, S .Bhattzcharya, S. Chaudhuri, J.Mat. Res. Bull 42 (2007) 576.

[10] A .Tanussevski, D. Poelman, J. Solar Energy Materials and Solar Cells 80 (2003) 297-303.

[11] A.Voznyi ,V. Kosyak, A.Opanasyuk, N. Tirkusova, L. Grase, A. Medvids, G. Mezinskis , J.Materials Chemistry and Physics 173(2016)52-61.

[12] T. Akbari, S.M. Rozati, J.Chemistry of Solid Materials 2 (2014) 33-39.

[13] Sekhar C. Ray, Malay K. Karanjai, Dhruba DasGupta, J.Thin Solid Films 350(1999)72-78.

[14] H. Amani Hamedani « Investigation of Deposition Parameters in Ultrasonic Spray Pyrolysis for Fabrication of Solid Oxide Fuel Cell Cathodes», doctorate thesis, Georgia Institute of Technology, (2008).

[15] M. Ajili, M. Castagné, N. K. Turki, J .Optik 126 (2015) 708–714.

[16] S. Philipe, doctorate thesis, University of valenciennes et du hainaut Cambrésis, (1995).

[17] C. Ballif, «Propriétés électriques et optiques de couches minces de WS_2 et MOS_2 en vue d'applications photovoltaïques», Doctorate thesis, Federal institute of technology in lausanne, (1998).

[18] Warren B E X-ray diffraction, New York: Dover, (1990).

[19] B.R. Sankapal, R.S. Mane, C.D. Lokhande, J.Materials Research Bulletin 35 (2000) 2027–2035.

[20] Cullity BD, Stock SR, Elements of X-ray diffraction. Upper Saddle River, NJ: Prentice-Hall, (2001).

[21] K.L. Chopra, Thin Film Phenomena, McGraw-Hill, New York, 270(1969).

[22] K. Gurumurugan, D.Mangalaraj, S.K.Narayandass, K.Sekar, C.P. Girija Vallabhan, J. Semicond Sci Technol 9 (1994)1827.

[23] Eze F, J. Mater Chem Phys 89 (2005) 205.

[24] Williamson GB, Smallman RC, Philos Mag 1 (34) (1956) 46.

[25] B.G. Jeyaprakash, R. Ashok kumar, K.Kesavan, A. Amalarani, J.American Science 6(2010) 3.

[26] G.Huertas, «Etude de Nouveaux Matériaux D'électrode Positive et D'électrolyte Solide Vitreux Sous Forme de Couches minces pour des Couches Minces Microbatteries au Lithium», doctorate thesis, University of Bordeaux I, (2006).

[27] A.Bougrine, A.el hichou, M.Addou, J. Ebothé, A. Kachouna, M. Troyon, J.Material Chemistry and Physics 80 (2003) 438-445.

[82] ع. عطاف، « ترسيب و تشخيص شرائح نيتريد السيليسيوم اللامتبلور »، أطروحة دكتوراه دولة، جامعة محمد خيضر- بسكرة، (2005).

[29] JI .Pankove, J. Optical processes in semiconductors, Dover, New York, (1975).

[30] McCarthy, G. Welton, J. Powder Diffraction 4 (1989) 156.

[31] G.H. Yue, D.L. Peng, P.X. Yan, L.S. Wang, W. Wang, X.H. Luo, J. Alloys Compound 468 (2009) 254–257.

[32] V. Robles , J. F. Trigo, C. Guillén, J. Herrero, J .Mater Sci 48 (2013) 3943–3949.

[33] Timothy H. Gfroerer , Photoluminescence in Analysis of Surfaces and Interfaces, Encyclopedia of Analytical Chemistry, R.A. Meyers (Ed), John Wiley & Sons Ltd, Chichester, (2000) 9209–9231.

[34] M.L.W.Thewalt, A.G. Steele, J.E. Huffman, J. Appl. Phys. Lett 49 (1986) 1444–1446.

[35] S. Kasap, P. Capper, Springer Handbook of Electronic and Photonic Material, Springer Science +Business Media, Inc, New York, USA, (2006).

Deposition times influence on tin sulfide thin films using $SnCl_2$ and $SnCl_4$ sources precursors

III.1. Introduction

In this chapter, we studied the effect of deposition time on the structural, optical and electrical properties of tin sulfide thin film produced by ultrasonic spray; also we comparatived between the physical properties of SnS films deposited from $SnCl_2$ and $SnCl_4$ at different deposition time.

The spraying deposition time t_d varied from 2 to 13 min and using two sources of tin: tin chloride II and tin IV chloride. Two initial types of solutions will be referred to as solution **1** and solution **2** and the films that were obtained from them will be referred to as films'serie **1**and films'serie **2** respectively.

Under these deposit conditions, good films are obtained. They are uniform and very adherent to the substrates.

III.2.The films thickness and growth rate

Figure.III.1 shows the variation of film thickness as a function of deposition time. At low deposition time 2 min, the nucleation step is very short, and with increasing in the deposition, the growth of the film becomes easier and linear.This indicates that the deposition of atoms on the first layer becomes faster with time. We note that there is no difference between the increases in film thickness between 2-6min for tow films series. After 6min, we can observe a slow increase in the films serie **1** and a rapid increase for films serie **2**.

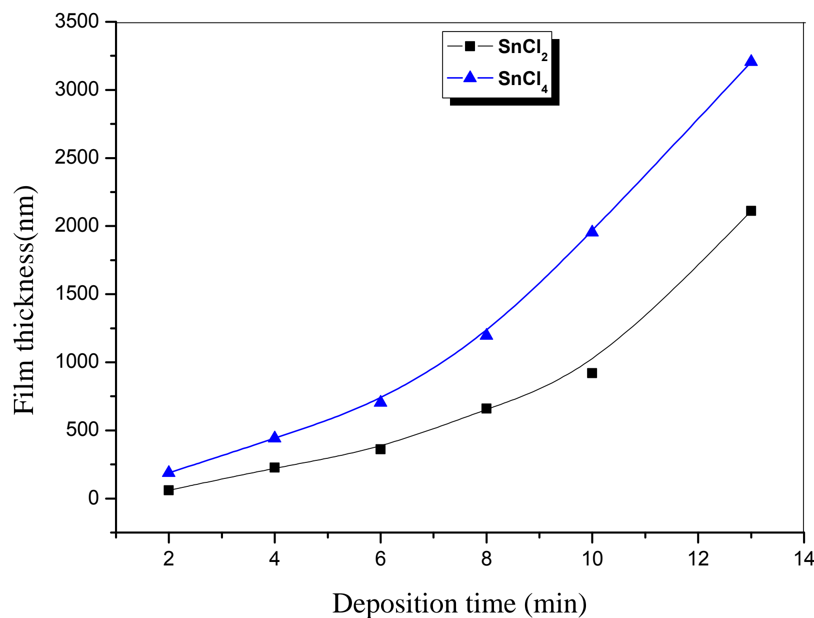

Fig.III.1: *Variation of film thickness as a function of deposition time.*

The dependence of the growth rate of tin sulfide films on deposition time is plotted in figure.III.2. The growth rate is estimated from the ratio of film thickness on the deposition time. As can be seen, the growth rate increases with the increasing of the deposition time for two sources.

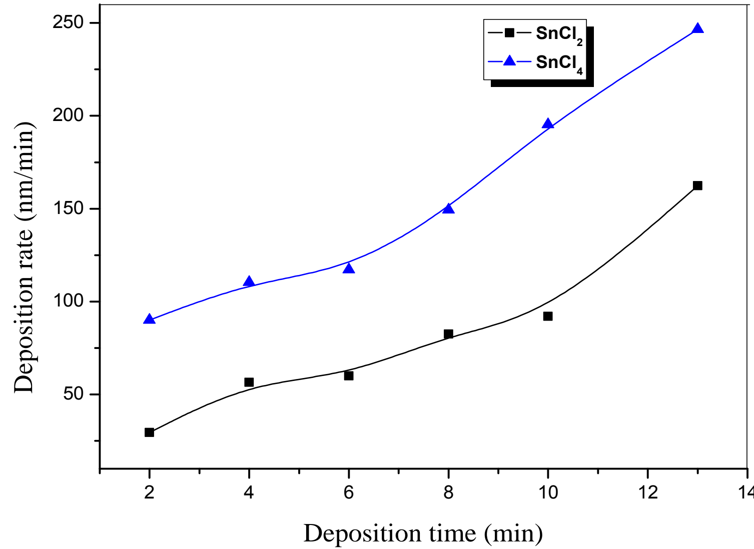

***Fig.III.2**: Variation of deposition rate as a function of deposition time*

III.3.Structural studies

Figure .III.3 shows the XRD spectra of tin sulfide samples deposited at different deposition time.

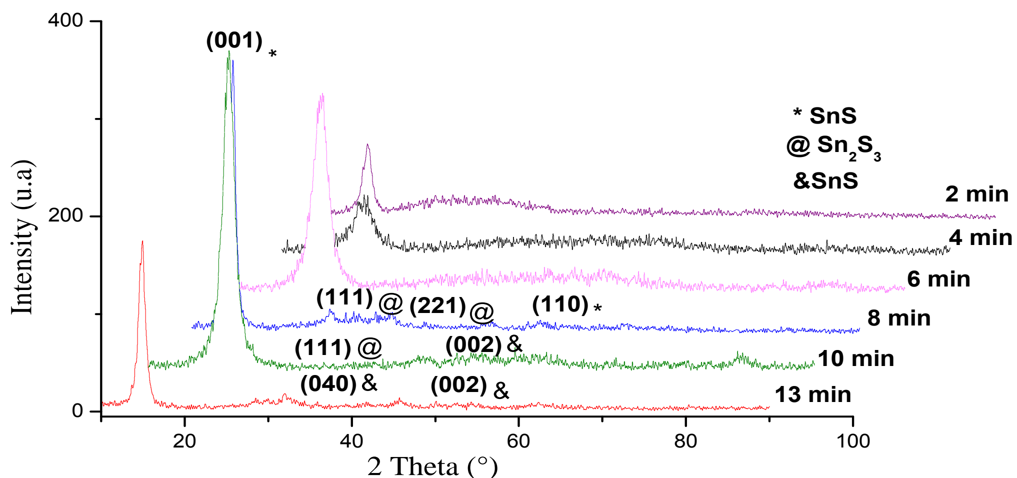

***Fig.III.3:** XRD pattern of SnS thin film sample with different deposition time.*

These results are compared with the results of ASTM file (American Society for Testing and Materials) Tin Sulfide, to take Miller indices (hkl) and the type of variety of this material.

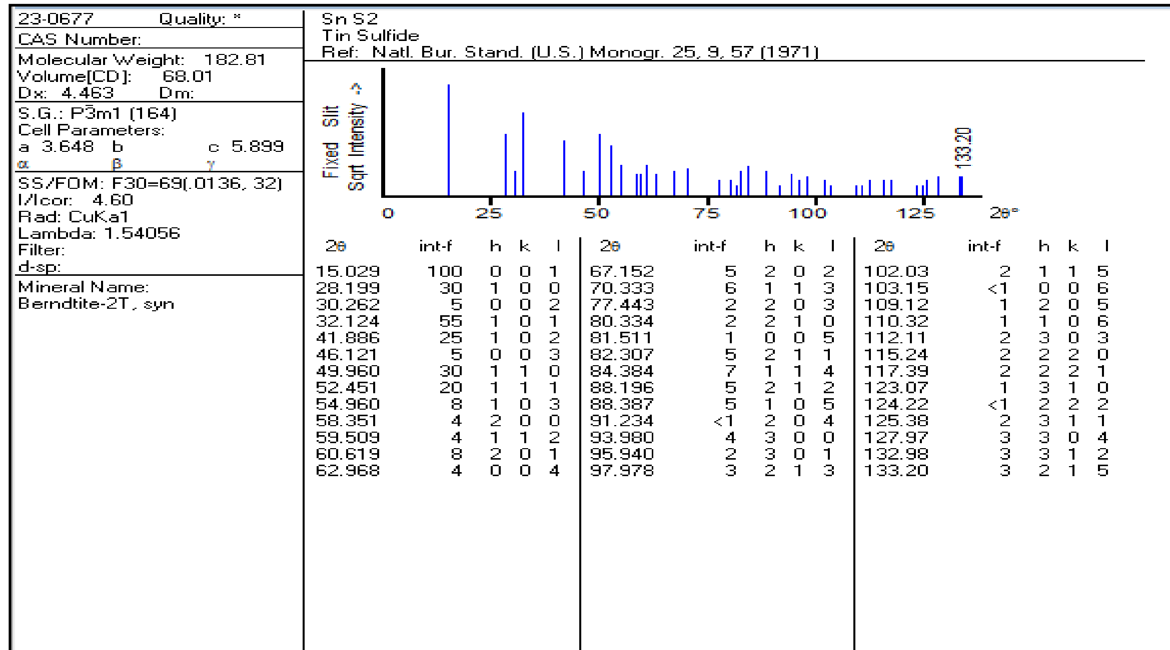

23-0677 Quality: *
CAS Number:
Molecular Weight: 182.81
Volume[CD]: 68.01
Dx: 4.463 Dm:
S.G.: P$\bar{3}$m1 (164)
Cell Parameters:
a 3.648 b c 5.899
α β γ
SS/FOM: F30=69(.0136, 32)
I/Icor: 4.60
Rad: CuKa1
Lambda: 1.54056
Filter:
d-sp:
Mineral Name:
Berndtite-2T, syn

Sn S2
Tin Sulfide
Ref: Natl. Bur. Stand. (U.S.) Monogr. 25, 9, 57 (1971)

2θ	int-f	h	k	l
15.029	100	0	0	1
28.199	30	1	0	0
30.262	5	0	0	2
32.124	55	1	0	1
41.886	25	1	0	2
46.121	5	0	0	3
49.960	30	1	1	0
52.451	20	1	1	1
54.960	8	1	0	3
58.351	4	2	0	0
59.509	4	1	1	2
60.619	8	2	0	1
62.968	4	0	0	4
67.152	5	2	0	2
70.333	6	1	1	3
77.443	2	2	0	3
80.334	2	2	1	0
81.511	1	0	0	5
82.307	5	2	1	1
84.384	7	1	1	4
88.196	5	2	1	2
88.387	5	1	0	5
91.234	<1	2	0	4
93.980	4	3	0	0
95.940	2	3	0	1
97.978	3	2	1	3
102.03	2	1	1	5
103.15	<1	0	0	6
109.12	1	2	0	5
110.32	1	1	0	6
112.11	2	3	0	3
115.24	2	2	2	0
117.39	2	2	2	1
123.07	1	3	1	0
124.22	<1	2	2	2
125.38	2	3	1	1
127.97	3	3	0	4
132.98	3	3	1	2
133.20	3	2	1	5

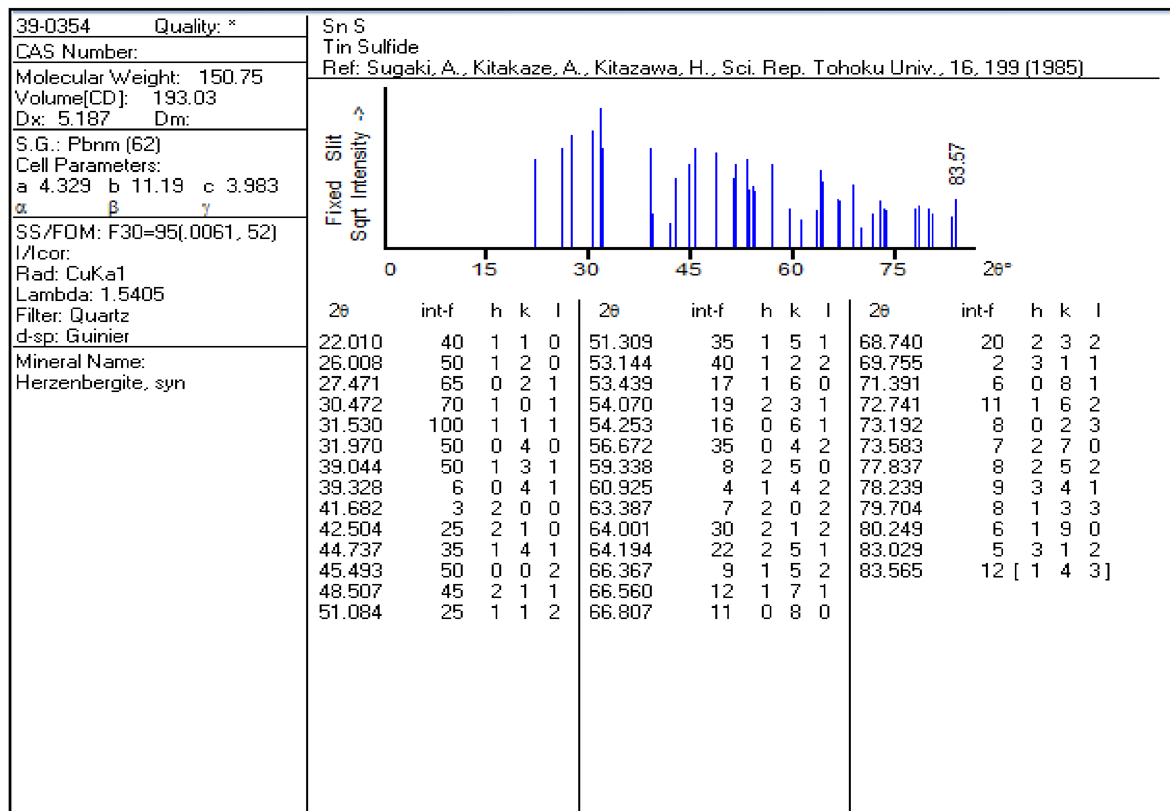

39-0354 Quality: *
CAS Number:
Molecular Weight: 150.75
Volume[CD]: 193.03
Dx: 5.187 Dm:
S.G.: Pbnm (62)
Cell Parameters:
a 4.329 b 11.19 c 3.983
α β γ
SS/FOM: F30=95(.0061, 52)
I/Icor:
Rad: CuKa1
Lambda: 1.5405
Filter: Quartz
d-sp: Guinier
Mineral Name:
Herzenbergite, syn

Sn S
Tin Sulfide
Ref: Sugaki, A., Kitakaze, A., Kitazawa, H., Sci. Rep. Tohoku Univ., 16, 199 (1985)

2θ	int-f	h	k	l
22.010	40	1	1	0
26.008	50	1	2	0
27.471	65	0	2	1
30.472	70	1	0	1
31.530	100	1	1	1
31.970	50	0	4	0
39.044	50	1	3	1
39.328	6	0	4	1
41.682	3	2	0	0
42.504	25	2	1	0
44.737	35	1	4	1
45.493	50	0	0	2
48.507	45	2	1	1
51.084	25	1	1	2
51.309	35	1	5	1
53.144	40	1	2	2
53.439	17	1	6	0
54.070	19	2	3	1
54.253	16	0	6	1
56.672	35	0	4	2
59.338	8	2	5	0
60.925	4	1	4	2
63.387	7	2	0	2
64.001	30	2	1	2
64.194	22	2	5	1
66.367	9	1	5	2
66.560	12	1	7	1
66.807	11	0	8	0
68.740	20	2	3	2
69.755	2	3	1	1
71.391	6	0	8	1
72.741	11	1	6	2
73.192	8	0	2	3
73.583	7	2	7	0
77.837	8	2	5	2
78.239	9	3	4	1
79.704	8	1	3	3
80.249	6	1	9	0
83.029	5	3	1	2
83.565	12	[1	4	3]

***Fig.III.4**: ASTM files of SnS_2 and SnS.*

The XRD patterns of the thin films deposited at (2-6min) show peak corresponding to SnS_2 hexagonal phase [1-3] (JCPDS card No 23-0677) with preferential orientation in the plane (001) around the angle $2\theta = 15.02$.The films grow at t_d from 8 to 13 min and the previous one (2 to 6 min) show the same prominent peak corresponding to SnS_2whereas other peaks observed at 8 min of 2θ values of 26.70°, 33.98° and 50.27° were found to match with reflections of minimum intensity from (111), (221) and (110) crystallographic planes of Sn_2S_3 and SnS_2 phase respectively. The peak seen at 10 min and 13 min of 2θ values of 45.56° is found with reflections from (002) plane of SnS phase (JCPDS card No 390354) and other peak appeared only at 13 min with (040) plane .The emergence of these peaks indicates that the increase of deposition time has the effect of improving the crystallinity of poly-crystalline layers. We can conclude that with increasing deposition time of the composition and constitution films are changed disulfide in mono sulfide. Similar results about the formation of SnS_2 phase using $SnCl_2$: $2H_2O$ precursor has been observed byK.T. Ramakrishna Reddy et al [4] and N. Koteeswara Reddy et al[5], they observed that the SnS_2 phase became predominant as the temperature increases to 300 ^{0}C obtained by spray pyrolysis.

The XRD diffraction spectra recorded in films serie **2** prepared with various deposition times are shown in figure.III.5

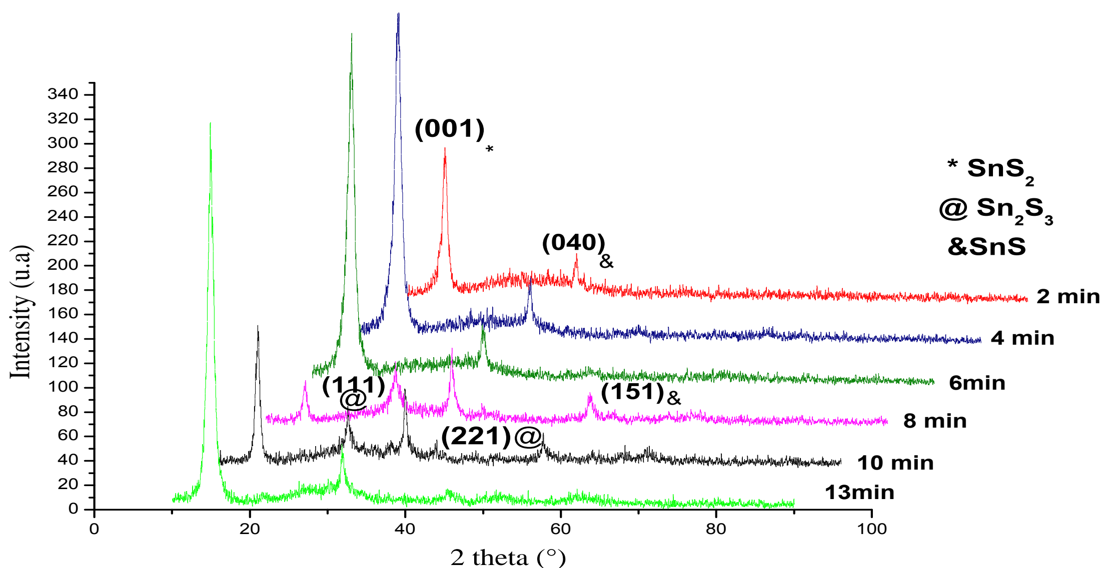

Fig.III.5: *XRD pattern of Sn_xS_y thin film sample with different deposition time.*

For the films serie **2**, it can be noted that the XRD patterns of the thin films at (2-6min) show peaks corresponding to SnS_2 hexagonal phase [6] with preferential from (001) planeand other peak of minimum intensity corresponding to SnSphase with orthorhombic in structure from (040) plane[7]. Moreover, the figure bellow displays the intensity of the peak (001) decrease with increasing deposition time; in contrary to the intensity of the peak (040) correspondent SnS phase. Hence, with rising deposition time, the analysis of the XRD pattern of film deposited after 6 min indicates the formation of Sn_2S_3 and SnS phase with other orientations (111), (221) and (151). Similar results about the formation of SnS_2phase by spray pyrolysis technique using $SnCl_4$: $5H_2O$ precursor has been observed byseveral studies [3-5]. Also the same observation by other groups using other deposition techniques [2, 8, 9]. But the difference between their work and our work is the appearance of the new phase.

The appearance of phase SnS in the films serie **2** at the first deposition time 2 min can be referred to the solubility of the solution or the energy of bindings between the atoms in both solutions. Solubility in solution **2** is bigger than the solubility of solution **1**, for that solution **2** produces a wide number of Sn atoms. Atoms Sn leads to two significant results: the formation of SnSand SnS_2 phases and the emergence of a third new phase called Sn_2S_3 at deposition time 8 min. The former phase appeared of big intensity at XRD analysis in the films serie **2** when compared to films serie **1**. As a result, on one hand, Sn_2S_3 appeared at 8 min and its intensity decrease at 10 min. On the other hand the intensity of the SnS_2 phase decreases. Consequently, Sn_2S_3 phase stability is inferior to SnS and SnS_2 stability.

A prominent (001) peak for two precursors indicates that the crystallite structure of the films is oriented with their c-axis perpendicular to the substrate plane. This is due to its surface energy and that the atoms will arrange themselves into the plane with the lowest surface energy [10, 11]. Thus, it can be deduced that the main effect on the chemical composition is caused by the precursor nature and by the deposition time. The use of both solutions **1**and **2** have proved that (001) reffered to as SnS_2 phase is the preferred orientation in all deposition times. Whereas, SnS and Sn_2S_3 phases clearly shows when using $SnCl_4$ at large deposition time 8, 10 and 13 min.

III.3.1.Texture coefficient, Crystallites size, Strain, dislocation density and lattice parameters

The lattice parameters of the dominate phase in tow films series were obtained comparing the XRD pattern of figure.III.3 and figure.III.5 with the data reported in the JCPDS card, the lattice constants are slightly different from those given in the standard JCPDS data.This could be an indication of stress in the film. From the results of the texture coefficient calculations, it was found that preferential orientation of deposited films with different deposition time of 2,4,6,8,10 and 13 min for two precursors was the (001) orientation. All the results are given in table.III.1 and table.III.2

Tab.III.1: *Structural properties of films serie* ***1*** *on different deposition time*

SnS					JCPDS card reference No 23-0677	
Deposition time (min)	h k l planes	Lattice parameters (A°) a c	Crystallite size (nm)	TC	Lattice parameters (A°) a c	2 θ(°)
2	(001)	a=3.638 c=5.932	11.62	1	a=3.648 c=5.899	15.02
4	(001)	a=3.533 c=5.760	14.52	1		
6	(001)	a=3.636 c=5.927	19.36	1		
8	(001) (111) (221) (110)	a=3.630 c=5.917	12.86	1.04 0.72 2.04 0.18		
10	(001) (111) (002)	a=3.638 c=5.931	11.22	2.01 0.73 0.24		
13	(001) (040) (002)	a=3.625 c=5.909	9.09	2.92 0.58 0.48		

Tab. III.2: *Structural properties of films serie* ***2*** *on different deposition time*

SnS					JCPDS card number 23-0677	
Deposition time (min)	h k l planes	Lattice parameters (Å)	Crystallite size (nm)	TC	Lattice parameters (A°) a c	2 θ (°)
2	(001) (040)	*a* = 3.582 *c* = 5.840	12.87	1.21 0.78		
4	(001) (040)	*a* = 3.600 *c* = 5.869	15.74	1.44 0.56	a=3.648 c=5.899	15.02
6	(001) (040)	*a* = 3.603 *c* = 5.873	17.71	1.41 0.59		
8	(001) (111) (221) (151)	*a* = 3.592 *c* = 5.856	20.24	0.073 0.83 2.91 0.17		
10	(001) (111) (221) (151)	*a* = 3.635 *c* = 5.925	23.61	0.23 0.76 2.83 0.14		
13	(001) (040)	*a* = 3.633 *c* = 5.923	28.33	1.45 0.54		

Figure.III.6 shows the variation of T_C (001) for two films.

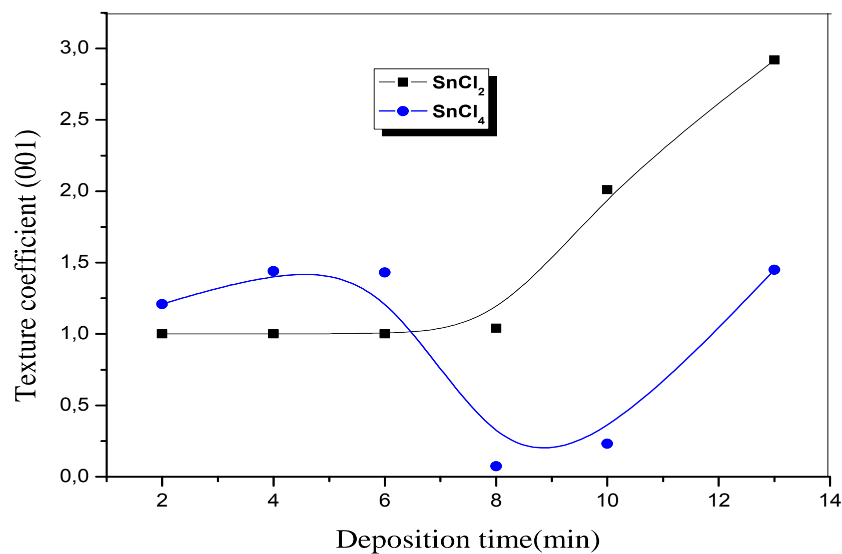

Fig.III.6: *Variation of preferential orientation as a function of deposition time for (001) plane.*

As seen, for films serie **1** the value of T_C (001) between 2-6 min takes average constant value and then increasing with increase in deposition time. Whereas, T_C of film **2** increasing when deposition time varied from 2-6 min and then decreased rapidly with increase in deposition time at 8 min after that increasing.

Figure.III.7 shows the variationthe crystallite size as a function of the deposition time. The values of crystallite size are comparable to those reported by other research [2, 12].We can divide the figure into 2 ranges:

-The range (I): 2-6 min: We found that the values of crystallite size are nearly the same either using precursor 1 or 2.

-The range (II): 6-13 min: The crystallite size increases when using precursor **2** and decreases when using precursor 1.This can be referred to the existence of Sn atoms in solution **2** which leads to an easy breaking down of bindings between Sn and Cl.All of this is supported in figure 2 that indicates the appearance of other phases. Also the concentration of the defect (grain boundary) is low in the films **2** in contrast with films serie **1**. For films serie **1**, the reduce of crystallite size according to the deposition time between (8-13 min) in the case of the developed films is likely caused by the emergence of other phases SnS and Sn_2S_3 this later leadsto the detriment of orientation (001), toward other direction (111), (110), (221) and (002). From these results we get to say that we have a weak restriction regime [13] because the crystallite size is very small. It is from the order of the rayon of an exciton in a bulk material (rayon of the exciton Bohr), less than 20 nm.Also this decreasing can be attributed to the force decreasing in between crystals attracting each other with Van der Waals force because the substrate remained in the solution longer than necessary [14]. For films serie **2** the estimated D value increases with the increasing deposition time, it can be due to the complete deposition process occurring.The latter passes through the nucleation, coalescence stage and the subsequent vertical growth. The same observation has been climbed by H. Moualkia et al [15]. Also the increase of the crystallite size with the increase of deposition time can be explained as the deposition time increases, the amount of solute reaching on the surface of the substrate increases to form film and therefore the electrostatic interaction between solute atoms becomes larger there, by increases the probability of more solute to be gathered together to form a crystallite [16].

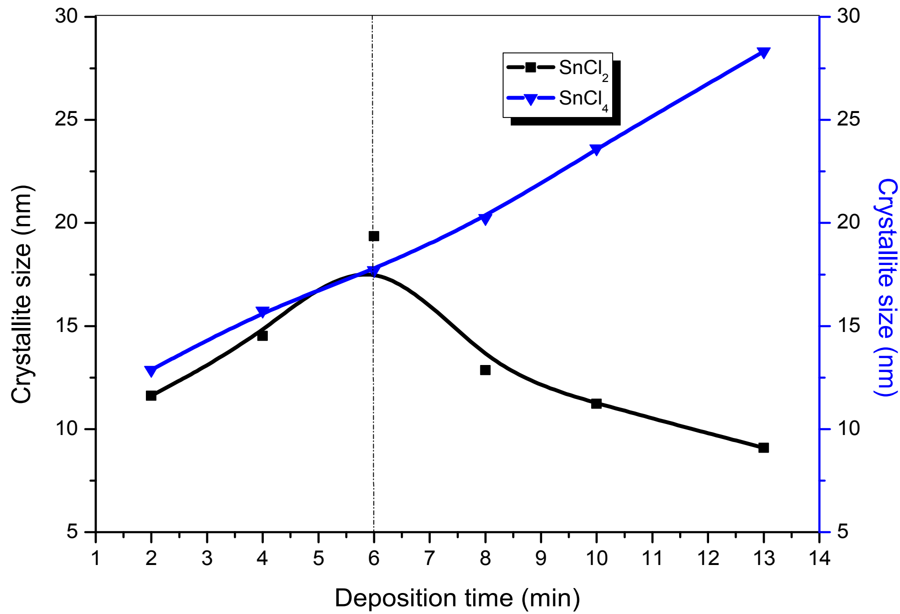

Fig.III.7: *Variation of the crystallite size as a function of the deposition time.*

Figure.III.8 shows the variation of ε versus the deposition time. Comparatively with the variation of crystallite size D, the internal strain behavior of the two films serie **1** and **2** follows an opposite trend of D. This comportment is due to the fact that grains growth is controlled by the strain in film network. This is due to the presence of internal strain in the film network cause a minimization in the grain growth driving forces, which prevent the grain size enlargement during the film formation [17, 18]. Similar behavior has been observed on SnS films deposited with chemical bath at increasing deposition time [19].

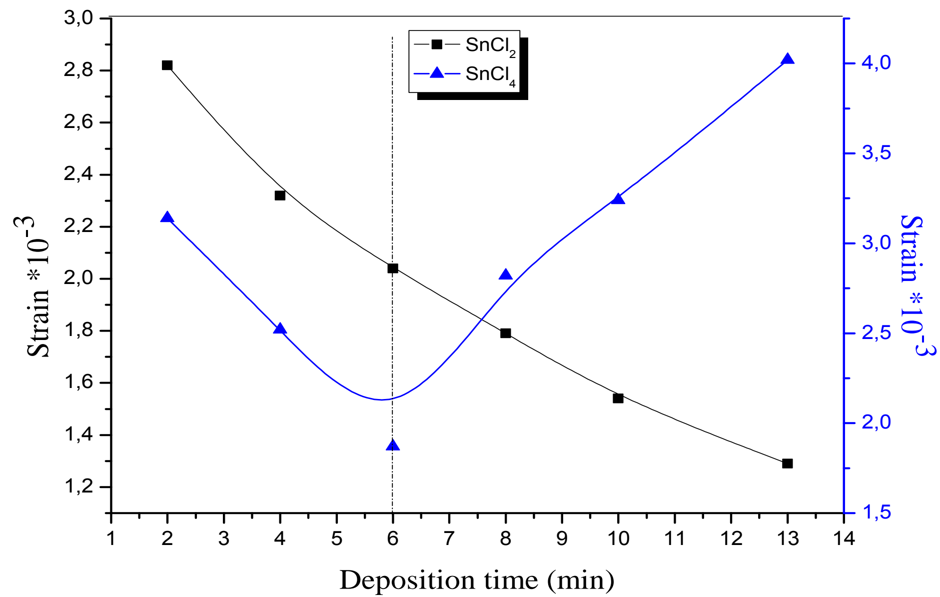

Fig.III.8: *Variation of strain ε in the films network as a function of the deposition time.*

Figure.III.9 represents the variation of dislocation density with deposition time for two precursors. It is clearly observed that in the films serie **1** the dislocation density decreases as increasing in the deposition time from 2 to 6 min. After that, it increases while the dislocation densitydecreases of the films serie **2** with increasing deposition time. It is clearly observable that there is an inter relationship between: crystallite size, strain and dislocation density.While there are increasing variations in the crystallite size, there are decreasing variations in the strain and dislocation density. Similarly this result has been achieved by another researcher [20].

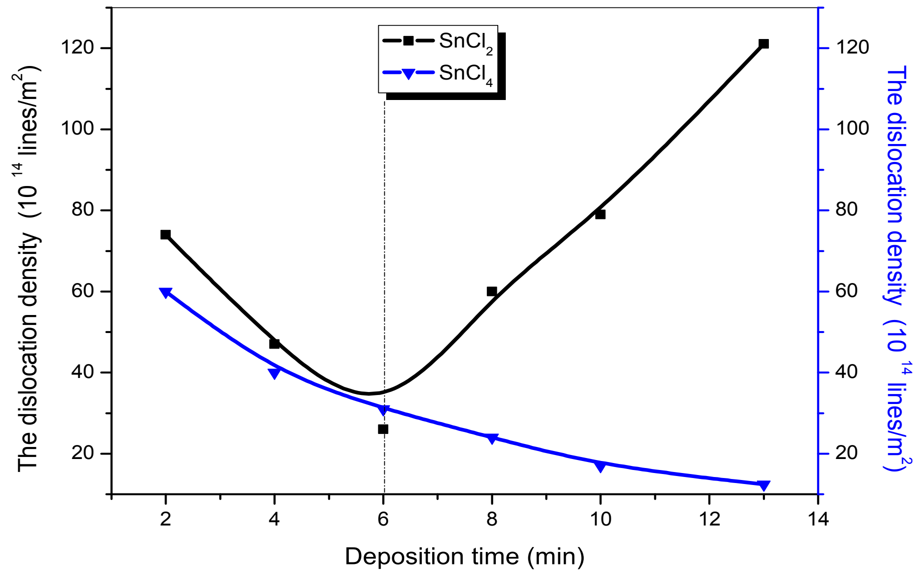

Fig.III.9: *Variation of dislocation density with deposition time.*

The variations number of crystallites shown in figure.III.10. For two series of films, the number of crystallites increased with increasing deposition time.The same variation observed by E. Guneri et al [14] in SnS deposited by chemical bath deposition with different deposition times.

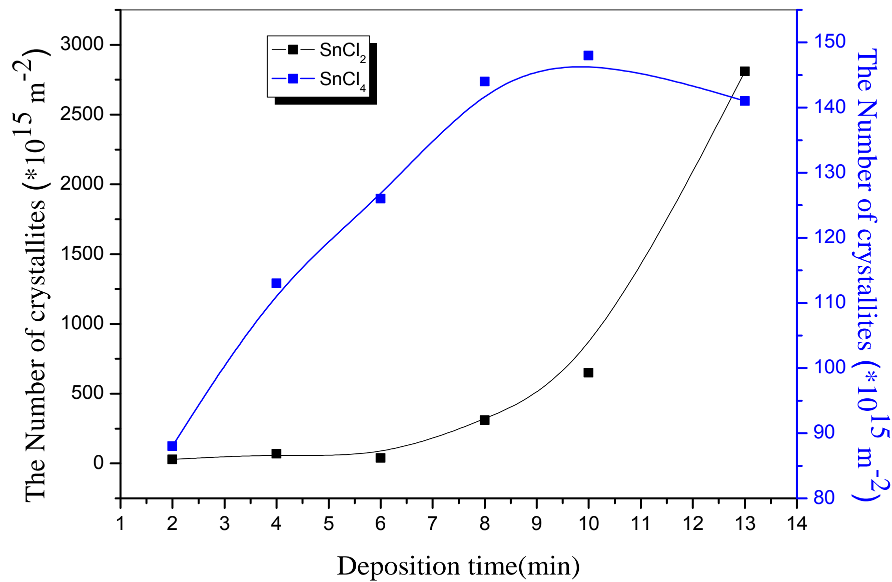

Fig.III.10*: Variation of number of crystallites with deposition time of SnS thin films.*

III.4.Optical studies

III.4.1.Transmittance

The optical transmittance with wavelength of tin sulfide films was measured in wavelength range of 300- 800 nm.The transmission spectra in deposited time range of 2–13 min are shown in figure.III.11 and figure.III.12 for two films.It can be noticed that the transmittance of film varied from 57.22 -3.1 % and from 55.22 -14.25% for two films respectively. There is a lack of interference fringes which are due to multiple reflections [21].Therefore, in one hand; the absence of these fringes in our films indicates that they have a rough appearance [6]. From the other hand, the transmittance decreases with increasing deposition time. This is due to the increase of the thickness of the films is controlled by deposition time. The optical transmittance for the film that has been prepared at 8 min using solution **2** was almost between the transmittance of film deposited at 4 min and 6 min. That leads to the appearance of the Sn_2S_3 phase which results in low disorganized reduce of transmittance but the small intensity of the later in films serie **1** exhibits a well decreasing of transmittance. Through the observation of figure.III.12 we can see that there is an interference fringes at 2, 4 and 6 min when using the solution **2** indicates that the texture appeared smoothly. At 13 min a low transmittance is obtained for both films series.

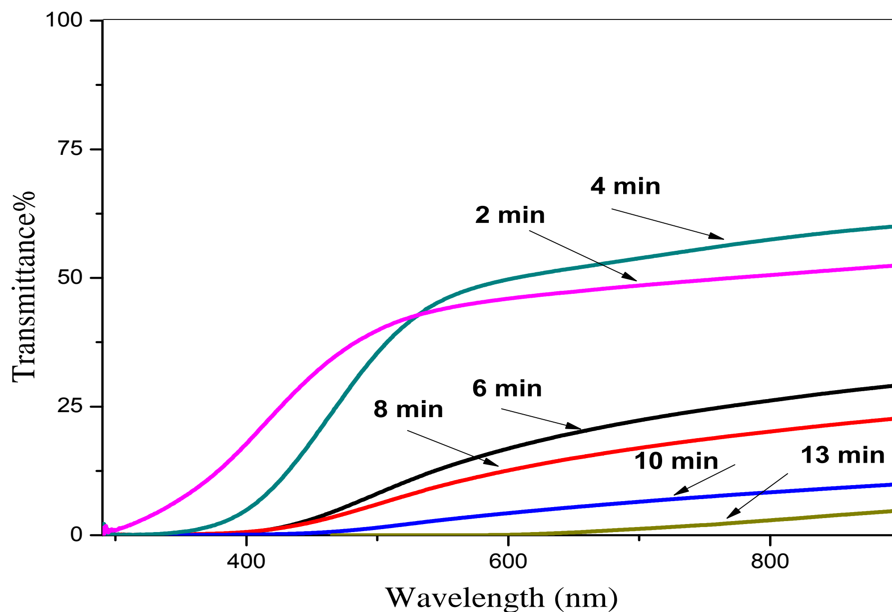

***Fig.III.11**: Transmission curves for films deposited at different deposition time using $SnCl_2$*

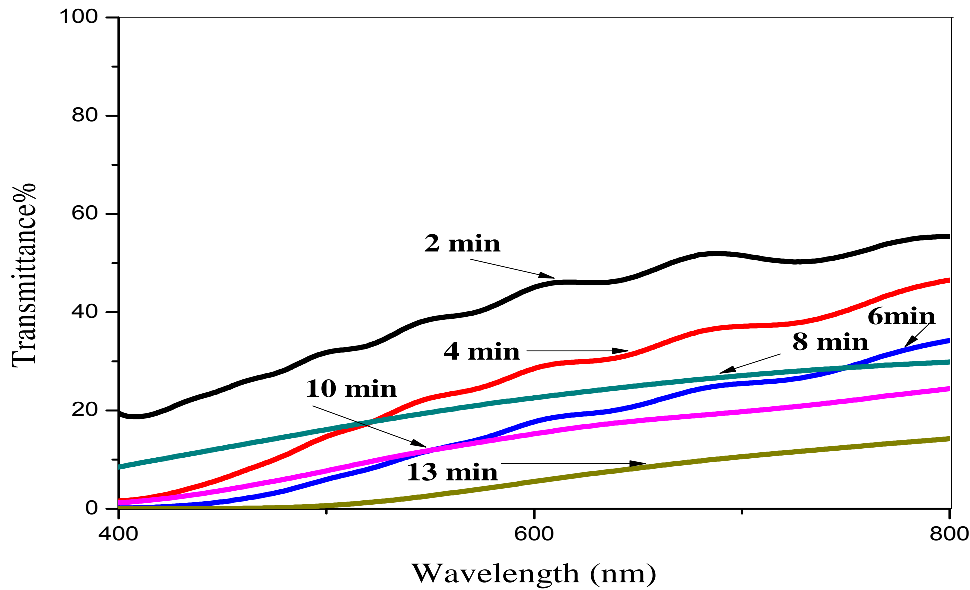

Fig.III.12: Transmission curves for films deposited at different deposition time using$SnCl_4$.

III.4.2.Optical band gap

In figure.III.13, for the two films, the optical band gap decreases with increasing deposition time. These values are in the range observed earlier [22, 23].T.H. Patel et al [24], have studied the effect of deposition time using chemical bath deposition, in their studies, they observed that there was areduce of optical band gap with increasing deposition time. These results agreed with ours. The decrease in optical band gap can be due to increasing inthe film thickness with increasing in the deposition time. They have also observed decrease in the optical band gap of SnS thin films with increasing of film thickness [21]. The difference in the optical band gap between the use of solution **1** and solution**2** in addition to the previous results, it appears that there is a strong decreasing in gap which can be arrived at 2.33eV for film serie **2** in comparatively to films serie **1**. Finally, we can conclude that $SnCl_4$ produces films in the deposition time 6-13 min more that are useful as absorbent film in solar cells in contrast with the prepared films in the same range of deposition time using $SnCl_2$.

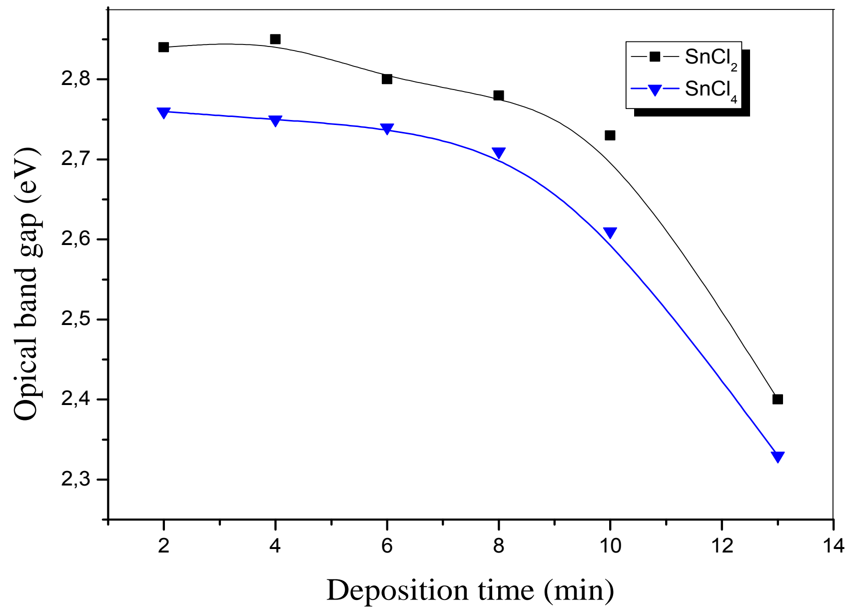

***Fig.III.13**: Variation of optical band gap at different deposition time.*

The variation in the calculated tail width E_{00} with deposition time is reported in the figure.III.14. For two films, the disorder varies inversely of the optical band gap. The widening of the gap is due to the reduction of the disorder in the film [12]. The disorder is characterized by the band tail width (valence and conduction).

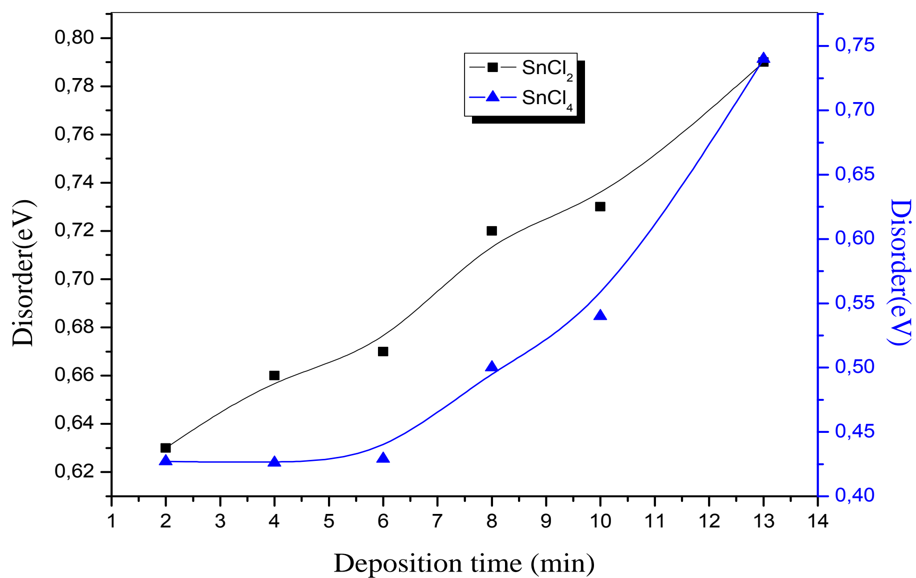

***Fig.III.14**: Variation of disorder of Sn_xS_y at different deposition time.*

III.4.3.Photoluminescence studies

The photoluminescence (PL) is one of the significant studies which can give us more important information on the crystal quality and purity of the material. The room temperature PL emission spectra of the Sn_xS_y thin films, deposited with different deposition time t_d = 2, 4, 6, 8 and 10 min using $SnCl_2$: $2H_2O$ are demonstrated in figure.III.15. PL spectra consist of four emission peaks centered at about 455(blue), 530 (green), 583 (yellow) and 648 (red). As energy corresponds to all the observed emission peaks 2.73, 2.34, 2.12 and 1.91 eV.Yang et al [25] have reported a PL peak at 590 nm for tin disulfide thin films. While, N.G. Deshpande et al [22] have observed two emission peaks of PL attributed to 549.78 nm (green) and 700.28 nm (red) emission of SnS_2. In our study, the strong PL peaks centered at 455nm is maximum for sample prepared with deposition time of 6min; this peak corresponds to the radiative recombination of bound excitons, whereas the explanation for the origin of the broad peaks at 530, 583and 648 nm (the most intense form samples prepared at the deposition time of 2 min) may be from the inner deep level emission [26].This deep level arises because of the stoichiometric variation in SnS_2 phase.Another possible explanation can be ascribed toemission from sulfide vacancies V_S or interstitial tin atoms I_T which considered to be the localizer states in the optical band gap. Other researcher has referred the origin of broad peaks to the impurities and native defects such as interstitial tin atoms [22].

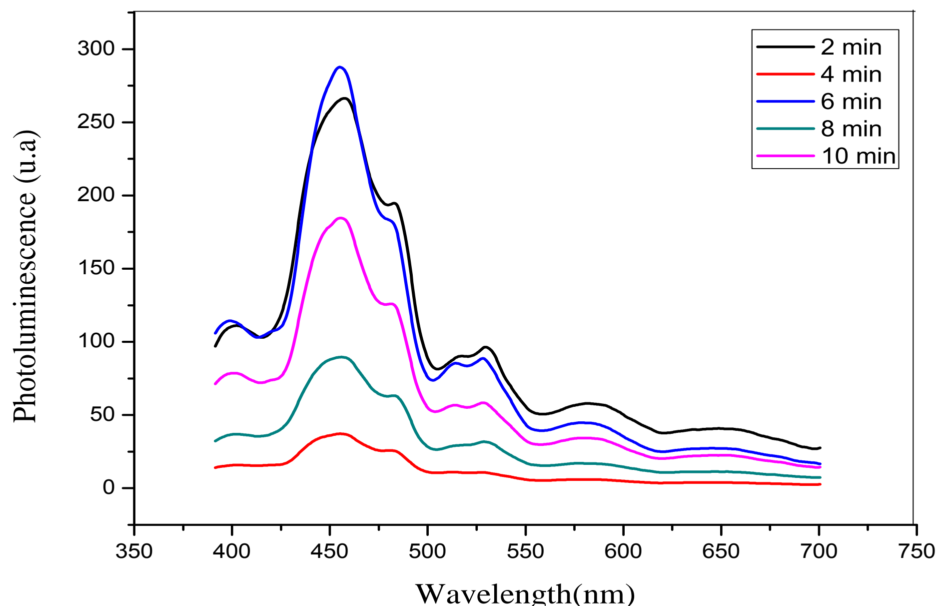

***Fig.III.15**: PL Spectra Vs Wavelength plot of Sn_xS_y thin films prepared at different deposition time.*

III.5. Electrical studies

In figure.III.16, we can notice that when the deposition time between 2-6 min has no effect of the resistivity for the films serie **1** then after that deposition time, it increased suddenly to the value of 2.45Ω.cm; these value were the same fond by precedent studied using $SnCl_2$: $2H_2O$ precursor [27].The lowest resistivity ($2x10^{-4}$Ω.cm) obtained for the deposition time equals to 6min is due to the better crystallinity of the films prepared at this deposition time. These results are strongly supported by XRD analysis (figure.III.3) which indicates that the film grown at 6 min have large grain size than the others films. An increase in grain size of this film leads to reduced grain boundary scattering, and thus a decrease in electrical resistivity. However, the higher electrical resistivity of the films formed at deposition time after 6 min refers to smaller grain size. Similar interpretations were obtained in SnS thin films deposited by chemical bath deposition technique with increasing deposition time by E. Guneri et al [14]. Although, the crystallite size of the films deposited at 8 ,10 and 13 min, is closed to that deposited at 2 and 4 min but the resistivity of the films deposited at 8 and 10 min is higher than those deposited at 2 and 4 min. This result is probably due to the presence of SnS_2 and other new phases like SnS and Sn_2S_3. This later might be responsible for the higher resistivity. T.H. Sajeesh [28] reported the similar regard. In their study, they explained that the high value of resistivity of the films preparedbelow 300 °C is a result of mixed valent compound Sn_2S_3 presence. Also Ramakrishna Reddy et al [4] interpreted the high resistivity of the film deposited for temperature <300 °C due to the appearance of SnS_2 and Sn_2S_3. The low resistivity in SnS_2 films can be due to a deviation in stoichiometry in this compound (excess of tin atoms) [29]. But the resistivity of films serie **2** decreasing in all deposition time from 2 to 13 min and the low resistivity appeared in the films deposited at 13 min which deduces that it is the appropriate film for the fabrication of solar cells. The value of resistivity is good agreement with the reported value [30-32]. In addition, for the films serie **2** can be interpreted the decreases of resistivity by the increase of the crystalline size with increasing deposition time.

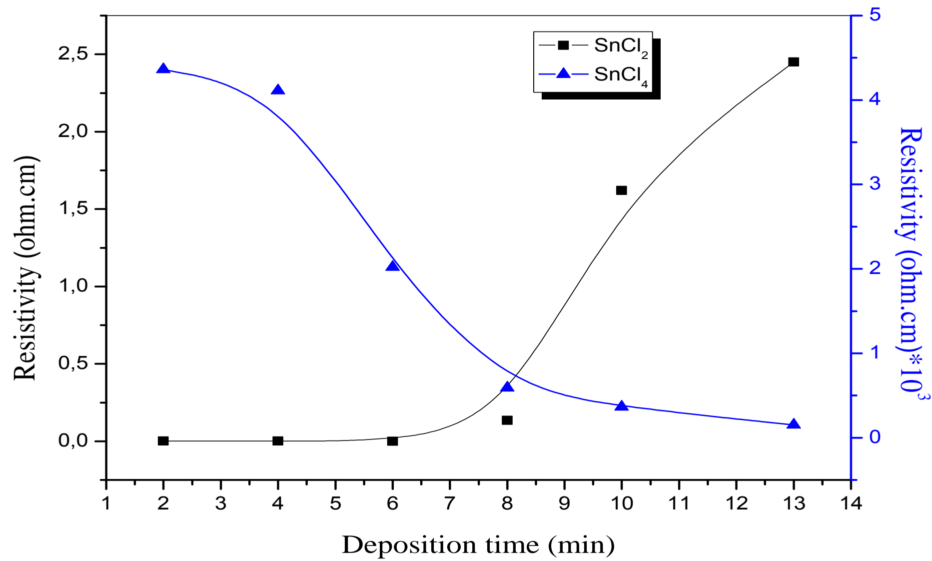

Fig.III.16: *Electrical resistivity of SnS thin films.*

III.6.Conclusion

In summary, we can say that in this study we have proved that the deposition time and the precursor both affect the thin films (**1** and **2**) and provide us with different behaviors and interesting characteristics. X-ray diffraction reveals a good crystalline structure with (001) orientation which corresponds to SnS_2 phase. Another phase SnS appeared in films **2** starting from 2 min.while, at films serie **1** it appears only when the film is deposited at 10 min and 13 min. Sn_2S_3 phase occurred only after 6 min. For both series of films, the optical tests show that the transmittance decreasing with increases the deposition time.The Photoluminescence spectra exhibited the luminescent peaks in the visible region, which shows its potential application in photovoltaic devices.For films deposited using solution **1**, the electrical resistivity (ρ) increased when SnS and Sn_2S_3 phases' appeared butthe electrical resistivity decrease with increases in the deposition timefor films deposited using solution **2**. Finally, we conclude thatthe films serie **2** produces better results from structural, optical properties compared to the films serie **1**. In addition, the deposition time has effects on these properties in which we can notice that there is two ranges from 2 to 6 min and 6 to13 min.These later, supplies better results that appear through: the crystallite size, optical band gap and resistivity for the film prepared using solution **2** compared to the film prepared using solution **1**. Lastly, the ideal condition for better solar cell efficiency is increasing the deposition time.

References of third chapter

[1] **I. B. Kherkhachi**, A. Attaf, H. Saidi, A. Bouhdjer, H. Bendjedidi, Y. Benkhetta, R. Azizi, J. Semiconductors37(2016) 032001.

[2] S.K. Panda, A. Antonakos, E. Liarokapis, S. Bhattacharya, S. Chaudhuri, J. Materials Research Bulletin 42 (2007) 576–583.

[3] C. Khélia, K. Boubaker, T. Ben Nasrallah, M. Amlouk, S. Belgacem,J. Alloys and Compounds477 (2009) 461–467.

[4] K.T.Ramakrishna Reddy, P.Purandar Reddy, R.W.Miles, P.K.Datta, J.Optical Materials 17(2001) 295-298.

[5] N. Koteeswara Reddy, K.T. Ramakrishna Reddy, J. Physica B368 (2005) 25–31.

[6] **I.B. Kherkhachi**, H.Saidi, A. Attaf, N.Attaf,A. Bouhdjar , H.Bendjdidi, Y. Benkhetta,R. Azizi, M.jlassi, J. Optik 127 (2016) 4043-4046.

[7] M. Kul, J.Vacuum 107 (2014) 213-218.

[8] L.L.Cheng, M. H. Liu, S.C.Wang, M. X .Wang, G .D. Wang,Q. Y. Zhou, Z.Q Chen, J. Semicond. Sci. Technol 28 (2013) 015020.

[9]J. Gajendiran, V. Rajendran, J.Adv. Nat. Sci.: Nanosci. Nanotechno 2 (2011) 015001.

[10] U.C. Oh, Jung Ho Je, J. Appl. Phys 3 (1993) 1692.

[11] S. Biswas, S. Kar, S. Chaudhuri, J, Appl. Surf. Sci 253 (2007) 9259.

[12] JI .Pankove, Optical processes in semiconductors, Dover, New York, (1975).

[13] L. Chopra. K, Thin Film Phenomena. NewYork: McGraw-Hill, (1969).

[14] E.Guneri, C.Ulutas, F.Kirmizigul, G.Altindemir, F.Gode, C.Gumus, J.Chalcogenide Letters 7 (2010) 685-694.

[15] H. Moualkia, S. Hariech, M.S. Aida, J. Thin Solid Films518 (2009) 1259–1262.

[16] A.Bouhdjer, A.Attaf, H.Saidi, H.Bendjedidi, Y.Benkhetta, I.Bouhaf, J.Semiconductors 36(2015) 082002.

[17] B.G. Jeyaprakash, R. Ashok kumar, K.Kesavan, A. Amalarani,J .American Science 6 (2010) 3.

[18] P. Prathap, G. Gowri Devi, Y.P.V. Subbaiah, K.T. Ramakrishna Reddy,V. Ganesan, J. Curr. Appl. Phys 8 (2008) 120.

[19] L.L.Cheng , M.H.Liu , M.X .Wang, S.C Wang ,G.D Wang , Q.Y Zhou, Z.Q Chen, J.Alloys and Compounds 545 (2012) 122–129.

[20] S. Velumani, K. Narayandass, D. Mangalaraj, J.Semicond. Sci. Technol 13 (1998) 1016–1024.

[21] C. Sekhar. Ray, Malay K. Karanjai, Dhruba DasGupta, J.Thin Solid Films 350 (1999) 72-78.

[22] N.G. Deshpande, A.A. Sagade, Y.G. Gudage, C.D. Lokhande, J.Alloy Compd, 436 (2007) 421–426.

[23] O. Parasyuk, I.D. Olekseyuk, L.V. Piskach, S.V. Volkov, V.I. Pekhnyo, J. Alloys Compd 399 (2005) 173–177.

[24] T.H. Patel, J. Surface Science 4 (2012) 6-13.

[25] Q. Yang, K. Tang, C. Wang, J. Zuo, D. Zhang, Y. Qian,J. Thin Solid Films 436 (2003) 203–207.

[26] G .Kiruthigaa, R .Manoharan C, S. Dhanapandian, International Recent Scientific Research 5 (4) (2014)796-798.

[27] K. kamli, « Elaboration et caractérisations physico-chimique des couches minces de sulfure d'étain par spray ultrasonique: Effet des sources d'étain», Memory of magister, University of Med Khider-Biskra, (2013).

[28] T.H. Sajeesh, A.R. Warrier, C. Sudha Kartha, K.P. Vijayakumar, J.Thin Solid Films 518 (2010) 4370–4374.

[29] M.Calixto-Rodriguez, H.Martinez, A.Sanchez-Juarez, J.Campos-Alvarez, A. Tiburcio-Silver, M.E. Calixto,J. Thin Solid Films 517 (2009) 2497–2499.

[30] C.D. Lokhande, J. Phys D Appl Phys 23 (1990) 703.

[31] B.R. Sankapal, R.S. Mane, C.D. Lokhande, J. Materials Research Bulletin 35(2000) 2027–2035.

[32] **I.B. Kherkhachi**, A. Attaf, H.Saidi, A. Bouhdjar, H.Bendjdidi, Y. Benkhetta, R. Azizi, J.Main Group Chemistry15(2016) 231-242.

Chapter IV

Effect of solution flow rate on properties of tin sulfide thin films

In this chapter, we have studied the effect of the solution flow rate on the different properties such as the structural, optical and electrical of tin sulfide thin layers deposited by ultrasonic spray method.

We divide this chapter into 2 parts:

IV.1. Party A: Solution flow rate affects on tin sulfide thin films prepared at 4 min

We fixed the deposition time at 4 min and the solution flow rate S_f varied from 25 to 60ml/h.

IV.1.1.The films thickness and deposition rate

Figure.IV.1 shows variation of film thickness as a function of spraying solution, from which it is seen that film thickness continuously goes on increasing as the quantity of spraying solution increases. The expected reason for this is supply of more number of ingredient ions with increase in quantity of spraying solution. In figure inset, we have drawn the variation of the deposition rate; the latter is estimated from the ratio of film thickness on the deposition time fixed at 4 min. As can be seen the deposition rate varies linearly with the flow rate. The same variation observed by precedent studied [1].

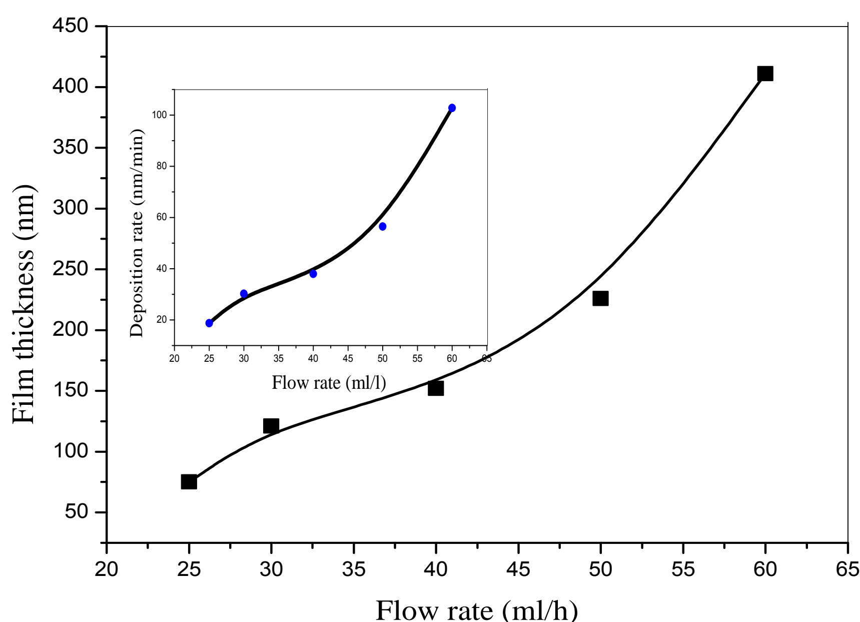

***Fig IV.1**: Variation of the films thickness and deposition rate as function of flow rate*

IV.1.2. Structural studies

In figure.IV.2 we reported the X-ray diffraction spectra of tin sulfide thin films deposited with different flow rates of the solution 25,30,40,50 and 60 ml/h.

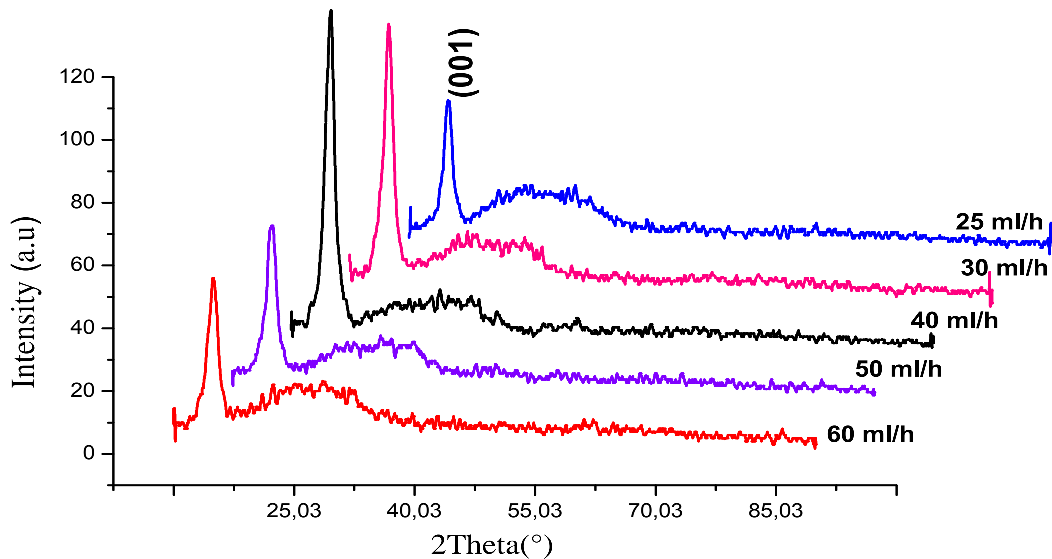

Fig.IV.2: *X-ray spectra of the samples of SnS_2.*

The XRD patterns for tin sulfide thin films grown at various flow rates are shown in figure.IV.2, it can be seen that all the films show a peak corresponding to SnS_2 hexagonal phase (JCPDS card No 23-0677) [2] with orientation in the plane (001) around the angle 2θ = 15.02°. Also, it can be shows that, the intensity of the peak (001) increase with increasing flow rate between 25-40 ml/l and after 40 ml/h decrease. The preferential orientation growth of the film is along the c-direction. C. Khelia et al [3] and L. Amalraj et al [4] have found the same peak (0 0 1) for film deposited by spray pyrolysis, in addition similar results about the formation of SnS_2 at various flow rate with (001) plane has been observed by other research [5].

IV.1.2.1. Lattice parameters, Crystallites size, Strain and Dislocation density

There is small difference for the peaks positions lattice parameters (a and c) between the experimental results and data. This may be caused by the defect in the cell of the crystal, which causes local changes in the lattice parameters. The results are shown in table.IV.1.

***Tab. IV.1**: Lattice parameters of SnS_2 thin film.*

SnS_2			**JCPDS card reference No 23-0677**
Flow rate (ml/h)	h k l planes	Lattice parameters (Å)	Hexagonal structure
25		a = 3.590 c = 5.852	*a* =3.648 *c* =5.899
30		a = 3.650 c = 5.950	
40	(001)	a = 3.614 c = 5.891	
50		a =3.533 c =5.760	
60		a = 3.653 c = 5.955	

The variations of the crystallite size together with the film strain are reported in figure.IV.3.

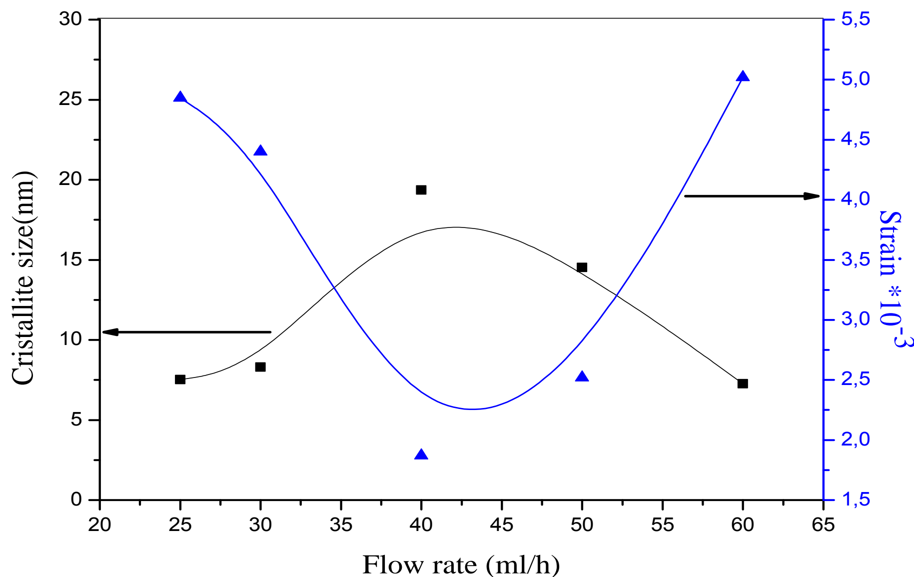

***Fig.IV.3**: Crystallite size and strain as a function of flow rate.*

The obtained crystallite size is ranged from 7.26 to 19.36 nm. The same order of crystallite size were observed by M. R. Fadavieslam [5] has found that the *average* crystallite size of 14.84 nm with variation of flow rates. The broad hump (25–40°) was ascribed to the amorphous glass substrates, which was also observed by other groups [4, 6, 7]. As seen, the crystallite size is increased with increasing the flow rate between 25-40ml/h, then decreasing. The decrease in crystallite size at higher S_f > 40 ml/min can be

attributed to adverse effect of S_f on nucleation which leads to poor crystallinity of film. This result is in good agreement with the XRD analysis which indicates that the best crystallinity is obtained for S_f = 40 ml/min. On the other hand an increase in the flow rate causes the decrease of strain in the formed crystallites entre 25-40ml/h, then increasing. The decrease in crystallite size in the thin layers of tin disulfide is due to the rise of the stress, this later is the results of internal strains [8].

Figure.IV.4 shows the variation of dislocation density and the number of crystalline with flow rate. It is observed that dislocation density decreased with increasing flow rate (25-40ml/h) then increased with increasing flow rate. Also according to this figure, the number of crystalline decreased slightly from $0.17x10^{18}$ to $0.049 x10^{18} m^{-2}$ with increasing flow rate from 25 to 40 ml/h and after that flow rate, it increased unexpectedly to the value of $1.06 x10^{18} m^{-2}$, in parallel we notice that the number of crystalline and the dislocation density are minimal for S_f = 40 ml/h. This behavior can be explained by the change of the particle's size (D) with S_f. Indeed, the smaller crystallites allow deposition in relatively large numbers and possibly the appearance of some linear defect (dislocation) and their development throughout the growing structure [9].

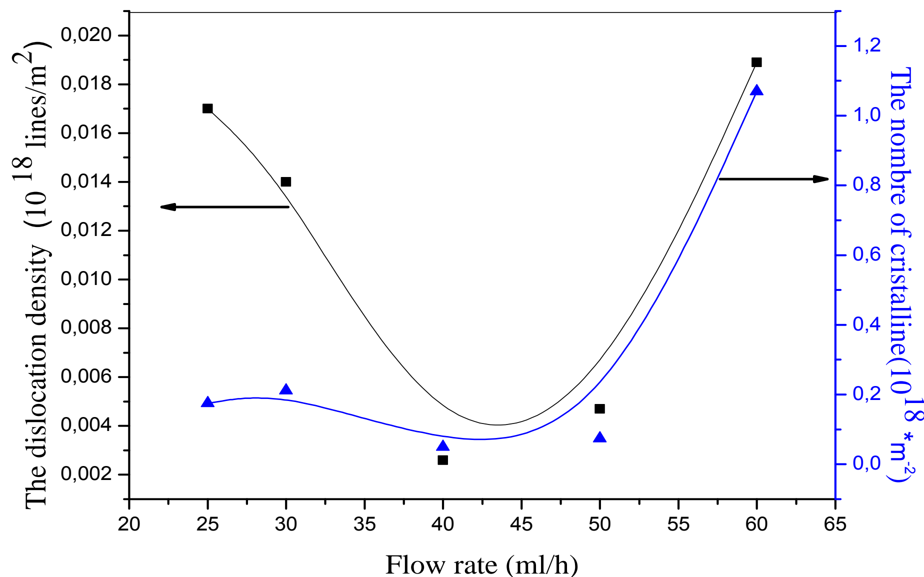

Fig.IV.4: *Variation of the dislocation density with flow rate of SnS_2 thin films.*

IV.1.3. Optical studies

Analysis of optical (transmission/absorption) spectra is one of the most useful techniques for the understanding of the band structure and energy gap of both crystalline and amorphous materials.

IV.1.3. 1.The transmittance

The optical transmittance measured as a function with wavelength of the tin disulfide (SnS_2) is depicted in figure.IV.5. The absence of interferences fringes in films transmittance spectra indicates that they have a should rough surface [10]. The films deposited with low flow rates 25ml/h exhibit higher transparency due to their low thickness. It can be seen that when the flow rate increases the transmittance decreases until 40 ml/h, then increases again with flow rate 50 ml/h (thickness of this film = 226 nm), and increase further.

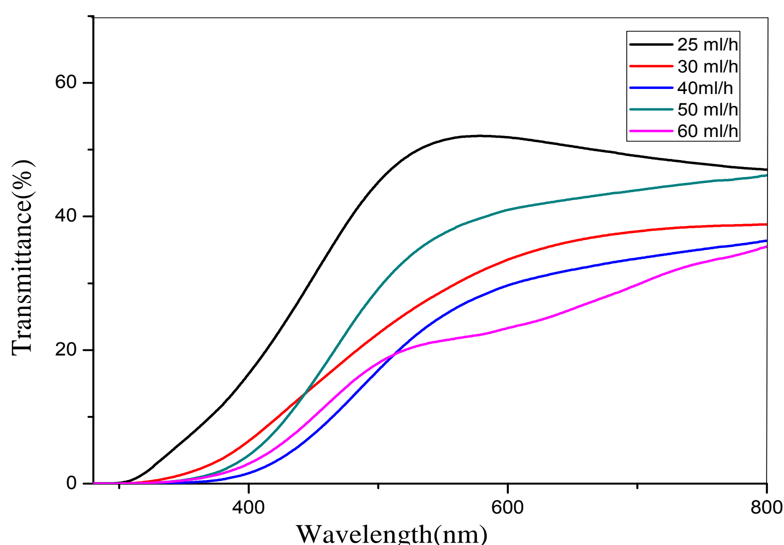

Fig.IV.5: *UV–visible transmittance spectrum of SnS_2 deposited at different flow rate.*

IV.1.3.2.The absorbance

Figure.IV.6 illustrates the variance of absorbance in the range of 300– 800 nm. It is evident that the absorption coefficient decreases with an increase in wavelength and a sharp decrease in absorption coefficient near the band edge indicate better crystallinity of the films, and the optical band gap.The films deposited at higher flow rate are more absorbent than the films deposited at lower flow rate.

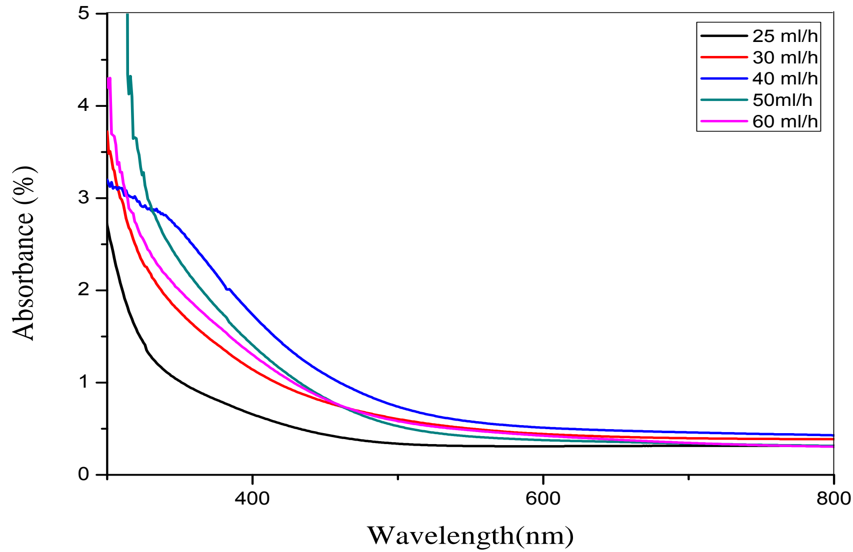

Fig.IV.6: *Spectral dependence of absorbance for SnS_2 films synthesized at different flow rates.*

IV.1.3.3.The optical band gap and disorder

The optical band gap and disorder of the films in various flow rates is determined from the plot of $(\alpha h\upsilon)^2$ versus $h\upsilon$ as shown in figure.IV.7. As can be seen, the optical band gap decreases with increasing flow rates. The values of optical gap are same with those obtained by precedent studies [11-14]. This decrease in optical band gap with increase in flow rate can be due to the increase in the film thickness. The similar results have been found in the previous research [15, 16]. The widening of the gap is due to the reduction of the disorder in the film [17].

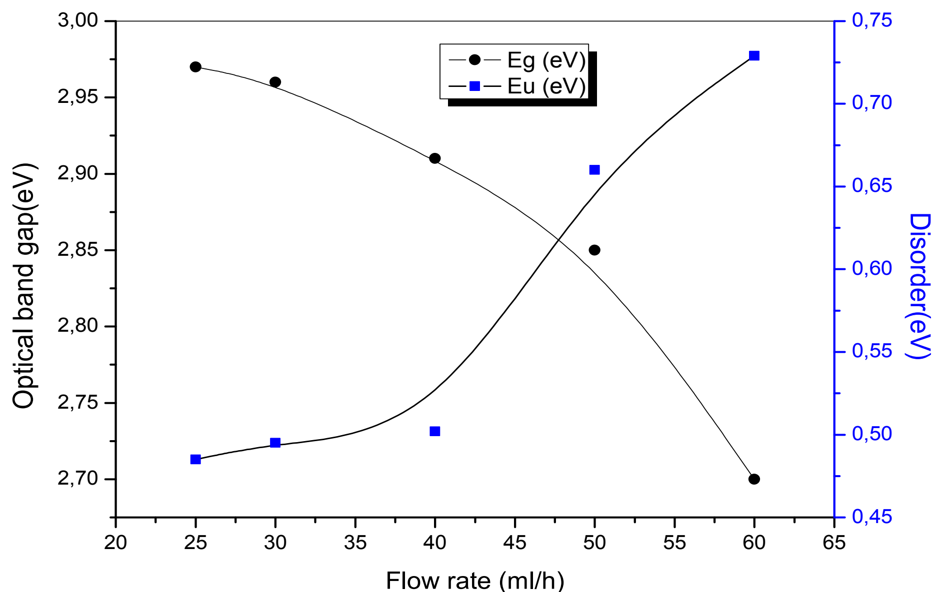

Fig.IV.7: *Variation of optical band gap energy and disorder of SnS_2 at different flow rate.*

IV.1.4. Electrical studies

The variation of films resistivity with flow rate is depicted in figure.IV.8. It is observed that resistivity decreases with increasing flow rate between 25-40 ml/h then increasing with increasing flow rate. The films showed average electrical resistivity of 5.67 $x10^{-4}$ Ω.cm. The electrical resistivity is improved, due to the grain coalescence structure and lowest resistivity of 3.2 $x10^{-4}$ Ω.cm is obtained at flow rate 40ml/h. This is mainly attributed to the decreasing of number of scattering centres and trapping centres in the grain boundaries in which the high dense and packed grains cause an increase of carrier mobility and electron concentration [18, 19]. This is supported by XRD analysis which indicates that the film grown at 40 ml/h have large grain size than the others films.The higher electrical resistivity of the films formed at flow rate after 40ml/h is due to decrease in grain size. Similar interpretation were obtained by Prathap et al. in Mo doped In_2O_3 films deposited by using the spray pyrolysis method [20] and obtained by E. Guneri et al in SnS thin films deposited by chemical bath deposition [21].

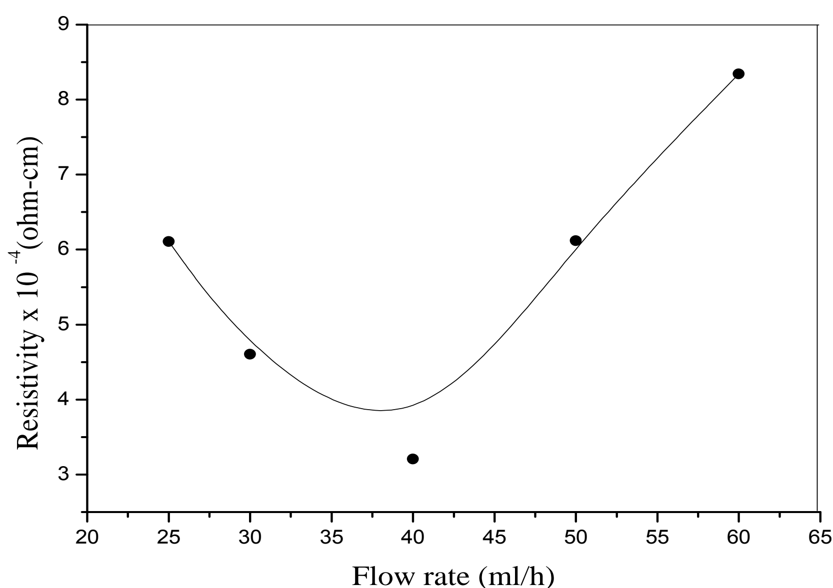

Fig.IV.8: *Variation of electrical resistivity with different flow rate.*

IV.2.Party B: Solution flow rate affects on tin sulfide thin films prepared at 6 min

We fixed the deposition time at 6 min and the solution flow rate S_f varied from 25 to 60ml/h.

IV.2.1.The films thickness and deposition rate

Figure.IV.9 shows variation in growth rate (nm/min) with solution flow rate. The growth rate increase with the increase of the solution flow rate due to the increase of film thickness (see figure.IV.9) as result of increase in spray volume flux over substrate surface.

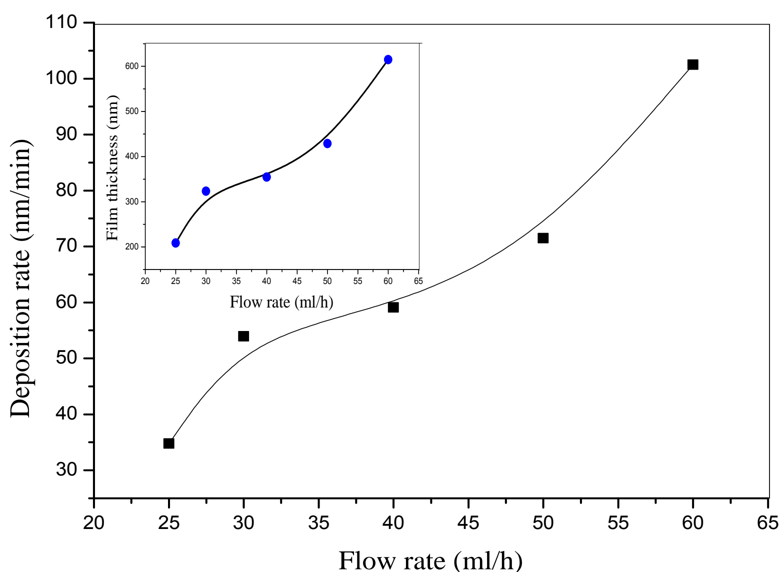

***Fig.IV.9**: Deposition rate dependence on solution flow rate, inset shows variation of film thickness as a function of solution flow rate.*

IV.2.2. Structural properties

The XRD patterns for tin sulfide thin films grown at 6min with different spray rate are shown in figure.IV.10. It is obvious that the SnS thin films reveal polycrystalline structure with peaks corresponding to SnS_2 hexagonal phase [6] with preferential from (001) plane and other peaks of minimum intensity corresponding to SnS,Sn_2S_3,$SnS_2$and SnO_2 phases with (100),(002),(112),(211),(221),(250),(003),(151),(310),(112),(102) and (110) plane. All peaks from XRD patterns coincide well with those given in the JCPDS card (no 23-0677, no. 390354 and no.14-0619) for tin sulfide and (no. 88-0287) for tin oxide. It is interesting to note that with the increasing of spray rates from 40 ml/h to 60 ml/h there is emergent of other peaks which corresponding to other SnS, Sn_2S_3 and SnO_2

phases. This indicates the possibility of controlling the phases by simply varying the flow of the solution. Indeed, the flow of cash coming into the surface of the growing film can alter and change the type of surface reactions involved in the formation of the film. On the other hand when comparing between the spectra XRD at different spray rate for tin sulfide thin films grown at 4 min and 6 min can be note that the film deposited at 6min show peak corresponding other phase. Also it is noted that the intensity of peak (001) increases with increased solution flow rate, and this is logical because it was well known that the (001) plane presents a lower surface free energy plane due to the high atomic density of this plane .

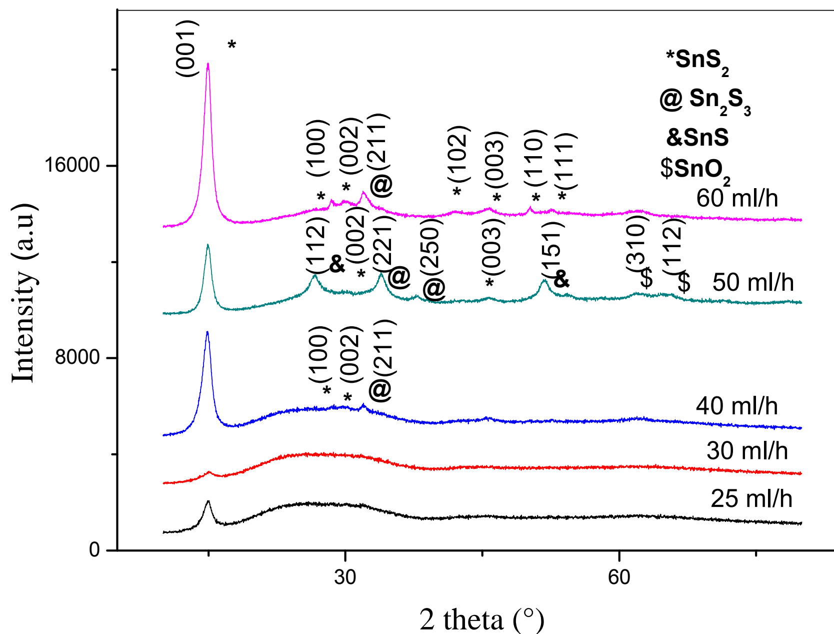

***Fig.IV.10**: XRD diffraction pattern of tin sulfide thin films prepared with different flow rate*

These results are compared with the results of ASTM files of SnS_2 and SnS (see the previous chapters) and ASTM files of Sn_2S_3 and SnO_2 are shown in figure.IV.11.

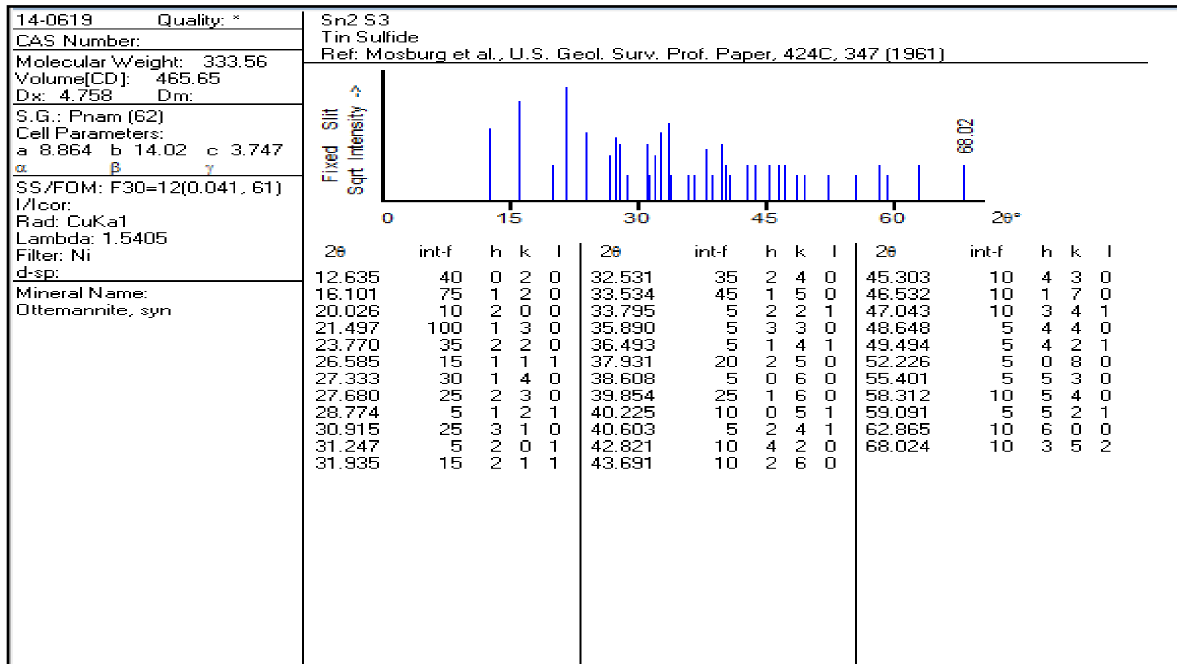

14-0619 Quality: *
CAS Number:
Molecular Weight: 333.56
Volume[CD]: 465.65
Dx: 4.758 Dm:
S.G.: Pnam (62)
Cell Parameters:
a 8.864 b 14.02 c 3.747
α β γ
SS/FOM: F30=12(0.041, 61)
I/Icor:
Rad: CuKa1
Lambda: 1.5405
Filter: Ni
d-sp:
Mineral Name:
Ottemannite, syn

Sn2 S3
Tin Sulfide
Ref: Mosburg et al., U.S. Geol. Surv. Prof. Paper, 424C, 347 (1961)

2θ	int-f	h	k	l	2θ	int-f	h	k	l	2θ	int-f	h	k	l
12.635	40	0	2	0	32.531	35	2	4	0	45.303	10	4	3	0
16.101	75	1	2	0	33.534	45	1	5	0	46.532	10	1	7	0
20.026	10	2	0	0	33.795	5	2	2	1	47.043	10	3	4	1
21.497	100	1	3	0	35.890	5	3	3	0	48.648	5	4	4	0
23.770	35	2	2	0	36.493	5	1	4	1	49.494	5	4	2	1
26.585	15	1	1	1	37.931	20	2	5	0	52.226	5	0	8	0
27.333	30	1	4	0	38.608	5	0	6	0	55.401	5	5	3	0
27.680	25	2	3	0	39.854	25	1	6	0	58.312	10	5	4	0
28.774	5	1	2	1	40.225	10	0	5	1	59.091	5	5	2	1
30.915	25	3	1	0	40.603	5	2	4	1	62.865	10	6	0	0
31.247	5	2	0	1	42.821	10	4	2	0	68.024	10	3	5	2
31.935	15	2	1	1	43.691	10	2	6	0					

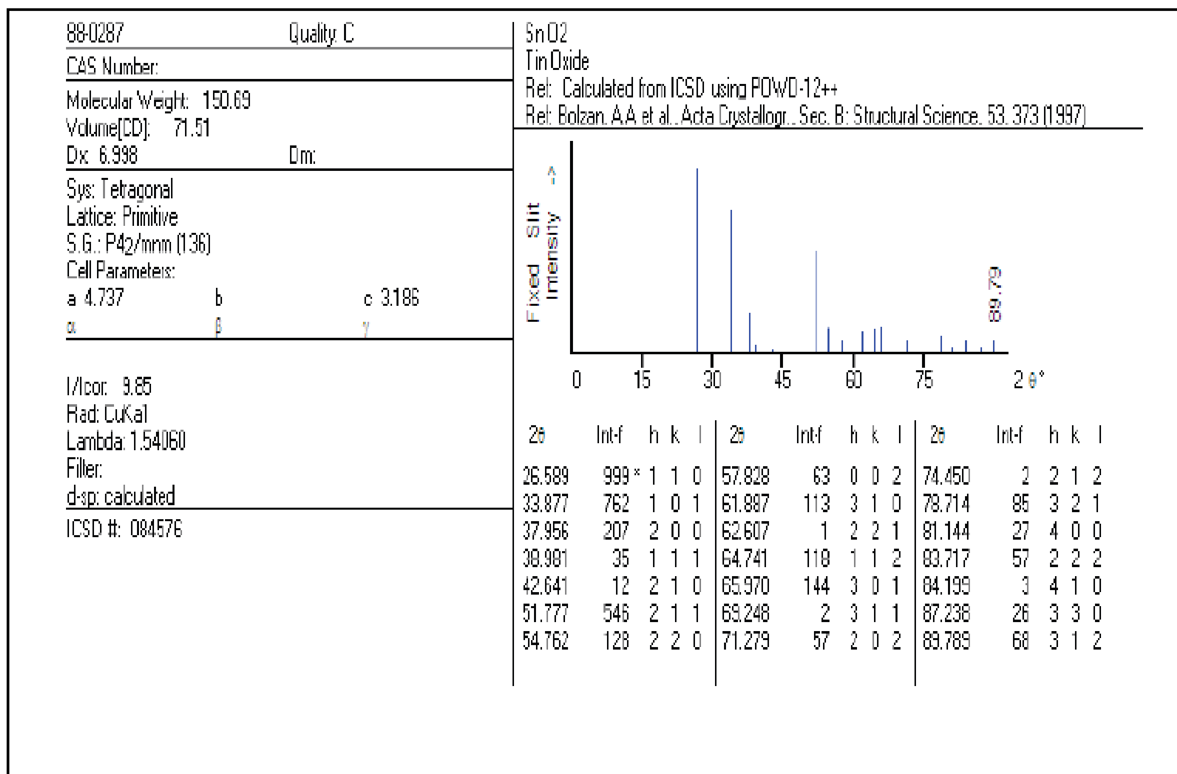

88-0287 Quality: C
CAS Number:
Molecular Weight: 150.69
Volume[CD]: 71.51
Dx: 6.998 Dm:
Sys: Tetragonal
Lattice: Primitive
S.G.: P42/mnm (136)
Cell Parameters:
a 4.737 b c 3.186
α β γ
I/Icor: 9.65
Rad: CuKa1
Lambda: 1.54060
Filter:
d-sp: calculated
ICSD #: 084576

Sn O2
Tin Oxide
Ref: Calculated from ICSD using POWD-12++
Ref: Bolzan, A.A et al., Acta Crystallogr., Sec. B: Structural Science, 53, 373 (1997)

2θ	Int-f	h	k	l	2θ	Int-f	h	k	l	2θ	Int-f	h	k	l
26.589	999 *	1	1	0	57.828	63	0	0	2	74.450	2	2	1	2
33.877	762	1	0	1	61.887	113	3	1	0	78.714	85	3	2	1
37.956	207	2	0	0	62.607	1	2	2	1	81.144	27	4	0	0
38.981	35	1	1	1	64.741	118	1	1	2	83.717	57	2	2	2
42.641	12	2	1	0	65.970	144	3	0	1	84.199	3	4	1	0
51.777	546	2	1	1	69.248	2	3	1	1	87.236	26	3	3	0
54.762	128	2	2	0	71.279	57	2	0	2	89.789	68	3	1	2

Fig.IV.11: *ASTM files of Sn_2S_3*

IV.2.2.1.Lattice parameters, crystallites size, strain and dislocation density

The lattice parameters were calculated using the observed values for the (0 0 1) plane and using the d values (inter-planar spacing) for the hexagonal structure and the results are given in table.IV.2. Comparing the observed parameters with the standard

values, the values of lattice parameter a and c of the sample deposited at 25, 30 and 60 ml/h are lower and whereas, lattice parameter of the sample deposited at 40and 50 ml/h are higher. This could be an indication of stress in the films.

***Tab. IV.2**: Structural parameters of SnS_2 thin film*

Flow rate (ml/h)	2θ (°)	d_{hkl} (A°)	a (A°)	c (A°)	c/a	ASTM file
25	15.012	5.860	3.597	5.860	1.629	a =3.648 c =5.899
30	15.073	5.860	3.597	5.860	1.629	
40	14.934	5.936	3.644	5.936	1.628	
50	14.954	5.936	3.658	5.936	1.622	
60	14.808	5.860	3.597	5.860	1.629	

Table.IV.3 shows the crystallite size for tin sulfide thin films at different solution flow rate with (001),(112),(151) and (211) plans corresponding to SnS_2, SnS and Sn_2S_3 phases respectively. It can be observed that, at lower solution flow rate 25 and 30ml/h, the crystallite size corresponding to (001) plane is almost constant, and with increase in S_f, the crystallite size becomes bigger. While the calculated average crystallite size corresponding to (112) and (151) plan value of 13.25 nm at 50 ml/h.Whereas the crystallite size corresponding to (211) plan do not change at 40 and 60 ml/h. This behavior observed in the crystallite size with solution flow rate was also supported by XRD results.

***Tab. IV.3**: Crystallite size dependence on flow rate with (211), (001), (112) and (151) plans*

Flow rate(ml/h)	Crystallite size(nm)		
	(211)	(001)	(112), (151)
25	-	10.252	-
30	-	10.253	-
40	16.119	22.731	-
50	-	17.859	12.74, 13.767
60	16.199	27.785	-

Figure.IV.12 presents variation of grain size and strain as a function of solution flow rate. The results show that grain size increases from 10 to 22 nm with increasing of the solution flow rate between 25-40ml/h, then slightly decrease again with flow rate 50 ml/h, and increase further. Generally the grain size increases with increase in flow of the solution. This increase controlled by the flow rate can be explained as follows:

For low values of the flow rate, may be the particles arrive over the substrate are virtually dry and they are distributed on the substrate slowly, and with increasing solution flow rate the droplets arriving on the substrate increases; the large grains which absorb other small grains, it is deposited over substrate, and a dense film is formed, hence the increase of the particle size. Therefore we can conclude that the porosity decreases and the particle size increases while the flow increases [22]. While the strain vary inversely.

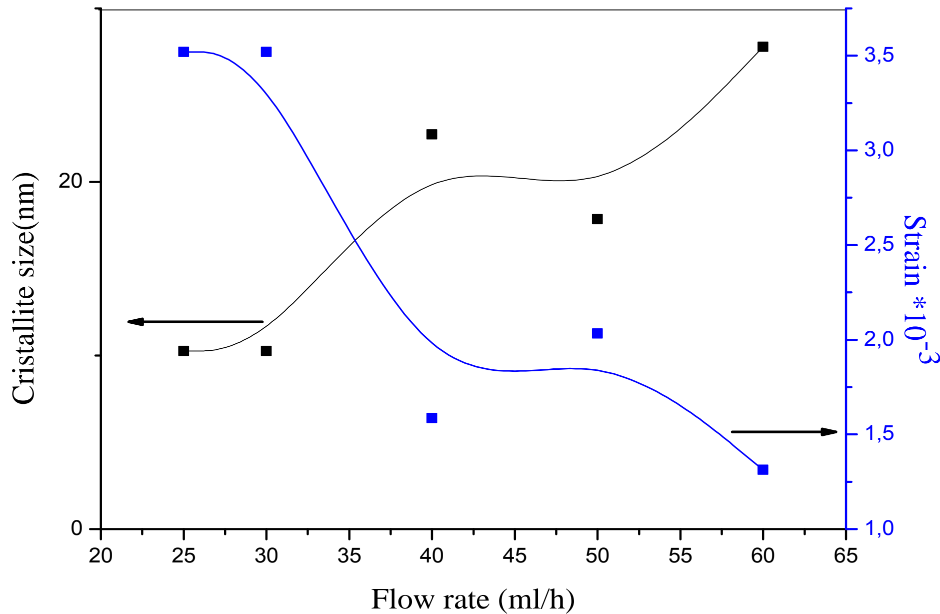

***Fig.IV.12**: Dependence of crystallite size and strain on flow rate.*

IV.2.3.Optical properties

IV.2.3.1.The transmittance

Figure.IV.13 shows the dependence of the optical transmission and spectra of the investigated thin films in the wavelength region 250–800 nm as a function of solution flow rate. It can be seen that the transmittance generally decreases with increasing the flow rate of 25 to 60 ml / h and this can be explained by the increase in thickness which induces an increase in the number of molecules (Beer law -Lambert) [23]. Furthermore, it is clear that the interference fringes absence in the spectrum of films. This can be attributed to the roughness of the interface air/film. On the other hand the films deposited at solution flow rate 60 ml/h show low optical transmittance (36%), thus we can say that our films applicable to the photovoltaic field.

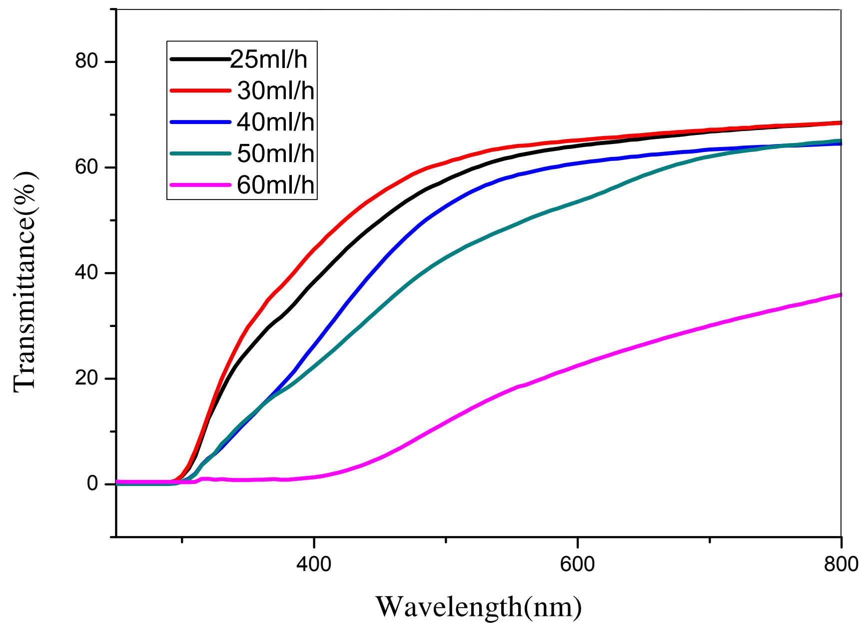

Fig.IV.13: *Optical transmittance spectra of tin sulfide thin films as a function of solution flow rate*

IV.2.3.2.The optical band gap and disorder

The optical band gap decreases with increasing flow rate while the disorder varies inversely (Figure.IV.14).

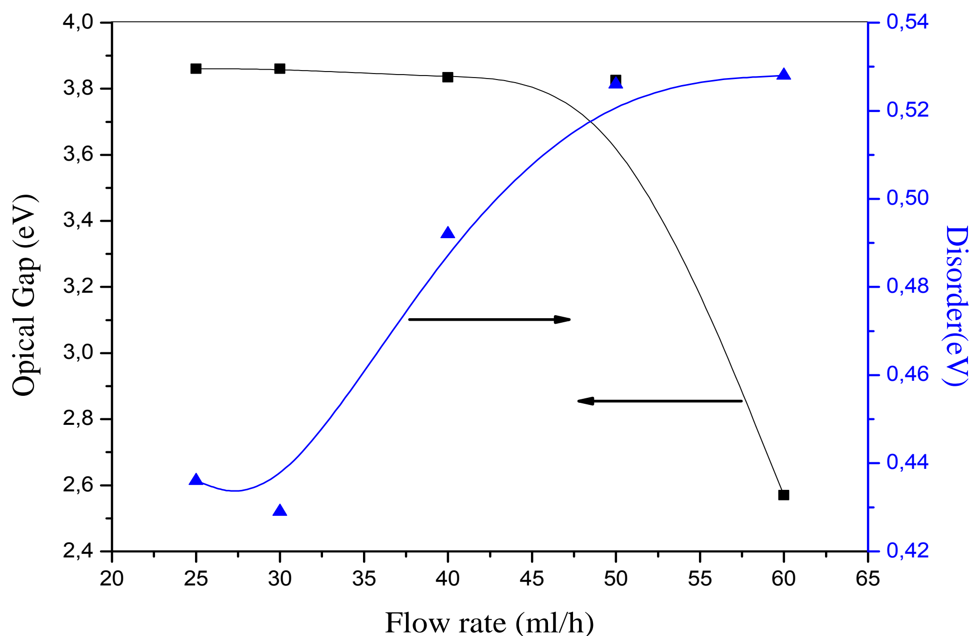

Fig.IV.14: *Variation of optical band gap and urbach energy of SnS at different flow rate.*

The optical gap values are larger than those reported by studies except the value of optical gap for film deposited at 60 ml/h is the same with those obtained by other research [11].The variation of the optical gap and the crystallite sizes reveals that the gap has an opposite behavior regarding the crystallite variation and as already mentioned above due to the small crystallite size, we have a quantum restriction regime that may modify the electronic films properties. It is manifested by the appearance of discrete energy levels. So the crystallite size decreases the optical gap is widened. The widening of the gap is due to the reduction of the disorder in the film [17].

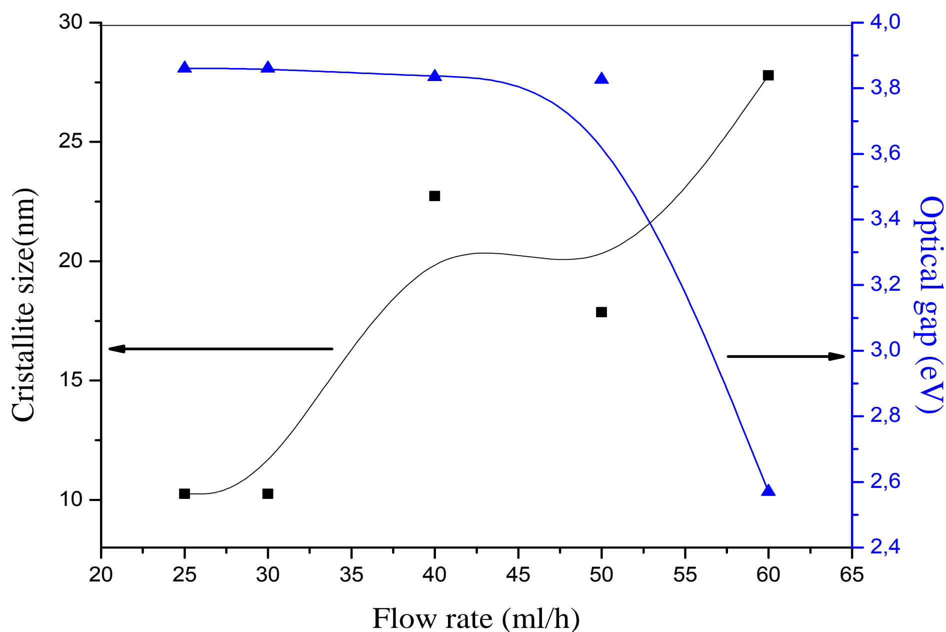

***Fig.IV.15**: Variation of crystallite size and optical band gap of SnS with various flow rates.*

IV.2.3.3.Photoluminescence properties

The room temperature photoluminescence (PL) spectrum of tin sulfide, deposited with different spray solution flow rates (S_f = 25, 30, 40, 50 and 60 ml/l) is given in figure.IV.16. PL spectra consist of three emission peaks centered at about 400(purple), 453 (blue), 530 nm (green). Here it is quite obvious that three emission peaks are the most intense for sample prepared at the spray flow rate of 25ml/h .The energy corresponding to all the observed emission peaks (3.1, 2.73 and 2.33 eV) is lower than the band gap energy of the films deposited at 25, 30, 40 and 50ml/h , they cannot be assigned to the direct recombination between electrons in the conduction and holes in the valence band while the

energy corresponding to the observed emission peaks (3.1 eV and 2.73 eV) is higher than the band gap energy of the film deposited at 60 ml/h ,this peak corresponds to the radiative recombination of bound excitons, where the explanation for the origin of the broad peaks at 400 and 530 nm may be from the inner deep level emission. This deep level arises because of the stoichiometric variation in SnS_2 phase .N.G. Deshpande et al [11] have reported a PL peak at 549.78 nm for tin disulfide thin films. The present result is very well agreeing with this observation. Also Chunrui Wang et al [24] have found the five bands appearing around 330, 360, 370, 390 and 420 nm. The later band is closely of band (400 nm) observed in our result.

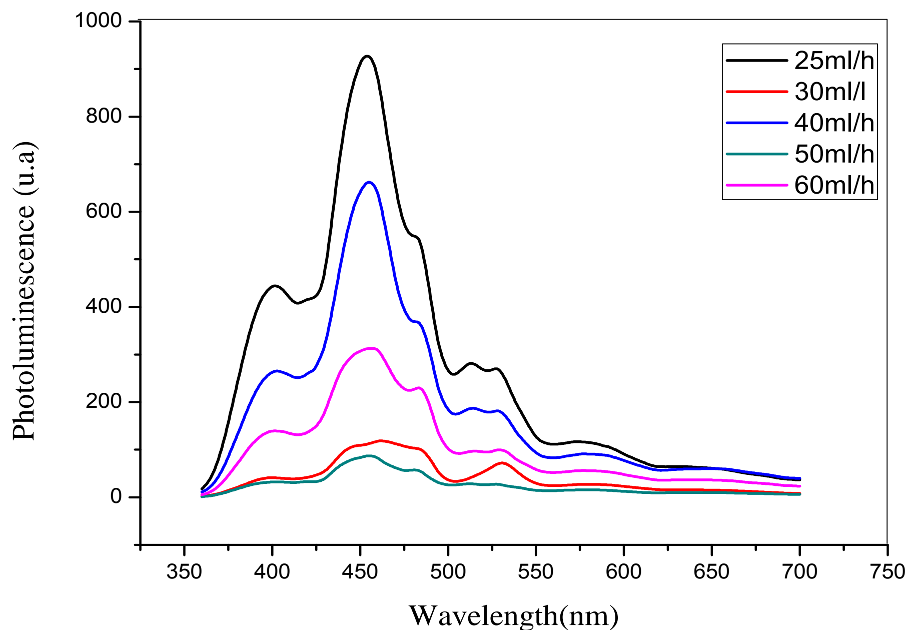

Fig.IV.16: *Photoluminescence spectra of SnS sprayed thin films.*

IV.2.3.4.The reflectance

Figure.IV.17 shows variation of reflectance as function of wavelength for tin sulfide films prepared at different flow rate. It is clear that the reflectance increases with the increase of the solution flow rate from 25-40 ml/h then decrease (at S_f = 50ml/h) and after that increase. This increase refers to the increase of thickness of films which is controlled by flow rate.The variation of reflectance is supported by the variation of transmittance. But we note that the values of reflectance are generally large and that's logical because the films are roughness and the interference fringes are not present in the spectra of transmittance.

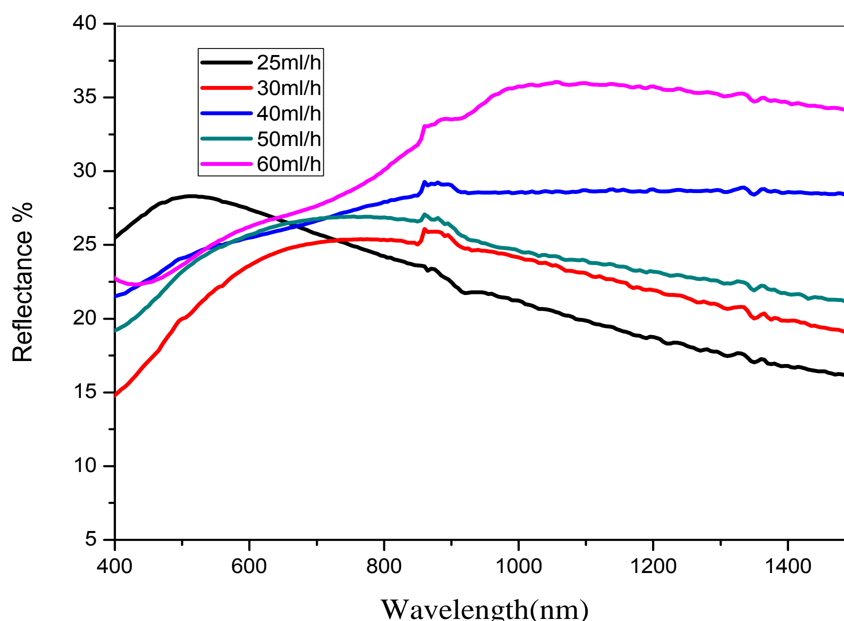

***Fig.IV.17**: Variation of reflectance for the SnS thin films deposited at various solution flow rate.*

IV.2.3.4.a.The refractive index

The refractive index of SnS films is shown in figure.IV.18. It was determined from this figure that the refractive index decreases with increase flow rate between 25-30ml/l then increase with increase flow rate to 40 ml/h after that it is almost constant. S. Mandalidis et al, found that the values of refractive indices exhibited by the SnS_2 films is almost constant (3) [25]. Similar observation reported by other authors for SnS_2 and Sn_2S_3 thin films [26, 27]. These results agree our studies. Anis Akkari et al observed that the values of refractive indices of SnS films varied from 1.7 to 2.7 [28]. Decrease of the refractive index indicates that the film density decrease. That is, when the incident light interacts with a material which has low amount of particles, there fraction will below, and thus the refractivity of the films decrease [29]. The presence of SnS and Sn_2S_3 phases according to the above X-ray patterns of films deposited at S_f>30ml/h due to the increase of the refractive index.

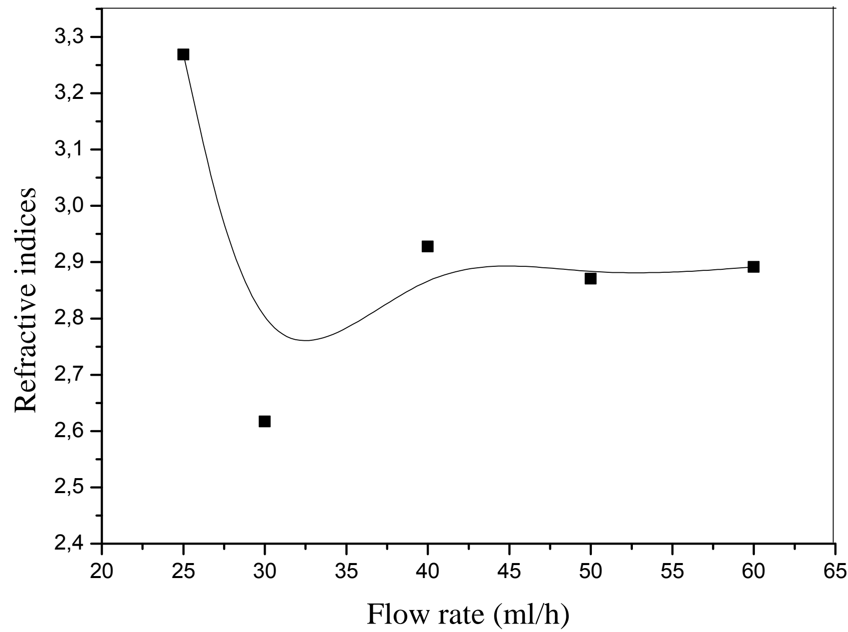

Fig.IV.18*: Variation of refractive index (n) for tin sulfide thin films grown at different flow rate*

IV.2.3.4.b.The extinction coefficient

The variation of extinction coefficient k with increase flow rate is shown in figure.IV.19.

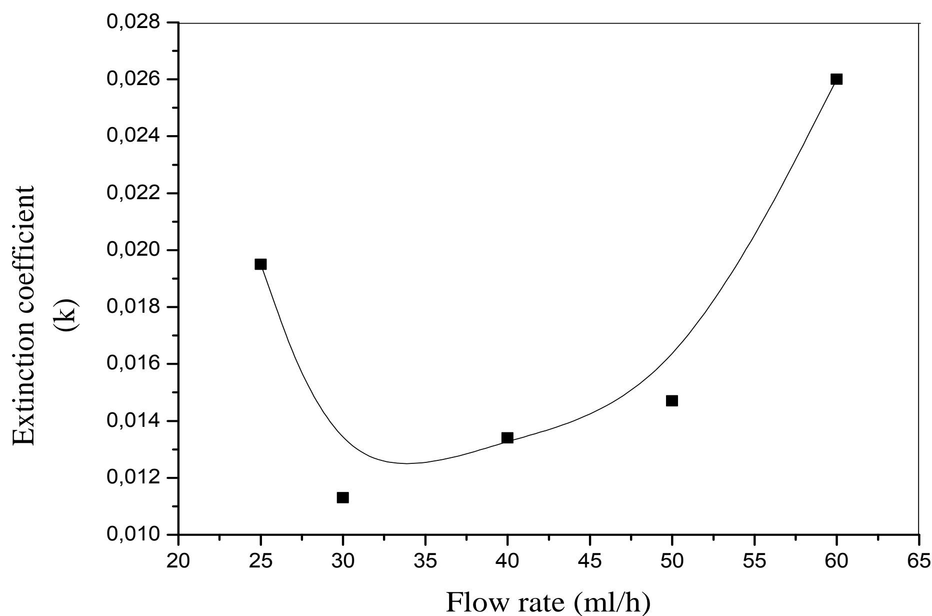

Fig.IV.19*: Plot of extinction coefficient 'k' of SnS grown for different flow rate*

It has been found that the extinction coefficient k is varying in the range of 0.011-0.026. S. Mandalidis et al [25] have also observed a similar value of extinction coefficient in the stoichiometric composition technique deposited SnS_2 single crystals. The low value of extinction coefficient as observed of film deposited at S_f =30 ml/h is a qualitative indication of surface smoothness and homogeneity of this films. In contrary for film deposited at S_f=60 ml/h which is the most roughness.

IV.2.3.4.c.The dielectric constant

The dielectric constant of tin sulfide thin films obtained at different solution flow rate presented in figure.IV.20.The sample obtained at 30 ml/h shows low values of the real and imaginary parts of the dielectric constant. Similar values to those reported by other authors for SnS_2 thin films [30].

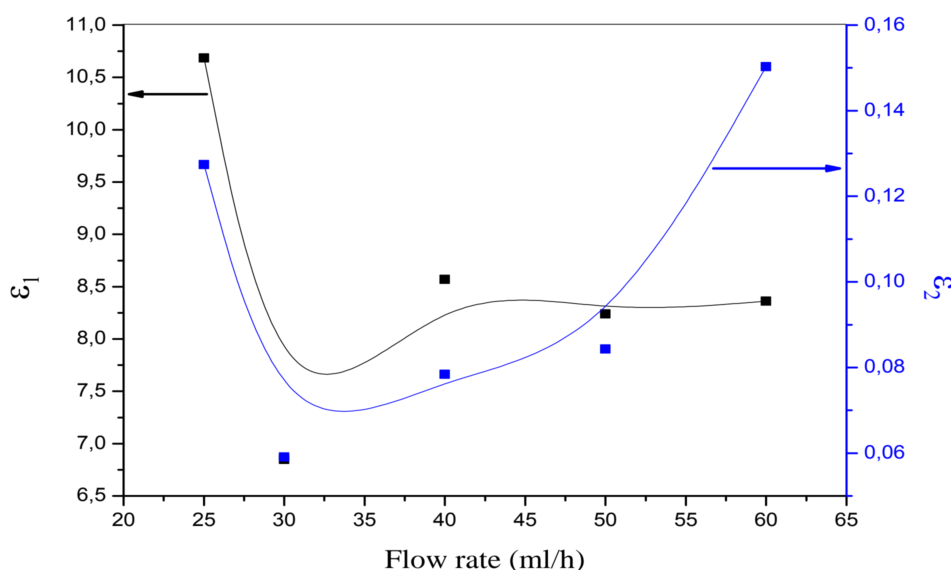

Fig.IV.20*: Variation of the real (ε_1) and imaginary (ε_2) parts of dielectric constant of SnS thin films as-grown at different flow rate*

IV.2.4.FTIR studies

Infrared (IR) refers broadly to that part of the eleactromagnetic spectrum between the visible and microwave regions.FTIR is conceivably the most powerful tool for identifying the functional groups or the types of chemical bonds. FTIR spectrums of tin sulfide thin films prepared at different flow rate of 25, 30, 40, 50 and 60 ml/h are presented in figure.IV.21. It is clearly observed that the adsorption band in the range of 500-800 cm^{-1} and of 1086 - 1350 cm^{-1} for films deposited at S_f =50 ml/h and 60ml/h and, with

decreasing the solution flow rate the intensity of these band disappears. Moreover, it can be seen for the solution flow rate equal to 60ml/ h bung a broad and strong band absorption and the intensity of peak is maximum and with decreased solution flow rate to 50ml / h this intensity reduce. The peaks appeared in interval 500-800 cm^{-1} in the spectrum are due to the formation of Sn – S , SnO and SnO_2 bond [31-33] .On other hand weak bonds observed at 1032 cm^{-1} for film deposited at 50ml/h and at 827 and 984 cm^{-1} for film deposited at 60ml/h. The peaks with the wave numbers of 827 and 984 cm^{-1} are ascribed to the stretching vibration of Sn-S bonds, indicating the formation of SnS film [34]. These peaks are in good agreement with the XRD results .This is supported by the transmittance and reflectance which indicate that the films deposited at 50 ml/h and 60 ml/h are plus roughness and absorbent. Finally, we conclude that the films obtained at higher flow rate are more absorbent.

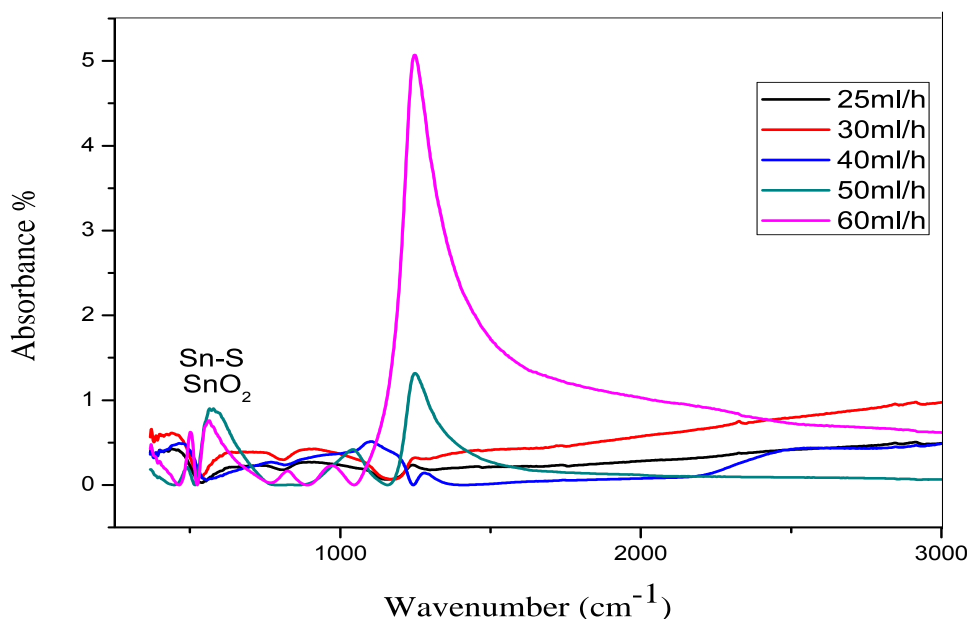

Fig.IV.21*: FTIR spectra of SnS films at different flow rate*

IV.3. Conclusion

The spray ultrasonic technique has been successfully used to obtain SnS_2 films at 4 min with various flow rates and SnS_2, SnS and Sn_2S_3 at 6 min, From the X-ray diffraction, we inferred that films have a hexagonal structure with preferential orientation (001) corresponding to SnS_2 phase and others small peaks (111), (112), (002), (211), (221) and (250) corresponding to SnS and Sn_2S_3 .In addition, SnO_2 phase appeared only at deposition time 6min and at flow rate 50 ml/h. The optical characterization showed that our films are absorbent and the high absorbance was detected for flow rate equal to 60 ml/h and the direct band gaps is 2.57 eV at 6 min. The films resistivity varies from 3.2 $x10^{-4}$to $8.34x10^{-4}$ Ω.cm. Finally, we conclude that the tin sulfide films deposited at 6 min and at higher solution flow rate with the values of band gap obtained are suitable for absorber layers in solar cells.

References of fourth chapter

[1] M. Messaoudi**,** «Elaboration et Caractérisation de Couches Minces SnS », Doctorate thesis, University of Mentouri-Constantine, (2016).

[2] **I.B. Kherchachi**, H.Saidi, A. Attaf, N.Attaf, A.Bouhdjar, H.Bendjdidi, Y. Benkhetta, R. Azizi, M.jlassi. J. Optik 127 (2016) 4043-4046.

[3] C. Khelia, K. Boubaker, T. Ben Nasrallah, Mr. Amlouk, S. Belgacem, J. Alloys and Compounds 477(2009)461-467.

[4] L.Amalraj, C.Sanjeeviraja, M.Jayachandran, J .Cryst Growth 234 (2002) 683–689.

[5] M.R.Fadavieslam, N.Shahtahmasebi, M. Rezaee-Roknabadi, M.M. Bagheri-Mohagheghi, J.Semiconductors 32 (2011) 113002.

[6] B.R. Sankapal, R.S. Mane, C.D. Lokhande, J.Materials Research Bulletin 35 (2000) 2027–2035.

[7] SK .Panda, A .Antonakos, E. Liarokapis, S .Bhattzcharya and S. Chaudhuri, J. Mat. Res. Bull 42(2007) 576.

[8] B.G. Jeyaprakash, R. Ashok kumar, K.Kesavan, A. Amalarani, J. American Science 6 (2010) 3.

[9] A. Akkari, « Synthèse et caractérisation physico-chimiques de couches minces de sulfure d'étain en vue de leur utilisation dans des dispositifs photovoltaïques », Doctorate thesis, University of Montpellier II, (2011).

[10] **I. B. Kherchachi**, A. Attaf, H. Saidi, A. Bouhdjer, H. Bendjedidi, Y. Benkhetta, R. Azizi, J. Semiconductors 37(2016) 032001.

[11] N.G. Deshpande, A.A. Sagade, Y.G. Gudage, C.D. Lokhande, J.Alloy Compd 436 (2007) 421–426.

[12] O.V. Parasyuk, I.D. Olekseyuk, L.V. Piskach, S.V. Volkov, V.I. Pekhnyo, J. Alloys Compd 399 (2005) 173–177.

[13] M.M. Kamel, M. M. Ibrahim, J .Solid State Electrochem 15 (2011) 683–688.

[14] V. Robles, J. F. Trigo, C. Guille´n, J. Herrero, J. Mater Sci 48 (2013) 3943–3949.

[15] O .Ogah, G .Zoppi, I. Forbes, R. Miles, J. Thin Solid Films 517(2009) 4702.

[16] MS. Selim, ME .Gouda, MG .El-Shaarawy, AM .Salema, WA .Abd El- Ghany, J. Appl Sci Res 7 (2011) 955.

[17] JI .Pankove, Optical processes in semiconductors; Dover, New York, (1975).

[18] D.Song, P. Widenborg, W. Chin, A. G. Aberle, J.Solar Energy Materials & Solar Cells 73 (2002)17.

[19] H. Kim, J.S. Horwitz, G.P. Kushto, S.B. Qadri, Z.H. Kafafi, D.B. Chrisey, J. Appl Phys Lett 78 (2001) 1050.

[20] P. Prathap, N. Revathi, K.T. Ramakrishna Reddy, R.W. Miles, J. Thin Solid Films 518 (2009) 1271–1274.

[21] E. Guneri, C .Ulutas, F .Kirmizigul, G .Altindemir, F .Gode, C. Gumus, J.Appl Surf Sci 257 (2010)1189.

[22] Ca. Matei Ghimbeu, « Préparation et Caractérisation de couches minces d'oxides métalliques semiconducteurs pour la détection de gaz polluants atmosphériques », Doctorate thesis, University of Paul Verlaine de Metz, (2007).

[23] M.Caglar, Y.Caglar, S.Ilican, J.Optoelectronics and Advanced Materials 8 (2006)1867.

[24] C. Wang, K. Tang, Q. Yang, Y. Qian, J. Chemical Physics Letters 357 (2002) 371–375.

[25] S. Mandalidis, J. A. Kalomiros, K. Kambas, A. N. Anagnostopoulos, J.Materials science 31 (1996) 5975-5978.

[26] J .Bords, J .Robertson, A .Jakobsson, J Phys C 11 (1978)2607.

[27] M. Khadraoui, N .Benramdane, C .Mathieu, A .Bouzidi, R. Miloua, Z. Kebbab, K.Sahraoui, R .Desfeux, J.Solid State Commun 150 (2010) 297.

[28] A. Akkari, M.Reghima, C.Guasch, N. Kamoun-Turki, J .Mater Sci 47 (2012) 1365-1371.

[29] R. Mariappana, T.Mahalingam, V.Ponnuswamy, J.Optik 122 (2011) 2216– 2219.

[30] V. Robles, J. F. Trigo, C. Guillen, J. Herrero, J .Mater Sci 48 (2013) 3943–3949.

[31] K. Nakamoto, IR Spectra of Inorganic and Coordination, Compounds-2nd Ed, Wiley Eastern NY, (1970).

[32] B. Orel, K. Lavancic Stangak, Z. Crnjak-Orel, P. Bukovec, M. Kosec, J. Non-Crystal. Solids 167 (1994) 272.

[33] M. Gartner, C. Savaniu, C. Parlog, M. Zaherescu, G. Craciun, O. Buiu, E. Szilagy, C. Cobianu, Proceedings of the International Semiconductor Conference, Sinae, Romania 1997 (1997)71–74.

[34] M. Kul, J.Vacuum 107 (2014) 213-218.

Substrate temperature effect on properties of tin sulfide thin films

In this chapter, we investigate the influence of substrate temperature T_s and determining the structural, optical and electrical properties of the tin sulfide thin films.

We divide this chapter into two parts:

V.1. Party A: Influence of substrate temperature for films deposited at 4 min and 50 ml/h

In this section, the deposition time was 4 min, the solution flow rate S_f was 50ml/h all of them were kept constant. However, the substrate temperature T_s varied from 100 to 400 °C.

V.1.1.The films thickness

The variation of film thickness with the increase in the substrate temperature shown in figure.V.1:

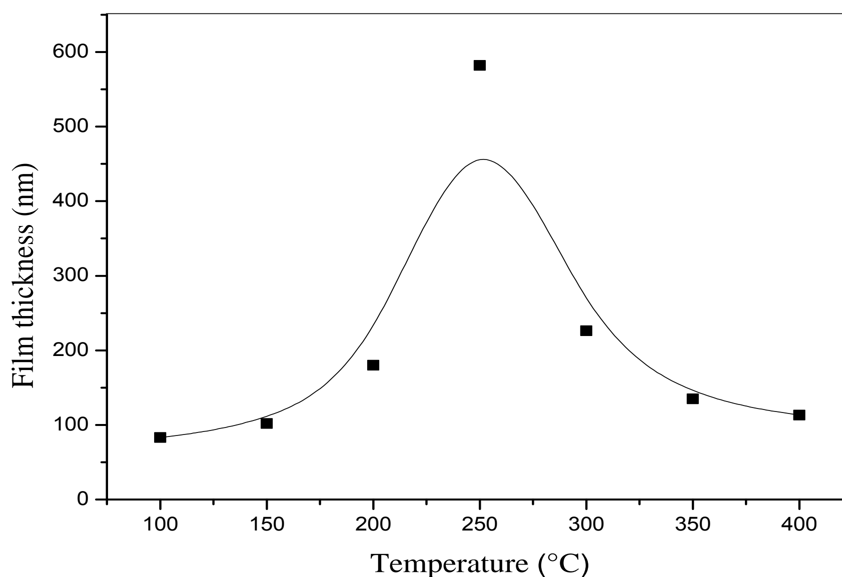

Fig.V.1: *The Variation of film thickness as a function of substrate temperature.*

In the interval [100-250°C] of the substrate temperature, the thickness increases steadily with increase of temperature. This increase in film thickness is due to the activation of the chemical reaction in surface species contributing to the film formation.

From 250°C, although the kinetics of reactions forming the tin sulfide should increase with temperature, there is a decrease in thickness. This can be explained by the decrease in the mass transported to the substrate heated at elevated temperatures [1]. This reduction in

thickness is caused by convective upward flow of hot air which deflects the fine droplet of their trajectory towards the substrate, and increases their re-evaporation of the compounds. Such a decrease in thickness with increase in T_S between 300-500°C for films fabricated using spray pyrolysis technique has been reported earlier [2].

V.1.2. Structural studies

Figure.V.2 represents the X-ray diffraction spectra of the films SnS prepared at different substrate temperatures.

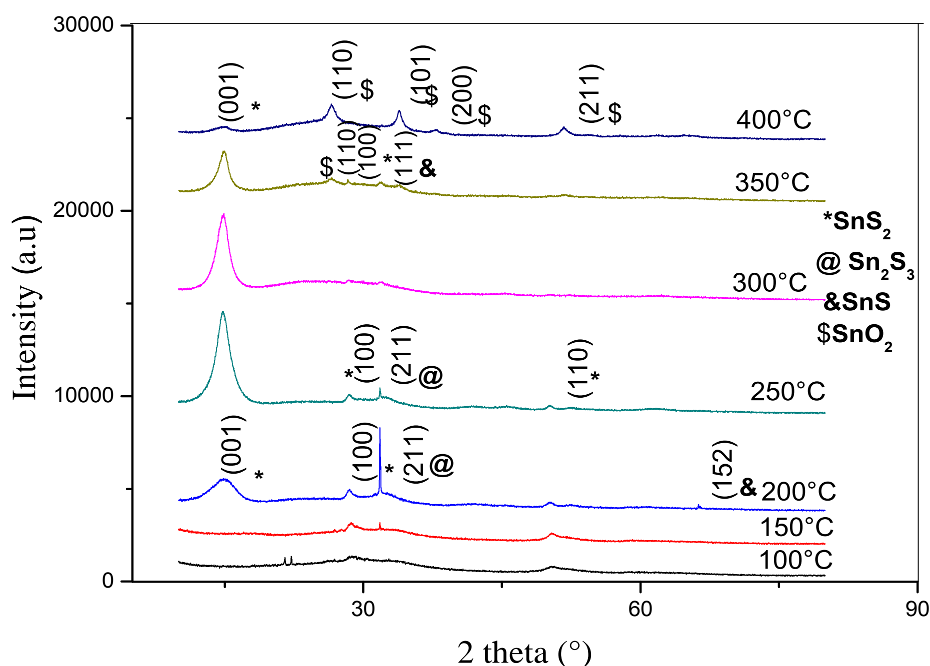

Fig.V.2: *XRD pattern of SnS thin film sample with different substrate temperatures.*

X ray diffraction data showed that layers grown at temperature 100°C and 150°C were fine grain polycrystalline of three small peaks which corresponds to the (100) and (110) direction of the SnS_2 phase and (211) direction of the Sn_2S_3 phase while those formed at temperature in the range 200-350°C indicated the presence of SnS_2, Sn_2S_3 and SnS phases. The Sn_2S_3 phase dominated at temperature 200°C with (211) plan of 2θ values of 31.78° (JCPDS card no. 14-0619) while the SnS_2 phase with (001) present increased with temperature and this phase became predominant at temperature 300°C (JCPDS card No 23-0677) and SnS phase appeared with (111) and (152) at 350°C and 200°C respectively (JCPDS card No 390354). Otherwise, the films grown at the highest temperature >300°C show an peak (001) corresponding to SnS_2 phase and SnO_2 phase

appeared with three directions (110), (200) and (211) (JCPDF no. 88-0287). Additionally, the intensity of the peak (001) decreases with increasing substrate temperature, in contrary for the intensities of the peaks correspondent SnO_2 phase. On other hand the films deposited at T_s =300°C show the better crystallization for the SnS_2 phase than those deposited at other temperature. Similar results about of predminant SnS_2 phase when increase the temperature to 300°C and appeared of SnS phase in the range 300-360°C too the dominant of Sn_2S_3 phase at low temperatures using spray pyrolysis obtained by several studies [3,4]. The influence of the substrate temperature on the crystal structure of SnS films was reported by other researchers such as, N. Koteswara Reddy et al [5] have studied the effect of T_s in the range 300–350°C using spray pyrolysis, in their studies observed one phase corresponding to SnS phase and M. Calixto-Rodriguez et al [6] have observed different SnS thin film compounds can be obtained by changing T_s=320–396 °C. Furtherer T.H. Sajeesh et al [2] have confirmed that all the films had predominant SnS phase, when T_S between 300-400°C by spray pyrolysis. A similar peak (211) corresponding to Sn_2S_3 phase has been observed by M. Khadraoui et al from $SnCl_2$ and thiourea, using the spray pyrolysis method at a low temperature 270 °C [5].

The presence of the SnO_2 phase at higher temperatures was probably due to the re-evaporation of the sulfur because of its high vapor pressure that is why the oxygen replaces. This has been confirmed by several authors [3, 7, 8].

The color of films deposited at low temperature is yellow and when temperature increase color of films changed to gray then brown and at higher temperatures tends to transparent. This color leads to present of the SnS_2, Sn_2S_3, SnS and SnO_2 respectively. The same color for SnS_2 and SnS phase observed by previous authors [9, 10], in adding up T.H. Sajeesh et al [2] have observed when T_S was in the range 300°C to 400 °C, all the films were having brownish gray color, they refers the color to predominant SnS phase. Whereas B.R. Sankapal et al [11] and panda el al [12] observed the SnS_2 films golden yellow in color.

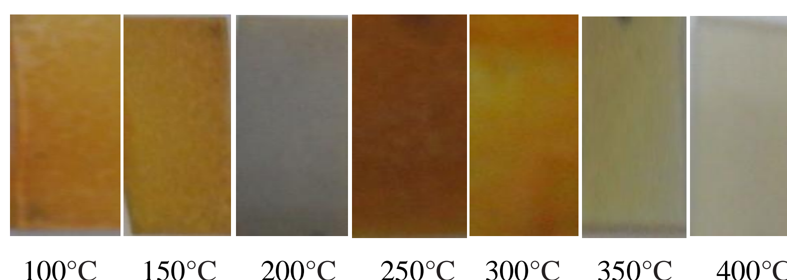

100°C 150°C 200°C 250°C 300°C 350°C 400°C

Fig.V.3: *The color of films Sn_xS_y with different substrate temperatures.*

V.1.2.1.Crystallites size, Strain, Dislocation density, Texture coefficient and lattice parameters

The X-ray diffraction spectra were exploited to determine the grain size, strain, dislocation density and number of crystallites in the films of tin sulfide. Grain size of the films was calculated from the peaks at 2θ=31.78°,15.02° and 31.81° corresponding to dominants Sn_2S_3,SnS_2 and SnS phases respectively with the methods described in the previous chapter . The results obtained are show in table.V.1. Through this table notes that the crystallite size of Sn_2S_3 phase is greater than SnS_2 and SnS phase. For SnS_2 phase, it can be seen the variation of grain size is opposite to the strain. From 200 to 300°C the crystallite size increases from 9.8 to 17.85 nm, after that decreases to reach 8.93 nm as maximum substrate temperature 400°C which is comparable to values reported in the literature [13]. Parallel, we note that the dislocation density and the number of crystallites per unit area is minimal for T_s=300°C. In effect, increases the substrate temperature or treatment are always accompanied by the increase in crystallite size, the reduction of the grain size at T_S<250°C and T_S >300°C probably due to the appearance of other phases. N. K. Reddy et al [14] have prepared films Sn_xS_y by the spray pyrolysis technique on glass substrates at temperature ranging between 100-450°C.The films obtained at 200-300°C showed peaks that correspond to Sn_2S_3 and SnS_2 phases with an average grain size of ~0.26 µm, the films deposited at 300–375°C showed peaks that correspond to SnS phase with an average grain size of ~ 0.37µm, and at growth temperatures >375 °C grain size was >0.44 µm. Otherwise T.H. Sajeesh et al [2] have studied the variation of the grain size depending on the substrate temperature for the tin sulfide produced by spray pyrolysis and concluded that the grain size decrease as T_S increased from 300 °C to 400 °C ;their results agree well with ours.

***Tab.** V.1: Structural parameters of spray ultrasonic Sn_xS_y films.*

Substrate temperature °C	Grain size (nm)		Strain **x10^{-3}**		Dislocation density x10^{14} lines/m^2	Number of crystallites x10^{16} m^{-2}
	(211) , (111)	(001)	(211), (111)	(001)	(001)	(001)
100	-	-	-	-	-	-
150	85.89	-	0.49	-	-	-
200	72.65	9.8	0.52	3.72	104.12	19.12
250	64.45	16.66	0.57	2.19	36.02	12.55
300	-	17.85	-	2.04	31.38	3.97
350	21.47 (SnS)	12.5	-1.74(SnS)	2.92	64	6.91
400	-	8.93	-	4.09	125.4	15.86

The variation of the texture coefficient implies the film growth in preferred orientation T_C (hkl) calculated for different preferred orientations (001) and (211) with different substrate temperature demonstrated in figure.V.4. From this figure it is observed that the high value of T_C (001) indicate the maximum preferential orientation of the film along the (001) plane at T_s=300°C correspond to single SnS_2 phase and the high value of T_C (211) at T_s=200°C which corresponding to Sn_2S_3 dominants phases.

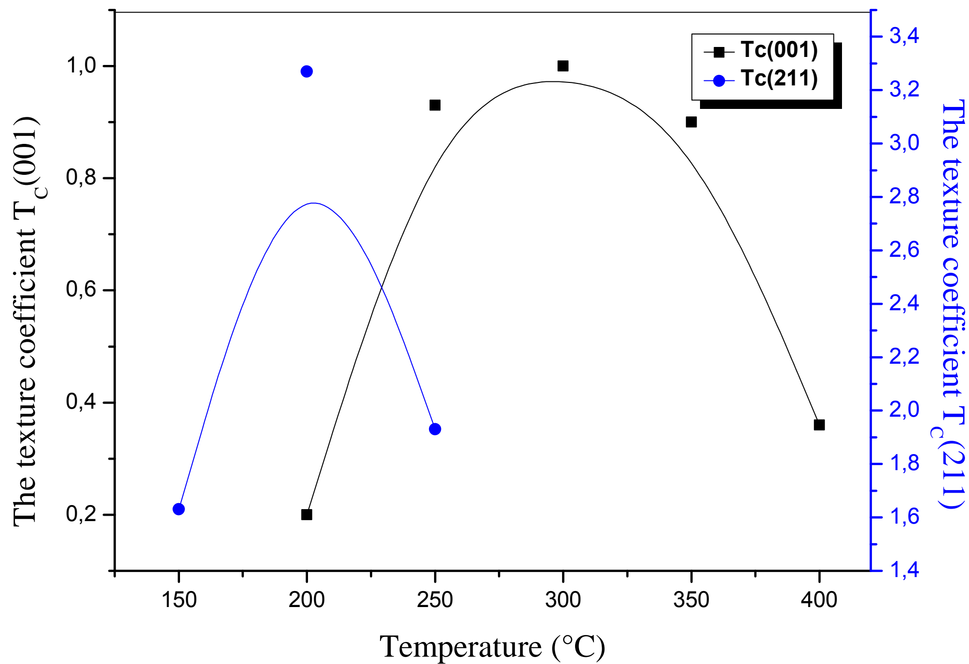

Fig.V.4*: Substrate temperature effect on the texture coefficient.*

The lattice parameters were calculated using the observed values for the (001) plane and using the d values (inter-planar spacing) for the hexagonal structure, which is given in chapter III. The results are given in table V.2. Comparing the observed parameters with the standard values (a = 3.648 A°, C = 5.899 A°), the values of lattice parameter a and c of the sample are differ and exhibit a more pronounced change as T_s increases.

Tab. V.2: *Lattice parameters of SnS_2 films deposited on the different substrates temperature*

Substrate temperature °C	**100**	**150**	**200**	**250**	**300**	**350**	**400**
Lattice parameters (A°) a and c	-	-	a=3.631 c=5.918	a=3.678 c=5.995	a=3.652 c=5.954	a=3.669 c=5.98	a=3.597 c=5.864

V.1.3. Optical studies

V.1.3.1.Transmittance

The optical transmittance of the films was measured in the wavelength range 300–900 nm, it can be used to determine many parameters characterizing a material for example: transparency, the optical band gap and the thickness of the layer ...etc. Figure. V.5 shows the transmittance spectrum for samples deposited at different substrate temperature. The average transmittance in the visible for samples obtained at the highest substrate temperatures (350–400°C) are around 32.36–46.33 %, lower than values for samples obtained at lower substrate temperatures (150–300°C), whose visible transmittance values are about 48.84%-64.78%. When the substrate temperature T_s=100°C, as can be seen in the spectra low transmittance. The average transmittance in the visible can be decreased with obtaining tin sulfide thin films with reduced thickness [15]. The absence interface fringes in the transmittance spectra indicate that the free surface of the films (film/air) is rough. This roughness causes light scattering and hence the reduction in transmittance of the films.

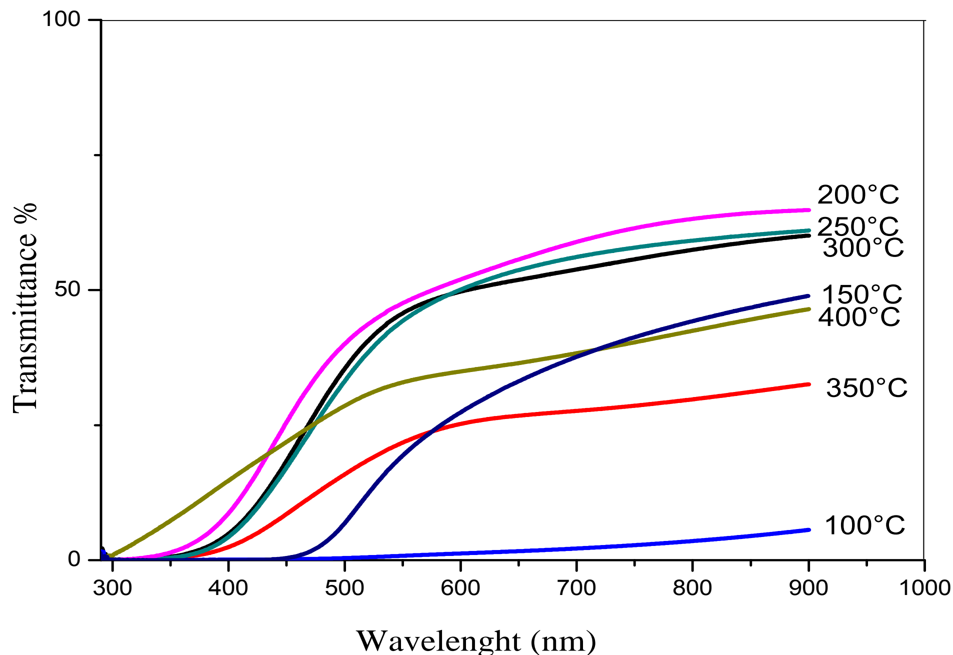

Fig.V.5*: Transmittance spectrum of tin sulfide thin films prepared at different substrate temperature*

V.1.3.2.Optical band gap

From transmittance spectra we deduce the optical gap E_g of tin sulfide films in accordance with the method described in the previous chapter. The band gap energy was calculated through $(\alpha h\upsilon)^2$ versus hυ plot, extrapolating to the point α = 0.

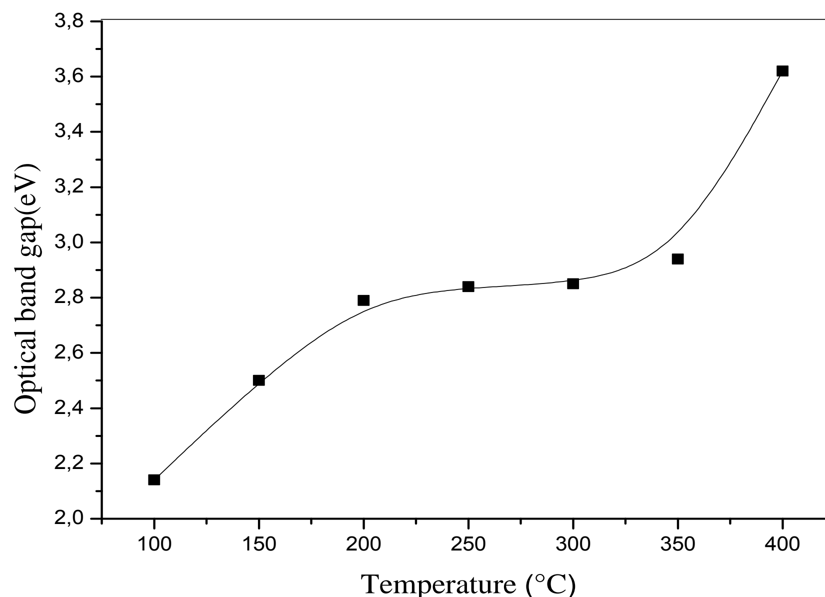

Fig.V.6: *Variation of optical band gap of films with T_S.*

Figure.V.7 shows the variation of the optical gap as a function of substrate temperature, it is seen from figure.V.6 that as the substrate temperature increases, the band gap increases from 2.14 to 2.85 eV. These values are close to the optical gap reported in the literature [16, 17]. Film deposited at 100°C has low band gap 2.14 eV, this is due to the presence of an amorphous phase in this film network as deduced from the XRD. Such behavior in amorphous silicon thin films a-Si: H [18] and silicon nitride thin films a-Si: N [19]. For samples prepared between 150-200°C, the gap is comprised between 2.50 - 2.79 eV, corresponding to the mixture SnS_2 and Sn_2S_3 phases. Thin films obtained at 250 and 300°C, the gap values of 2.84 eV and 2.85 eV respectively which corresponds to the SnS_2 phase, it is close to its value for SnS_2 bulk material. This is due to the good crystallinity of these films .Otherwise, the sample obtained at 350°C and 400°C has an optical gap value of 2.94 eV and 3.62 eV, the high value of optical gap is due to present of SnO_2 phase. The reduce of optical band gap at lower substrate temperature; this is due to lesser grain size and quantum confinement. The same interpretation obtained by previously studies [20]. In

conclusion, the layers deposited at lower substrate temperatures are more absorbent than those deposited at higher temperatures. This effect is due to phase change system Sn_xS_y, as also reflected by XRD patterns.

V.1.3.3. Photoluminescence studies

Photoluminescence (PL) technique measures the spectrum emitted by the radiative recombination of photogenerated minority carriers, is a direct way to measure the band gap energy. However, the large amount of impurities induces a large free carrier density in the bands. Consequently, different carrier interactions cause remarkable modifications of the lineshape and spectral energy of the PL features.

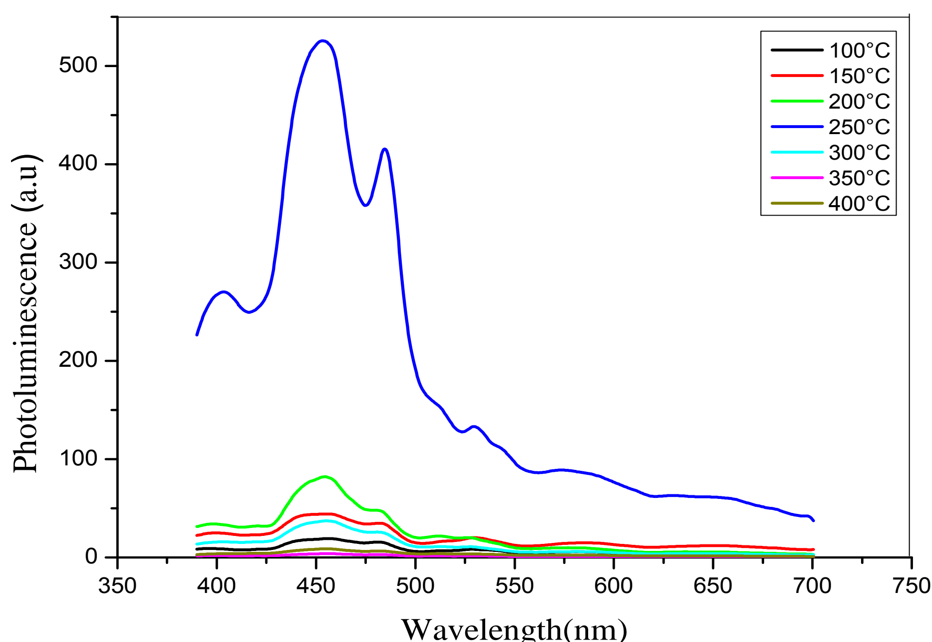

Fig.V.7: *PL spectra of tin sulfide at different substrate temperature*

Figure.V.7 shows the PL spectra for the tin sulfide thin films taken at different substrate temperature. It exhibits strong emission peak at 455nm corresponding to blue emission and other small peak at 483nm corresponding to green emission. As can be seen the film deposited at 250°C the intensity PL of peaks are higher than films deposited at others temperatures and those have demonstrated broad peaks, in addition other new peaks 403.13 nm (3.07 eV) appeared at this temperature. The peak band emission at 455 nm (2.73 eV) due to recombination of bound excitons [21], whereas the occurrence of other peak at 483 nm (2.56 eV) might be attributed to strains produced due lattice mismatch

between substrate and film. This is in close agreement with the XRD results. Another possible explanation for the origin of this latter peak might be deep level emission due to impurities and native defects such as interstitial tin atoms in SnS thin films.

V.1.4. Electrical studies

The electrical resistivity (ρ) of the as-grown films formed at different substrate temperatures is shown in figure.V.8.

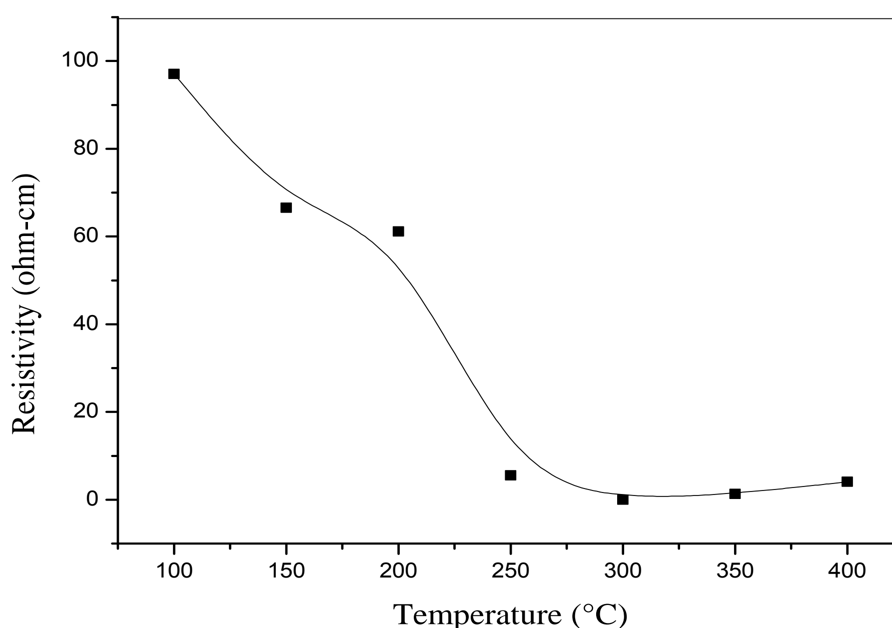

Fig.V.8: *Variation of electrical resistivity with substrate temperature for as-deposited films.*

The electrical resistivity varies from 97.03Ω.cm to 6.1×10^{-1}Ω.cm with increasing deposition temperature. It can be seen that the resistivity decreases rapidly with substrate temperature up to T_s=300°C and above this temperature, it still continues to increase but slowly. N. Koteeswara Reddy et al [14] have found the electrical resistivity varies from 300Ω.cm to 10^{-1}Ω.cm of SnS films deposited at different substrate temperatures. The reported value is the same range as the present value. The higher electrical resistivity of the films formed at lower substrate temperatures <200°C is due to the grains can't grow sufficiently large so that the inter-crystalline regions are wider and hence they offer high resistivity to the movement of charge carriers [14, 22]. Also the presence of binary phases like SnS_2 and Sn_2S_3 that are highly resistive might be responsible for the higher resistivity

[3, 4]. However, the films formed at substrate temperatures >200 °C, have shown low resistivity, which is due to presence of compound phases like SnS_2, SnS and SnO_2 phases that are lowly resistive might be responsible for the lower resistivity. The lowest resistivity ($6.1x10^{-4}$ Ω.cm) obtained for the substrate temperature T_S= 300°C is due to the better crystallinity. These results are strongly supported by XRD analysis (figure V.2) which indicates that the film grown at 300°C have large grain size than the others films.T.H. Sajeesh et al observed that the resistivity decreased with the increase in T_S and high value of resistivity of the films prepared below 300 °C was probably due to presence of mixed valent compound Sn_2S_3 [2]. These results agree our results.

V.2. Party B: Influence of substrate temperature for films deposited at 6 min and 40 ml/h

In this section, the deposition time was 6 min, the solution flow rate S_f was 40ml/h all of them were kept constant. However, the substrate temperature T_s varied from 100 to 400°C.

V.2.1. The films thickness deposition rate

Figure.V.9 shows the evolution of the films thickness and deposition rate with substrate temperature, it was found that the films thickness increased from 138 nm to 628 nm with increasing substrate temperature from 100°C to 250°C and then it decreased to 263 nm for the substrate temperature of 400 °C.

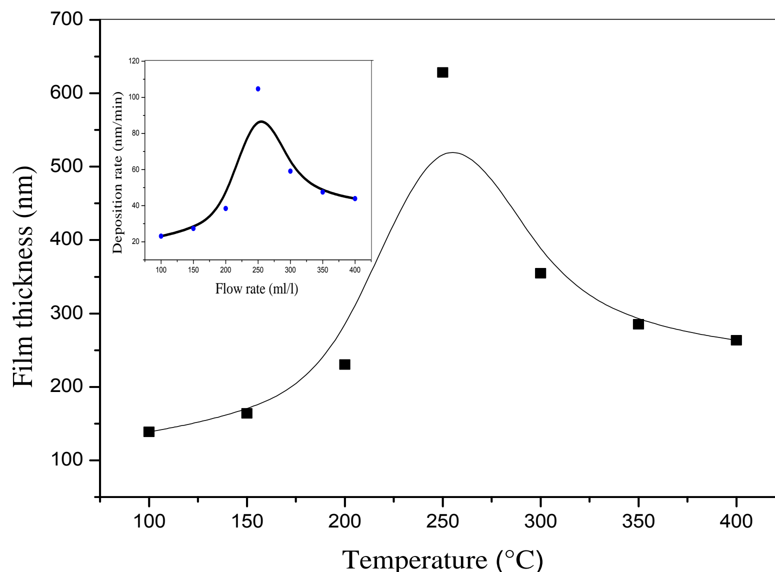

Fig.V.9: *The Variation of film thickness and deposition rate as a function of substrate temperature.*

The decrease might be due to the re-evaporation of the compounds at elevated temperatures. Such a decrease in thickness with increase in T_S for films fabricated using CSP has been reported by other research [23]. This was reported in the figure that inserts the variation of the deposition rate with substrate temperature. Moreover it is clear that the values of the films thickness and deposition rate for films deposited at 6 min are very greater than films deposited at 4 min.

V.2.2. Structural studies

Figure.V.10 showed the XRD diffraction profiles of the spray pyrolysised tin sulfide thin films deposited at 6 min with various substrate temperatures of 100, 150, 200,250,300,350 and 400°C, respectively.

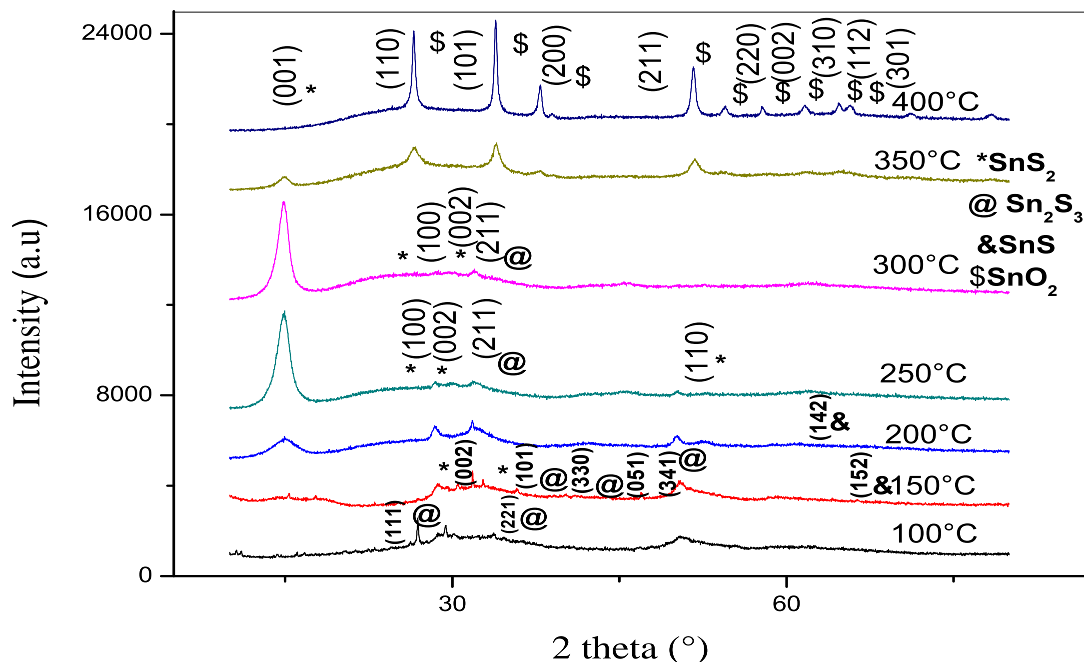

Fig.V.10: *XRD pattern of Sn_xS_y films prepared at substrate temperature.*

The X-ray diffraction data indicated that the layers grown at lower temperatures (100–300°C) show peaks corresponding to SnS_2, Sn_2S_3 and SnS phases. It was observed that the Sn_2S_3 phase was dominant at lower temperatures whereas SnS_2 became predominant as the temperature increases to 300°C, indicating that the latter phase is growing at the expense of the former while SnS phase appeared at 150°C and 200°C with (142) and (152) plan respectively. The film formed at temperatures in the range 350–400°C

showed peaks that correspond to SnS_2 and SnO_2 phase. Moreover, the intensity of the peak (001) correspond SnS_2 phase disappears with increasing substrate temperature to 400°C, in contrary for the intensities of the peaks correspondent SnO_2 phase. Similar results have been observed by C. Khelia et al in their study of substrates temperatures on the structural properties of α SnS_2 films prepared by spray pyrolysis [24]. The films grown at higher temperatures had sulfur deficiency due to its re-evaporation and so a possible explanation of the observations is that the tin-rich surface reacted with atmospheric oxygen to form SnO_2 [3, 6, 14].

Figure.V.11 shows the variation of intensity of diffraction peaks (001), (211), (152) and (142) with variation in T_s.

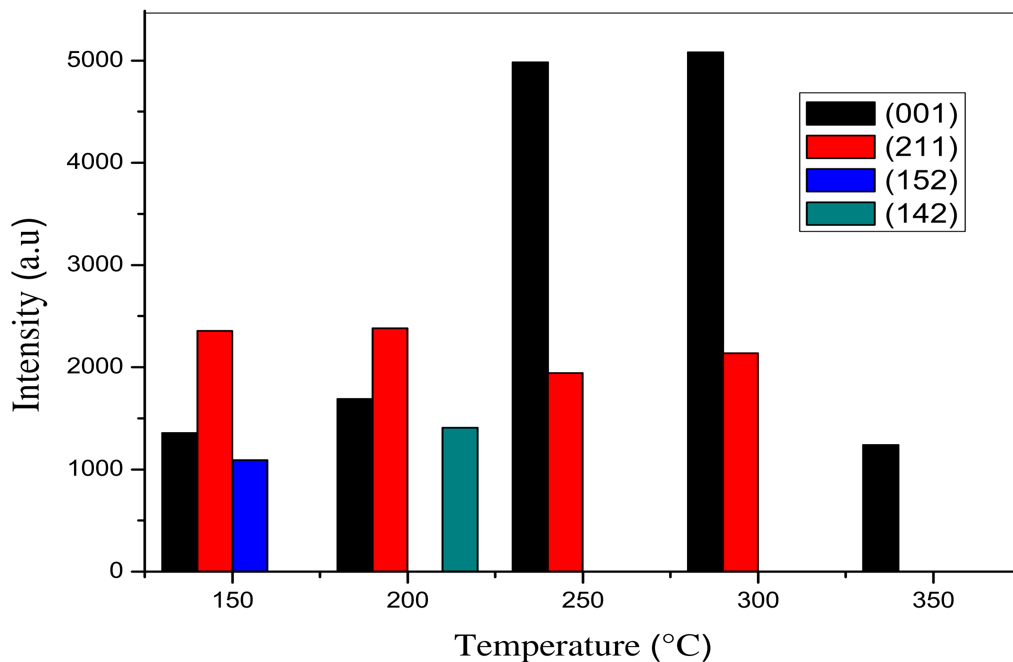

Fig.V.11: *Substrate temperature effect on the film texture*

As seen from this figure, the increase in intensity of peak (001) of the SnS_2 phase reveals the enhancement crystallinity of these films. This is due to the high crystalline quality with increase substrate temperature to 300°C and after this temperature the intensity decrease, this reduce can be due to a presence of SnO_2 phase. Whereas,(211) corresponding to Sn_2S_3 phase initially display steady intensity till T_s = 200°C and then it slightly decreases when substrate temperature between 250-300°C after that disappears at

350°C and 400°C. However, SnS phase appeared with orientation along (152) and (142) plane. The figure bellow displays the intensity of these peaks increased slightly as the T_S increased from 150 °C to 200°C.This indicates the dependence of composition, preferential orientation and crystallization on substrate temperature.

V.2.2.1.Lattice parameters, Crystallites size, Strain and Dislocation density

The lattice parameters of the SnS_2 films are shown in table.V.3.It is clear that the lattice parameters is different than the reported value of parameters with the standard values (a = 3.648 A°, c = 5.899 A°) (see table.V.3).

***Tab.V.3:** Lattice parameters of SnS_2 films deposited on the different substrates temperatures*

SnS_2				**ASTM file**	
Temperature (°C)	2θ(°)	Plan (hkl)	Lattice parameters (A°) a c	Hexagonal structure (A°)	**2θ(°)**
100	\		\		
150	15.34		a = 3.53 c =5.76	a =3.648 c =5.899	**15.02**
200	15.00	(001)	a = 3.61 c =5.88		
250	14.94		a = 3.64 c = 5.94		
300	14.93		a=3.63 c=5.93		
350	15.03	\	a = 3.61 c = 5.88	\	
400	\		\		

The average grains size D of SnS is estimated using Scherer's formula are reported in table.V.4.We found that the film deposited at substrates temperatures in the range 100-200°C showed a higher value of average grain size and a maximum value (D = 60.69 nm) at the temperature 150°C because at these temperatures the phase Sn_2S_3 most favorable . But after 100°C is observed that the average grain size decrease with increasing temperature to 250°C as there is competition in growth between the two phases (Sn_2S_3 and SnS_2) and this confirmed by the XRD spectrum. Also we note that the value of the average grain size at substrates temperature between 250-350°C is small because SnS_2 phase is predominant in these temperatures and it is most stable when the temperature equal to

300°C. On the other hand we see that the increase in temperature to 400°C helps to develop the grain size is due to the appearance of SnO_2 phase.

The other structural parameters like strain (ε), dislocation density (δ) and number of crystallites (n_c) calculated for the (001) reflection are shown in table.V.4.These parameters change with substrates temperature. This behavior was attributed to the change in the chemical stoichiometry in the films leading to the formation of different phases such as Sn_2S_3, SnS, SnS_2 and SnO_2.

Tab.V.4: *Structural parameters of spray ultrasonic Sn_xS_y film.*

Temperature (°C)	D (nm)			Average grain size (nm)	Strain $x10^{-3}$	Dislocation density $x10^{14}$ lines/m^2	Number of crystallites $x10^{16}$ m^{-2}
	(211)	(001)	(152), (142)				
100	-	-	-	48.64	-	-	-
150	85.9	38.72	30.36	60.69	0.94	6.67	0. 28
200	85.9	8.93	9.83	29.40	4.09	125	32.3
250	9.2	10.41	-	16.36	3.4	92.2	55.5
300	16.11	22.73	-	16. 51	1.59	19.3	3
350	-	17.86	-	17.08	2.03	31.34	5
400	-	-	-	43.94	-	-	-

V.2.3. Optical studies

V.2.3.1.Transmittance

Figure.V.12 shows the transmittance spectrum for samples deposited at different substrate temperature. From this figure, when Ts is increased a significant change in the absorption edge towards lower wavelengths is clearly observed. This effect may be due to the change of phases Sn_2S_3, SnS, SnS_2 and SnO_2, as revealed by XRD measurements. The average transmittance in the visible for samples obtained at the highest substrate temperatures (300–400°C) are around 72.32–64.45 %, higher than values for samples obtained at lower substrate temperatures (100–250 °C), whose visible transmittance values are about 42.61-57.13 %. The average transmittance in the visible can be increased with obtaining tin sulfide thin films with reduced thickness [15]. In addition, at higher temperature, the thermal energy provides bond formation thus it leads to have an increase in transparency. The same variation of transmittance with increase substrate temperature observed by K. Vijayakumar et al [10].

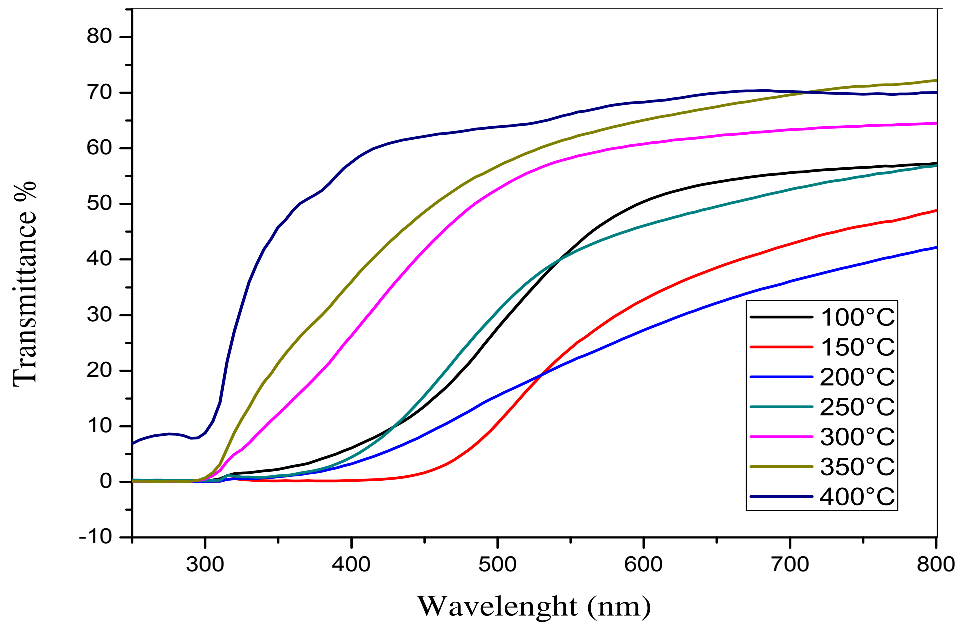

Fig.V.12: *Transmittance spectra of tin sulfide thin film prepared at different temperature*

V.2.3.2.The absorption coefficient

The absorption coefficient of the as-grown films formed at different substrate temperatures is shown in figure.V.13.

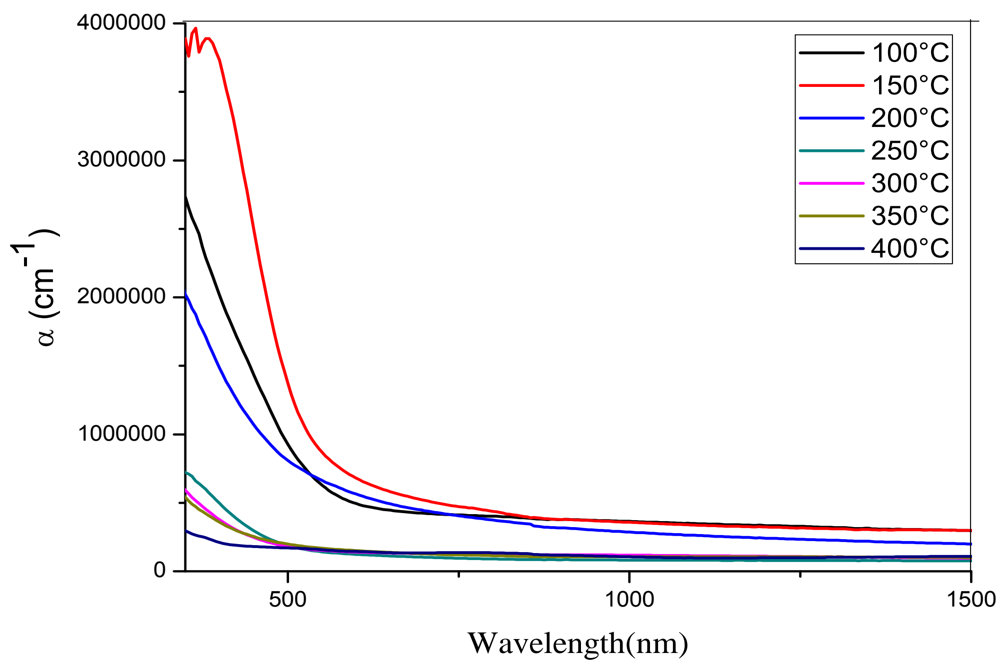

Fig.V.13: *Spectral shape of α versus wavelength of SnS thin layers system grown at different substrate temperature*

Tin sulfide have high absorption coefficient (10^6 cm^{-1}) in the wavelength range from 350 to 1500 nm. These results indicate that tin sulfide SnS compound show absorbing properties favorable for applications in solar cell devices. The same value of absorption coefficient found by T.H. Sajeesh [25] and the similar variation observed by K.Vijayakumar et al on SnS_2 thin films prepared at different substrate temperature using spray pyrolysis technique [10]. In the range of visible light, the film obtained at 400°C has the smallest absorption coefficient, and this indicated that the absorption coefficient declines at higher temperature.

V.2.3.3.The optical band gap and disorder

The variation of optical energy band gap (Eg) with substrate temperature is shown in figure.V.14. It is seen from figure.V.14 that as the substrate temperature increases; the optical band gap initially decreases from 2.76 to 2.37 eV and then increases to 3.89 eV. The observed low optical band gap of the films formed at lower temperatures was due to the presence of additional phases of Sn_2S_3 and SnS, which were known of lowly optical band gap. However the high optical band gap observed in the films formed at substrate temperatures, >250°C, correlated to the presence of the SnO_2 phase. This is supported by the XRD analysis. The optical band gap value is in agreement with the reported data on α SnS_2 and SnO_2films grown by spray pyrolysis [24] and the same variation has been found by another researcher [14]. The disorder varies inversely.

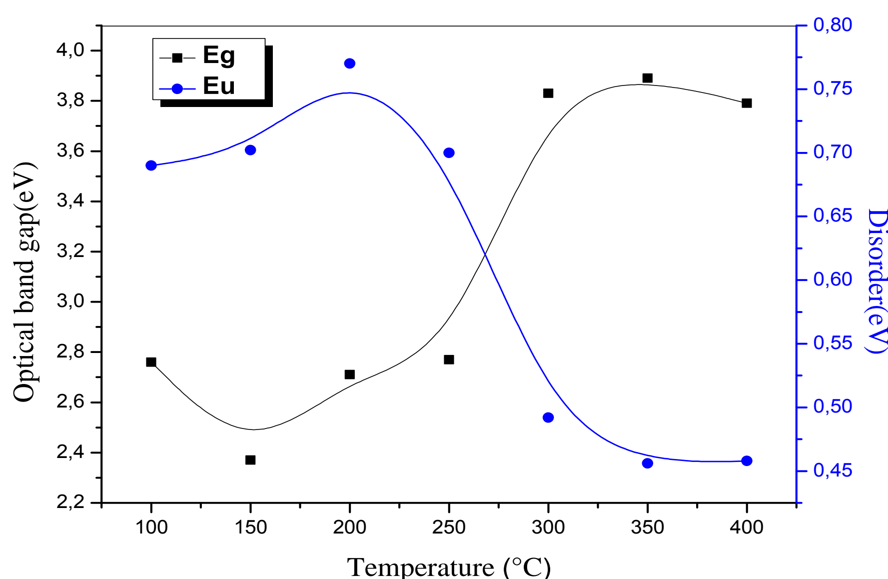

Fig.V.14: *Variation of optical band gap and disorder of the tin sulfide thin films grown at different substrate temperature*

V.2.3.4.Photoluminescence studies

From the PL measurement (Figure.V.15) all the samples [from 100°C to 400°C] showed three peaks centered at 400 nm, 453 nm and 530 nm, which were already described in chapter IV. Here the intensity of purple and blue emission of samples deposited at substrate temperature 250,300 and 400°C are higher than for samples obtained at other substrate temperatures (100°C,150°C,200 °C and 350°C) while the intensity of green emission is the most for films prepared at 250 °C and 300 °C. Qing Yang et al [26] found peak at 590 nm for SnS_2 films deposited by solvothermal process and J. Jeong et al show a broad peak at around 396 nm SnO_2 thin films [27]. This peak is in good agreement with our results.

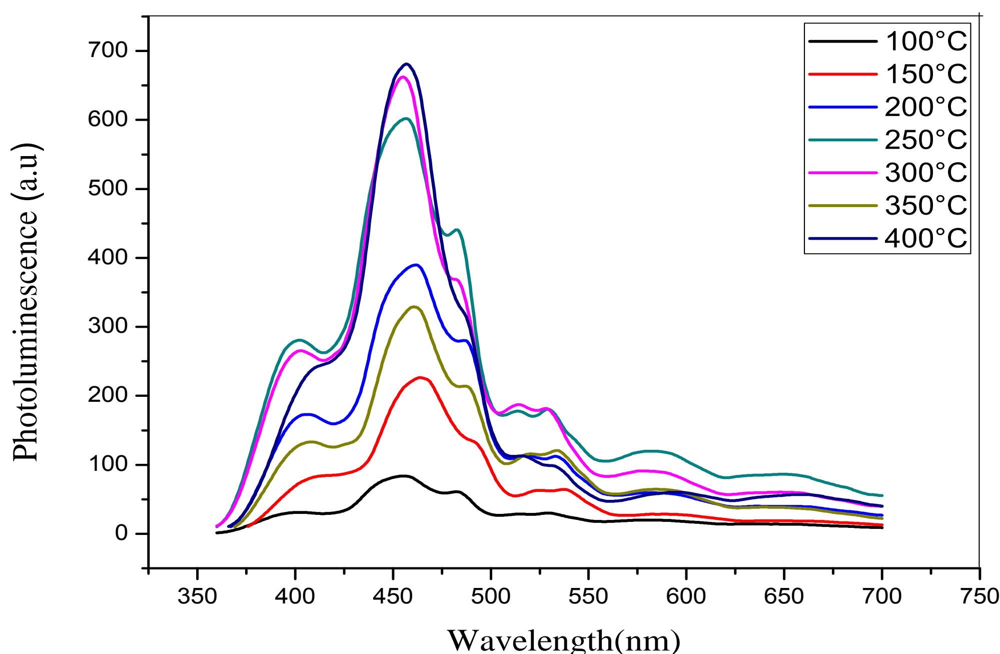

Fig.V.15: *PL spectra of different substrate temperature.*

V.2.3.5.The reflectance

The spectral shapes of reflectance R, for tin sulfide thin film system obtained at different substrate temperature (T_S =100 to 400°C) are shown in figure.V.16. Through this figure, it is noted that the value of the reflectance for the films deposited at T = 250 ° C maximum is probably due to the maximum value of the thickness (d = 628 nm). The reflectance values of the films are comparable to those reported in the literature, as has been observed by Mariappan R. et al [28]. The high value of transmission with a small reflectance in range of wavelengths can be therefore of importance that the material in

applications of effective particular energy devices. But we note that the values of reflectance are generally large, and this is logical because the films are rough as the interference fringes do not exist in the spectra of transmittance. However the presence of interference fringes of film deposited at 400°C on R spectra which confirms that, this film has uniform thickness as well as flat and smooth surfaces [29,30].

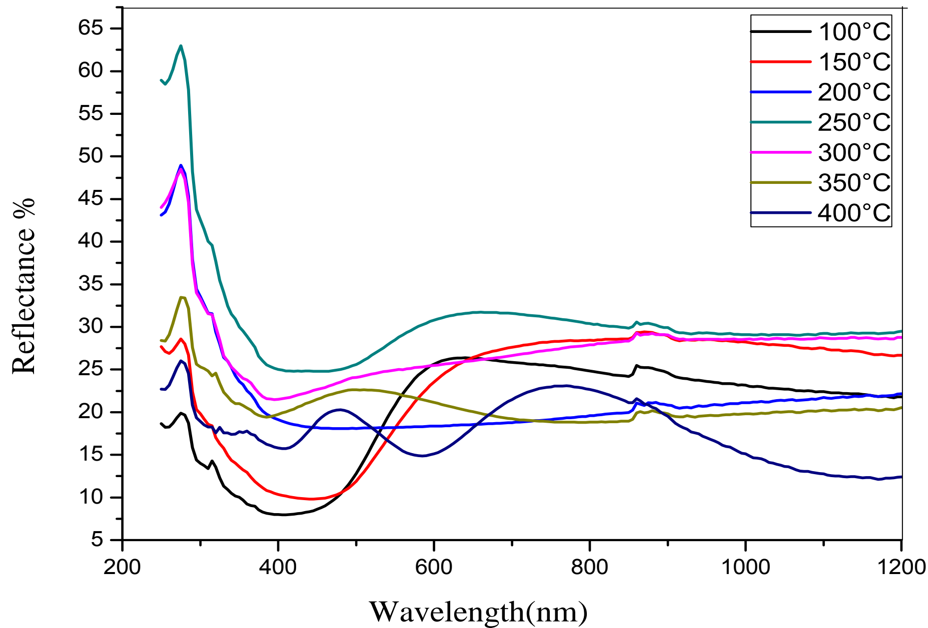

Fig.V.16: *Spectral shape of reflectance R of SnS thin layers for different substrate temperature.*

V.2.3.5.a. The refractive index and extinction coefficient

The refractive index and extinction coefficient characterize the optical properties of any solid material. Dispersion plays an important role in the research for optical materials, as it is a key factor in optical communication and in designing devices for spectral dispersion. The refractive index of the tin sulfide SnS films evaluated from the reflectance data indicated that its average value was ~2.58. The same values have been reported by other authors [29] for SnS films deposited by chemical bath deposition. The sample obtained at 250°C has maximum values of refractive index 3.52, very similar to those reported by other studies for SnS_2 thin films [31].The value of refractive index at lower substrate temperature is in good agreement with the value obtained by M. Khadraoui et al on Sn_2S_3 thin films grown by spray pyrolysis [32]. The extinction coefficient of these films was about of 0.053. The curves obtained are shown in figure.V.17.

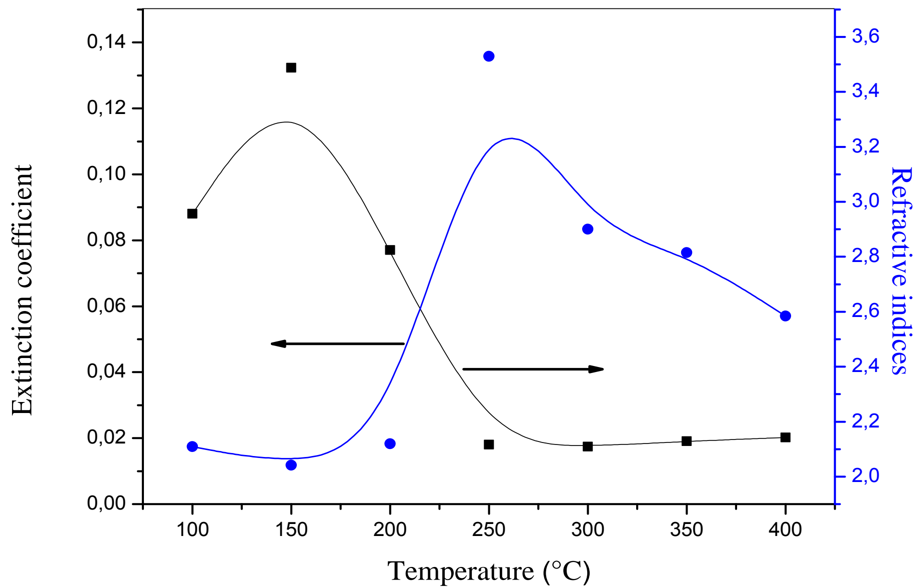

Fig.V.17: *Variation of refractive index (n) and extinction coefficient (k) for tin sulfide thin films grown at different substrate temperature*

V.2.3.5.b.The dielectric constant

The fundamental electron excitation spectrum of the films was described by means of a frequency dependence of the complex dielectric constant. Real and imaginary parts of the dielectric constant are related to the *n* and *k* values. The variation of the real (ε_1) and imaginary (ε_2) parts of the dielectric constant for different substrate temperatures is illustrated in figure.V.18.

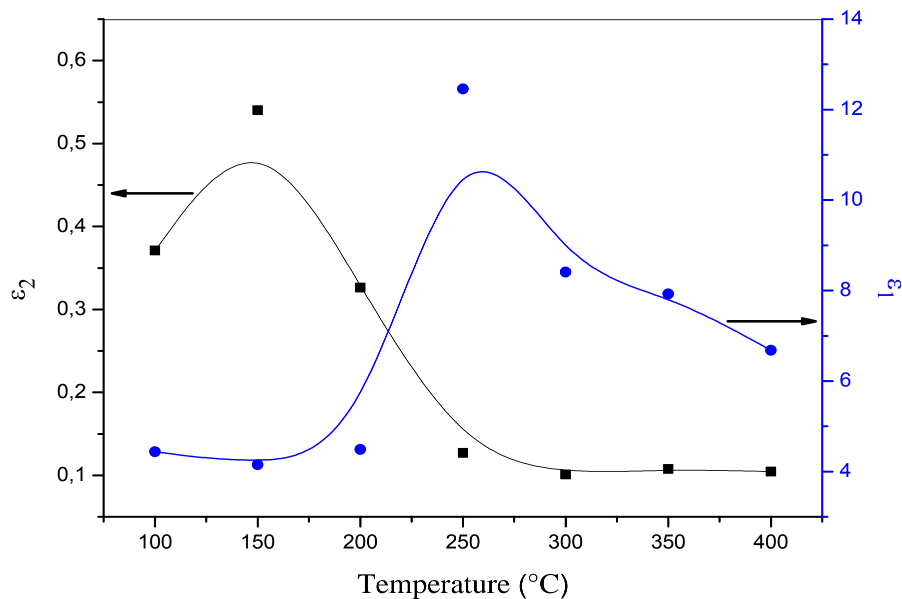

Fig.V.18: *Variation of real and imaginary part of the dielectric constant of the tin sulfide thin films*

The figures revealed that the values of the real part are higher than that of the imaginary part. From the optical data, it is observed that refractive index (*n*), the extinction coefficient (*k*), the real (ε_1) and imaginary (ε_2) parts of the dielectric constant follow the same pattern.

V.2.4. FTIR studies

Figure.V.19 shows the Fourier Transform Infrared (FTIR) spectrum of tin sulfide film deposited at different substrate temperature.

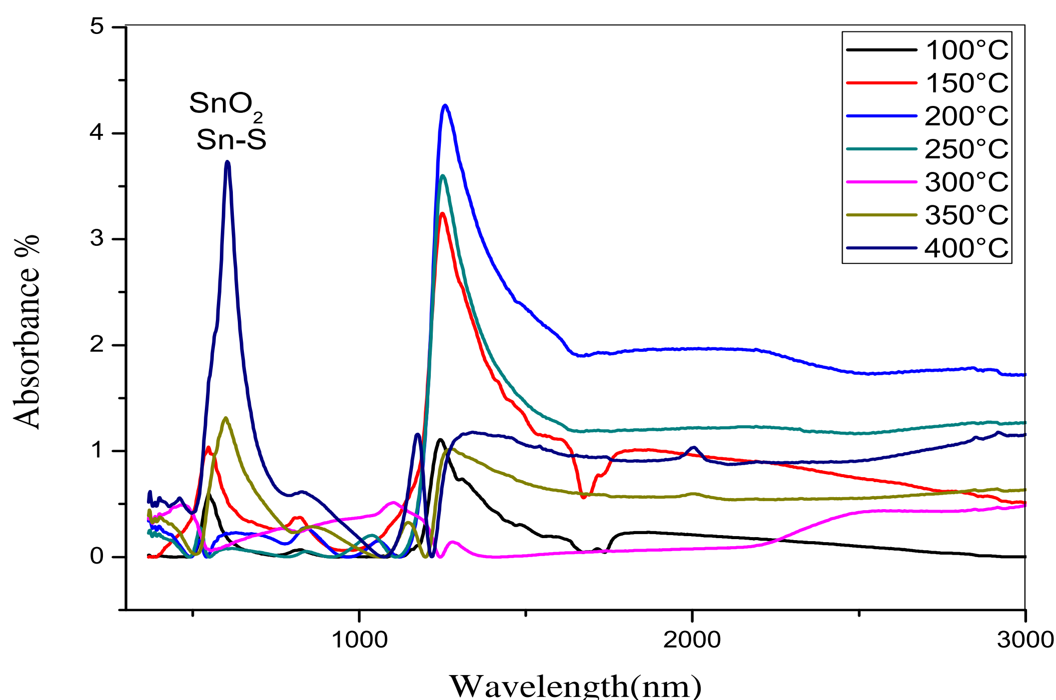

Fig.V.19: *FTIR spectra of SnS thin films deposited at various substrate temperature*

In this spectrum the absorption band located in the spectral region 500-800 cm^{-1} are observed for samples obtained at T=100,150, 350 and 400°C. In addition, with the decrease in substrate temperature the intensity of the band is reduced and diverted to small wavelength. Too, we observed the existence a broad band located in the interval 1086 - 1350 cm^{-1} at T = 150, 200 and 250°C, and with increasing the substrate temperature the width and the intensity of band decrease. Also we can see that our peaks were large that's because the most grains size were small so weak crystalline structure [33]. The peaks appeared in interval 500-800 cm^{-1} in the spectrum are due to the formation of Sn–S and SnO_2 bond [34, 35]. Here, the observed intensity was increased proportionately with the

increase of substrate temperature to 400°C. These results are strongly supported by XRD analysis which indicates that the SnO_2 phase was dominant at film grown at substrate temperature 350 °C and 400°C. On other hand , the absorption band situated in the spectral region 1086 - 1350 cm^{-1} is most intense for films prepared at lower substrate temperature (150, 200 and 250°C), which confirmed that these films were highly absorbing than other films. This is affirmed by the optical transmittance, the absorption coefficient spectra and XRD analysis which designate that the low substrate temperature gives films more absorbent.

V.3. Conclusion

Tin sulfide thin films prepared by spray pyrolysis technique have shown SnS_2, SnS and Sn_2S_3 structure depending on the substrate temperature at which the process was conducted. The tin sulfide films tend to grow in the SnS phase when the substrate temperature is comprise between 150-200°C for the deposition time equal 6 min. while the films grown at 4min show SnS phase when the substrate temperature is 200°C or 350°C. By the contrary, the SnS_2 phase is achieved by increasing the substrate temperature to 300°C with preferential orientation along the (001) plane. Otherwise, the Sn_2S_3 phase was dominant at lower temperatures. The samples obtained at lower temperatures presented energy band gap between 2.37 and 2.77 eV and very high absorption coefficient ($>10^6$ cm^{-1}), so that their application in solar cells could be as absorbent material. Whereas the samples obtained at higher substrate temperatures, presented band gap energy between 3.79 and 3.89 eV and, therefore, could be used as a window layer in photovoltaic devices.

References of fifth chapter

[1] T. Serin, N. Serin, S. Karadeniz, H. Sarı, N. Tugluoglu, O. Pakma, J. Crystalline Solids 352 (2006) 209–215.

[2] T.H. Sajeesh, A.R. Warrier, C. Sudha Kartha, K.P. Vijayakumar, J.Thin Solid Films 518 (2010) 4370–4374.

[3] N. Koteeswara Reddy, K.T. Ramakrishna Reddy, J.Solid-State Electronics 49 (2005) 902–906.

[4] K.T.Ramakrishna Reddy, P.Purandar Reddy, R.W.Miles, P.K.Datta, J.Optical Materials 17(2001)295-298.

[5] N. Koteeswara Reddy, K.T. Ramakrishna Reddy,J.Thin Solid Films 325 (1998) 4–6

[6] M.Calixto-Rodriguez, H. Martinez, A.Sanchez-Juarez, J.Campos-Alvarez, A.Tiburcio-Silver, M.E. Calixto, J.Thin Solid Films 517 (2009) 2497–2499.

[7] G.H. Yue, D.L. Peng, P.X. Yan, L.S. Wang, W. Wang, X.H. Luo, J. Alloys and Compounds 468 (2009) 254–257.

[8] N Koteswara Reddy, K T Ramakrishna Reddy, G Fisher, R Best and P K Dutta, J. Phys. D: Appl. Phys. 32 (1999) 988–990.

[9] S. C. Ray, M. K. Karanjai, D. DasGpta, J. Thin Solid Films 350 (1999) 72-78.

[10] K. Vijayakumar, C.Sanjeeviraja, M. Jayachandran, L. Amalraj, J. Mater Sci: Mater Electron 22 (2011) 929–935.

[11] Sankapal. B.R, Mane. R.S, Lokhande .C.D, J.Res. Bull 35 (2000) 2027–2035.

[12] S.K. Panda, A. Antonakos,E. Liarokapis, S.Bhattacharya, S. Chaudhuri, J.Materials Research Bulletin 42 (2007) 576–583.

[13] **I.B.Kherkhachi**, A. Attaf, H. Saidi, A. bouhdjar, H. Bendjdidi, Y. Benkhetta,R. Azizi, M.S. Aida, J. Optik 127 (2016) 2266–2270 .

[14] N. Koteeswara Reddy, K.T. Ramakrishna Reddy, J. Physica B 368 (2005) 25–31.

[15] V. Robles, J. F. Trigo, C. Guillén, J. Herrero, J .Mater Sci 48 (2013) 3943–3949.

[16] N.G. Deshpande, A.A. Sagade, Y.G. Gudage, C.D. Lokhande, J.Alloy Compd 436(2007) 421–426.

[17] O. Parasyuk, I.D. Olekseyuk, L.V. Piskach, S.V. Volkov, V.I. Pekhnyo, J. Alloys Compd 399 (2005) 173–177.

[18] Street R. A, Hydrogenated amorphous silicon, Cambridge University Press, (1991) 92.

[19] M.S .Aida, A. Attaf, M. L.Benkedir, The optical properties of sputtered amorphous silicon nitride films: effect of RF power, Phil Mag B 73 (1996) 339.

[20] B.G. Jeyaprakash, R. Ashok kumar, K.Kesavan, A. Amalarani, J.American Science 6 (2010) 3.

[21] **I.B. Kherkhachi**, H.Saidi ,A. Attaf, N.Attaf ,A. Bouhdjar , H.Bendjdidi , Y. Benkhetta ,R. Azizi, M.jlassi. J. Optik 127 (2016) 4043-4046.

[22] M. R. Fadavieslam, N. Shahtahmasebi, M. Rezaee-Roknabadi, M. M. Bagheri-Mohagheghi, J.Semiconductors 32 (2011) 113002.

[23] K.L. Chopra, S.R. Das, Plenum Press, New-York, (1983).

[24] C. Khélia, F.Maiz, M. Mnari, T.Ben Nasrallah, M.Amlouk, S.Belgacem, J.Eur. Phys. AP 9 (2000) 187-193.

[25] T.H. Sajeesh, K.B. Jinesh, C. Sudha Kartha, K.P. Vijayakumar, J.Applied Surface Science 258 (2012) 6870– 6875.

[26] Q.Yang, K.Tang, C.Wang, J. Zuo, D. Zhang, Y. Qian, J.Thin Solid Films 436 (2003) 203–207

[27] J. Jeong, S.P. Choi, C.J. Chang, D.C. Shin, J.S. Park, B.T. Lee, Y.J. Park, H. J. Song, J. Solid State Commun 127 (2003) 595.

[28] R. Mariappan, T. Mahalingam, V. Ponnuswamy, J.Optik 122 (2011) 2216– 2219.

[29] A. Akkari, M. Reghima, C. Guasch, N. Kamoun-Turki, J. Mater Sci 47 (2012) 1365–1371.

[30] S.Wang, S.Wang, J. Chen, P. Liu, M.Chen, H. Xiong , F. Guo, M. Liu, J .Nanopart Res 16 (2014) 2610.

[31] S. Mandalidis, J. A. Kalomiros, K. Kambas, A. N. Anagnostopoulos, J. Materials science 31 (1996) 5975-5978.

[32] M. Khadraoui, N. Benramdane, C. Mathieu, A. Bouzidi, R. Miloua, Z. Kebbab, K. Sahraoui, R. Desfeux, J.Solid State Communications 150 (2010) 297-300.

[33] F. Liu, B. Quan, Z.Liu, L. Chen, J. Materials Chemistry and Physics 93 (2005) 301-304.

[34] K. Nakamoto, IR Spectra of Inorganic and Coordination, Compounds-2nd E, Wiley Eastern NY, (1970).

[35] M. Gartner, C. Savaniu, C. Parlog, M. Zaherescu, G. Craciun, O. Buiu, E. Szilagy, C. Cobianu, Proceedings of the International Semiconductor Conference, Sinae Romania 1997 (1997)71–74.

General conclusion and perspectives

Our study related to the deposition and characterization of the tin sulfide thin films elaborated by the ultrasonic spray technique on glass substrates.

We studied the effect of three experimental parameters on the properties of these layers, namely the deposition time for two types of source of tin (tin chloride II and IV), the solution flow rate and substrate temperature. After their preparation, the films were characterized by several techniques (X-ray diffraction, UV-visible spectrophotometry, photoluminescence and four points).

To investigate the influence of different operating conditions of deposit on their structural, optical and electrical properties determined to optimal settings for the best layer of tin sulfide applied to the solar cells in particular.From the study of deposition time, for tin chloride **II** and **IV** as a source of tin, X-ray diffraction reveals a good crystalline structure with (001) orientation which corresponds to SnS_2 hexagonal phase and other phase SnS appeared of films deposited using tin chloride **IV** starting from 2 min while at films deposited using tin chloride **II** it appears only when the film is deposited after 8 min.On the other hand, Sn_2S_3 phase occurred only after 6 min for two precursors. Through the calculation of the grains size, we found that the deposition time has an influence on the grains size which is varied from 9.09 nm to 19.36 nm for the first source and 12.87 nm to 28.33 nm for the second source. However, for the solution flow rate we noticed that all the films have a hexagonal structure with preferential orientation (001) corresponding to SnS_2 phase but at 6min, we found that others small peaks (100), (002), (112), (211), (221), (250), (003), (151), (310), (112), (102) and (110) corresponding to SnS and Sn_2S_3. Good crystallinity is obtained at substrate temperature of 300°C for SnS_2, 150 and 200°C for SnS and at lower temperature (below 250 °C)for Sn_2S_3. Moreover at higher substrate temperature (after 350 °C) tin sulfide converts to transparent conducting tin dioxide SnO_2.

The optical characterization showed that our films are absorbent with high absorption coefficient ($>10^6\ cm^{-1}$), the transmittance varies between 3.1 % and 72% and the optical gap is varied between 2.14 eV and 3.89 eV. PL showed the emission peaks attributed to purple, blue, green, yellow and red emission. FTIR studies reveal the strong absorbance of tin sulfide thin films. Finally, the optical constants refractive index, extinction coefficient, and dielectric constant showed changes associated to the corresponding crystalline phases.

The measure of electrical resistivity of tin sulfide films by four points showed that the value obtained depending on the deposition parameters used.

Through the obtained results we found that, the tin sulfide thin films deposited at high deposition time and solution flow rate and at low substrate temperature are more suitable for utilization as the absorber layer in solar cells application but the films deposited at low deposition time and solution flow rate can be a potential candidate for optoelectronic as well as thin film solar cell devices. However, the films deposited at high substrate temperature could be used as a window layer in photovoltaic devices.

In conclusion, with varying deposition time, the precursors, solution flow rate and substrate temperature, different stoichiometries of tin sulfide can be obtained, enabling different use in photovoltaic applications.

Considering the results obtained on the optimization of the parameters structural, optical and electric of the layers containing Tin Sulphide, we propose to achieve these studies by characterizing the layers where the SnS phase appears, by MEB under the optimal conditions. So, efforts should be made to optimize the performance of this promising material, and improved the properties of its conditions to be more suitable for solar cells application.

Publications produced through this work

"**Structural, optical and electrical properties of Sn*x*S*y* thin films grown by spray ultrasonic**"

I.B.Kherkhachi, A.Attaf, H.Saidi, A.Bouhdjer, H.Bendjedidi, Y. Benkhetta, R. Azizi, J. Semiconductors Vol. 37, No. 3 (2016) .

"**Influence of solution flow rate on the properties of SnS_2 films prepared by ultrasonic spray**"

I.B. Kherkhachi, H.Saidi ,A. Attaf, N.Attaf ,A. Bouhdjar , H.Bendjdidi , Y. Benkhetta ,R. Azizi, M.jlassi. J. Optik 127 (2016) 4043-4046.

"The synthesis, characterization and phase stability of tin sulfides (SnS_2, SnS and Sn_2S_3) films deposited by ultrasonic spray"

I.B.Kherkhachi, A. Attaf, H.Saidi, A. Bouhdjar, H.Bendjdidi, Y. Benkhetta, R. Azizi, J.Main Group Chemistry 15 (2016) 231-242.

دراسة الشرائح الرقيقة لكبريتيد القصدير(SnS) المحضرة بالطرق الكيميائية للتطبيقات التكنولوجية

الملخص

موضوع هذه الرسالة يتناول تحضير ودراسة خصائص الشرائح الرقيقة لكبريتيد القصدير(SnS) باستخدام تقنية الرش الفوق الصوتي. العينات المحضرة قسمت إلى ثلاث سلاسل وفقا لشروط الترسيب : وهي زمن الترسيب (حضرنا سلسلتين الأولى استخدامنا فيها كلوريد القصدير II والأخرى استخدامنا فيها كلوريد القصدير IV كمصدر للقصدير)، تدفق الرذاذ ودرجة حرارة المسند. الشرائح المحضرة عولجت باستخدام تقنيات تشخيص مختلفة : الخصائص البنيوية ، الضوئية والكهربائية .
الدراسة البنيوية بينت أن الشرائح الموضعة في كل أزمنة الترسيب وخاصة المحضرة بواسطة كلوريد القصدير IV ذات بنية سداسية وفق المستوى المفضل (001) وكذلك المحضرة في كل التدفقات وعند درجة الحرارة 300 درجة مئوية لها نفس البنية. بينما عند استعمال كلوريد القصدير II عند أزمنة الترسيب اكبر من 6 دقائق وفي درجات حرارة المسند 150و 200 و350 درجة مئوية يظهر SnS وفق البنية المعينة متعامدة المحاور ، ولكن عند استعمالنا كلوريد القصدير IV يظهر SnS في كل أزمنة الترسيب. في حينSn_2S_3 يبرز في أزمنة الترسيب اكبر من 6 دقائق و يكون مفضل في درجات حرارة المسند المنخفضة. نتائج الدراسة الضوئية وضحت أن شرائح كبريتيد القصدير ماصة قي المجال المرئي للضوء وقيمة النطاق الممنوع من رتبة 2.8eV و هذا مما يجعلها مرشحة للتطبيقات الضوئية. قياسات الناقلية الكهربائية للشرائح المحضرة بينت أن قيمة هذه الأخيرة تتعلق بشروط الترسيب.

الكلمات المفتاحية: الشرائح الرقيقة، الشرائح الماصة، كبريتيد القصدير، الرش الفوق الصوتي، الخصائص البنيوية، الخصائص الضوئية، الخصائص الكهربائية.

Study of thin layers of tin sulfide (SnS) elaborated by chemical means for technological applications

Abstract

The present work deals with the deposition and characterization of tin sulfide thin film prepared by ultrasonic spray for the photovoltaic application. Sets of films were prepared by varying three deposition parameters namely deposition time (using tin chloride II and IV as the tin source), the spray flow rate and the substrate temperature (using the chloride tin II as a source of tin) .The films were subjected of various characterizations: structural, optical and electrical.The structural characterization of the films revealed that they have a hexagonal structure with a preferential orientation (001) at all deposition time and particularly films prepared with tin chloride IV as the tin source, at all spray flow rate and at temperature of 300 °C. However, we noted the presence of SnS phase with an orthorhombic structure at superior deposition time after 6 min for tin chloride II and all deposition time for tin chloride IV also appeared at substrate temperature 150° C, 200 °C and 350 °C. On the other hand, we observed Sn_2S_3 at higher deposition time for two sources of tin and at low substrate temperature. The optical characterization shows that tin sulfide films are absorbent in the visible, the value of the optical gap is about 2.8 eV; its indicating their photovoltaic applications. Measurements of the resistivity showed that the value of the latter depending on the deposition conditions.

Keywords: Thin films, films absorbent, Tin sulfide, Ultrasonic spray, Structural properties, optical properties, electrical properties.

Etude des couches minces de sulfure d'étain élaboré par voie chimique douce en vue d'applications technologiques

Résumé

Ce travail de thèse porte sur l'élaboration et la caractérisation des couches minces de sulfure d'étain préparées par spray ultrasonique pour des applications photovoltaïques. Les échantillons ont été élaborés en variant, séparément, trois paramètres: le temps de dépôt (on utilisant le chlorure d'étain II et IV comme source d'étain), le débit d'atomisation et la température de substrat (on utilisant le chlorure d'étain II comme source d'étain).Les films ont subi diverses caractérisations:structurale, optique et électrique.La caractérisation structurale des films a révélé que ces derniers ont une structure hexagonale avec une orientation privilégiée (001) à tout temps de dépôt et surtout les films préparés avec le chlorure d'étain IV comme source d'étain, à tout le débit et une température de 300°C. Cependant, nous avons noté la présence de SnS phase avec une structure orthorhombique à temps de dépôt supérieur de 6 min pour le chlorure d'étain II et à touts temps de dépôt pour le chlorure d'étain IV et encore des températures de 150° C, 200°C et 350°C. Mais, nous avons observé Sn_2S_3 à temps de dépôt supérieur de 6 min pour les deux sources d'étain et à faible température du substrat. La caractérisation optique montre que les films de sulfure d'étain sont absorbants dans le visible, la valeur du gap optique est de l'ordre de 2.8 eV ; ce qui indique leur applications photovoltaïques. Les mesures de la résistivité ont montré que cette dernière dépende des conditions de dépôt.

Mots clés : Couches minces, Couches absorbante, Sulfure d'étain, Spray ultrasonique, Propriétés structurales, Propriétés optiques, Propriétés électriques.